Survey of regulatory factors involved in the waveform changes coupled with Ca^{2+} of *Chlamydomonas* flagella

March 2018

Department of Picobiology, Graduate School of Life Science, University of Hyogo

Junya KIRIMA

ACKNOWLEDGEMENTS

Firstly, I want to thank my supervisor Prof. Kazuhiro Oiwa for the opportunity to work in his group on such an exciting project. I am grateful for the many opportunities Prof. Kazuhiro Oiwa has given me during my Ph.D. course. I am grateful to Drs. Akane Furuta, Ken'ya Furuta, Takayuki Torisawa, Takashi Sagawa, Hiroto Tanaka, Hitoshi Sakakibara, and Hiroaki Kojima for their indispensable advice, support with the research, and insightful discussions. Technical support was kindly provided by Ms. Maki Yoshio, Ms. Misako Amino, Ms. Yumi Nakajima, Ms. Yu Yamano, and Ms. Misaki Shiraga. I also thank my supervisors, Profs. Yoshinobu Mineyuki, Yoshiki Higuchi, and Hiderou Yoshida, for their guidance and support throughout my Ph.D. course. External supervisors helped make my Ph.D. degree possible. I thank Profs. Toshiki Yagi and Winfield S. Sale for all your help and critical advice on my project. I thank my many good friends in the picobiology department, who have encouraged and kept me going over these five years. I also thank the picobiology office staff who supported my Ph.D. life. Finally, I thank my family for their encouragement.

This work is supported by a Fellowship from the Leading Graduate School of Picobiology at the University of Hyogo (JK).

ABBREVIATIONS

- Abs350nm: absorbance at 350 nm
- BLAST: Basic Local Alignment Search Tool
- BPB: bromophenol blue
- BRB80: 80 mM PIPES-KOH, 1 mM $MgCl_2$, 1 mM EGTA, pH 6.8
- BSA: bovine serum albumin
- Blocking buffer: 3% bovine serum albumin (BSA), 5% glycerol, 20% fish gelatin in PBS, pH 7.4
- CBB: Coomassie Brilliant Blue
- CP: central pair
- DMT: doublet microtubule
- DRC: dynein regulatory complex
- DTT: dithiothreitol
- EDC: l-ethyl-3-(3-dimethylaminopropyl) carbodiimide
- EGTA: ethylene glycol-bis(2-aminoethylether)-*N,N,N′,N′*-tetraacetic acid
- EM: electron microscopy
- FAP: flagellar-associated protein
- Fixative solution: 50 mM HEPES-NaOH, 3 mM EGTA, 1 mM $MgSO_4$, 25 mM KCl, pH 6.8 with 3% formaldehyde and 0.1% glutaraldehyde
- GTP: guanosine triphosphate
- HEPES: 2-[4-(2-hydroxyethyl)-1-piperazinyl]ethanesulfonic acid
- HMDEK: 30 mM HEPES-NaOH, 5 mM $MgSO_4$, 1 mM DTT, 1 mM EGTA, 50 mM K-Acetate, pH 7.4
- High salt-concentration HMDE solution: 0.6 M KCl, 30 mM HEPES-NaOH, 5 mM $MgSO_4$, 1 mM DTT, 1 mM EGTA

- IDA: inner dynein arm
- MALDI-TOF: matrix-assisted laser desorption/ionization- time-of-flight
- MIP: microtubule inner protein
- MT: microtubule
- MTSB-NH_4Cl buffer: 50 mM HEPES-NaOH, 3 mM EGTA, 1 mM $MgSO_4$, 25 mM KCl, 50 mM NH_4Cl, pH 6.8
- NCBI: National Center for Biotechnology Information
- NP-40: Nonidet P-40
- OAD: outer arm dynein
- ODA: outer dynein arm
- ONL: orange nano-lantern
- PBS: phosphate-buffered saline
- PF: protofilament
- PIPES: piperazine-*N, N'*-bis(2-ethanesulfonic acid)
- PSB-T buffer: 10 mM Na-PBS, pH 7.4 with 0.02% Tween-20
- PVDF: polyvinylidene difluoride
- RS: radial spoke
- S.D.: standard deviation
- SDS: sodium dodecyl sulfate
- Sarkosyl: *N*-lauroylsarcosine
- TAP: Tris-acetic acid-phosphate.

TABLE OF CONTENTS

CHAPTER 1

General introduction

Cilia and flagella are motile organelles common in various types of eukaryotic cells. They range from several μm to dozens of μm in length with diameters of approximately 0.2 μm. The beating of motile flagella/cilia plays important roles in generating a driving force for swimming of protozoa and spermatozoa, making a mucus flow on epithelial cells for airway clearance, and transportation of substances. Defects in the function, organization, and/or integrity of these organelles are closely associated with several medical problems that are collectively named ciliopathy (Brown and Witman, 2014) (**Figure 1.1**).

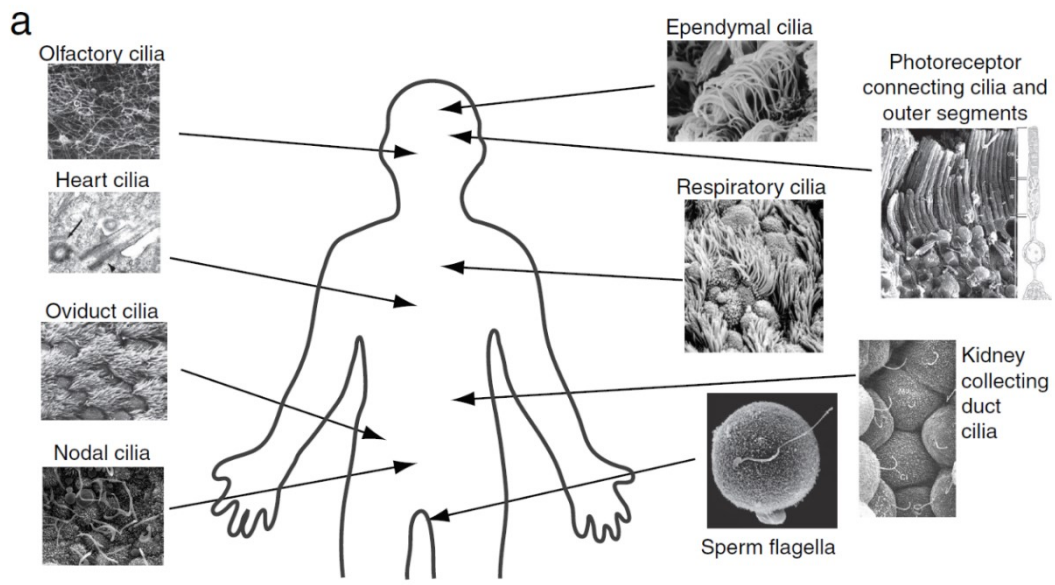

Figure 1.1 **Cilia and flagella are found throughout the human body**

Selected locations of motile and non-motile cilia in the human body. Reprinted with permission from Brown and Witman (2014).

Proteomics and genomics studies have shown that axonemes are composed of 200-600 types of protein components (Dutcher, 1995; Merchant et al., 2007; Pazour et al., 2005). The scaffold structure of cilia and flagella is called the axoneme, and it is composed of nine doublet microtubules surrounding a pair of singlet microtubules (known as the "9+2" structure) (**Figure 1.2 A, B**). This is a highly conserved structure among protozoa to vertebrates. The various proteins in the axoneme form functionally and structurally distinct axonemal components, such as the inner dynein arm (IDA), outer dynein arm (ODA), nexin-dynein regulatory complexes (N-DRC), radial spoke (RS), and central pair (CP), which are essential to generate cilia/flagella beating (Adams et al., 1981; Bui et al., 2008; Heuser et al., 2009; Pigino et al., 2011; Smith and Sale, 1992a).

The motor protein generating motive force of flagella movement is a dynein. A dynein is the generic name for the ATPase, which generates force and movement on microtubules. The two major classes are the axonemal dyneins and the cytoplasmic dyneins. The axonemal dyneins are further classified into two subclasses, outer arm dyneins and inner arm dyneins, based on their localization in the axoneme. They form two distinct rows, which are the outer arm and the inner arm (**Figure 1.2 C**). Although discrimination into these classes was originally based on their function and localization, phylogenetic analyses of full-length dynein sequences have confirmed differences between various dyneins. Recently, eleven classes of dyneins (two cytoplasmic, two outer arm, and seven inner arm) have been identified.

A *Chlamydomonas* flagellum contains at least seven subspecies of inner arm dyneins (dynein a - g) that are arranged along a doublet in a 96 nm repeat length. Judging from the subunit compositions, they are divided into three groups. Each 96-nm repeat of inner arm dyneins contains one copy of inner arm dynein f (I1), which has two distinct heavy chains, three intermediate chains, and several light chains. The second group contains monomeric heavy chains that each associate with one actin molecule and the Ca^{2+}-binding protein centrin (dyneins b, e, and g). The third group contains monomeric heavy chains that each associate with one actin molecule and a dimer of the essential light chain, p28 (dyneins a, c, and d). Cryo-electron tomography has revealed the three-dimensional

arrangement of inner arm dyneins in an axoneme and showed that six single-headed dynein subspecies are located as one straight array along the length of the A-tubule and their head domain pairs form three dyads (Bui et al., 2008; Ishikawa et al., 2007). **(Figure 1.2 D)**.

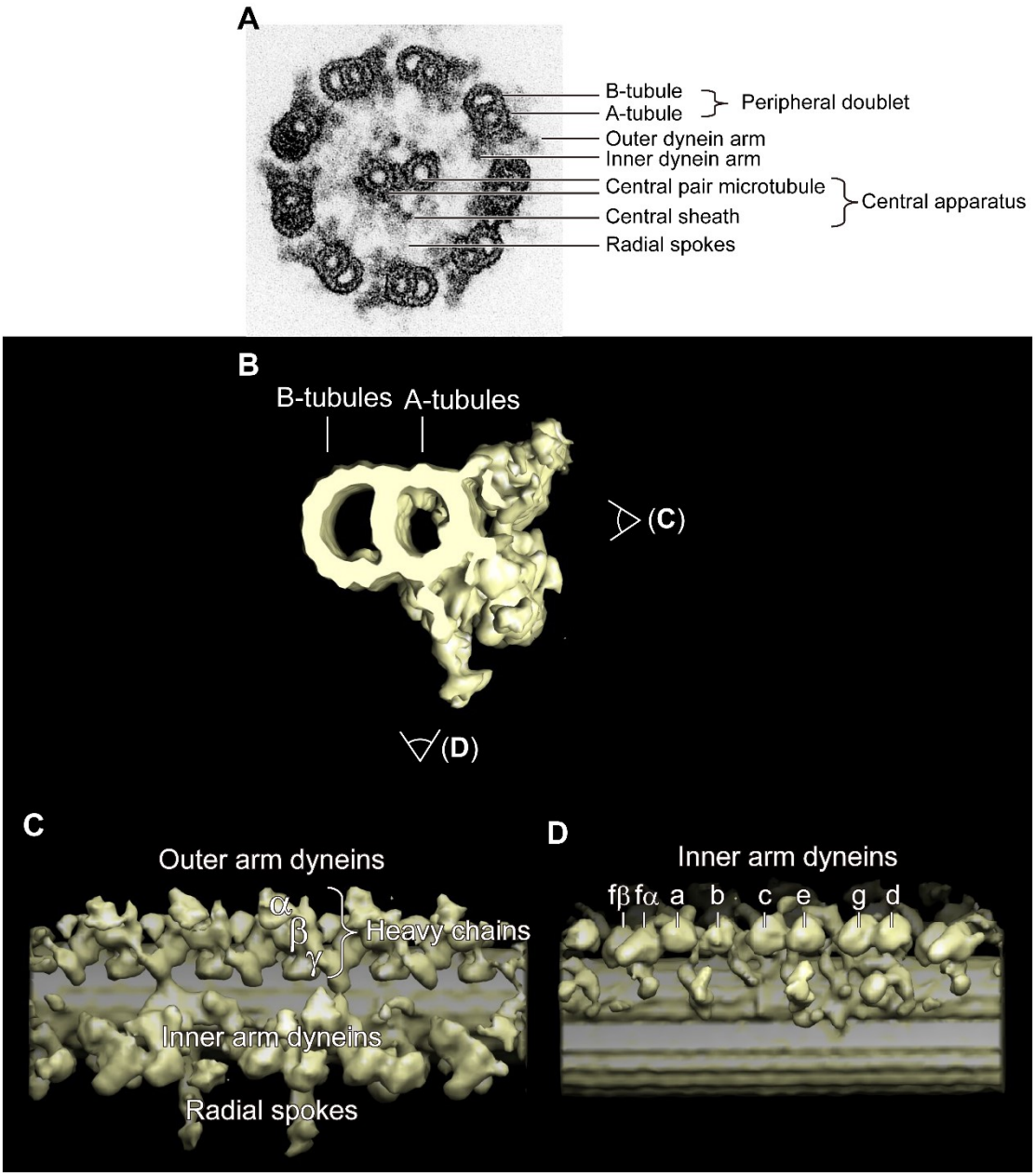

Figure 1.2 **Structure of axoneme and axonemal components**

Cross-section of a negatively stained axoneme (A) and cryo-electron tomogram of a DMT with axonemal components, represented by a surface rendering (B-D). (A) The scaffold of a eukaryotic flagellum is called an axoneme, and is composed of nine DMTs surrounding a pair of singlet microtubules (the central-pair microtubules). Axonemal components are arranged along the doublet and central pair microtubules. (B) The DMT is composed of a tubular A-tubule and a C-shaped B-tubule. Most axonemal components are attached to the A-tubule. Note that

some electron-dense materials are found on the inner wall of the DMT in both A- and B-tubules. These are known as microtubule inner proteins (MIPs). (C) The surface of the A-tubule viewed from the B-tubule of the adjacent doublet. Outer arm dyneins, inner arm dyneins, and radial spokes are arranged along DMTs with structural repeats, which are integral multiples of tubulin dimer structural repeat, 8 nm. In *Chlamydomonas*, the outer arm dyneins are composed of three heavy chains (HC): α–, β–, and γ–HC. Three ring-like motor domains of HCs are stacked like poker chips. (D) The surface of the A-tubule viewed from the central-pair microtubules. At least seven inner dynein subspecies (a to g) are found in a 96 nm-structural repeat. Only inner dynein arm f has two heavy chains (fα and fβ). In this tomogram, the structure of the radial spoke is not presented for clarity. Modified after Ishikawa (2012).

Bending of cilia/flagella is generated by shear between adjacent microtubules generated by dyneins **(Figure 1.3)**. Isolated dynein molecules showed various mechanical properties *in vitro*, such as a wide range of microtubule sliding velocities, variation of force generation, torque generation, various degree of processivity, and so on (Hirakawa et al., 2000; Kagami and Kamiya, 1992; Sakakibara et al., 1999; Sakakibara and Nakayama, 1998). Therefore, these inner and outer arm dyneins have such distinct motility that the coordination among these dyneins is considered to be essential for the systematic formation and propagation of flagellar bends.

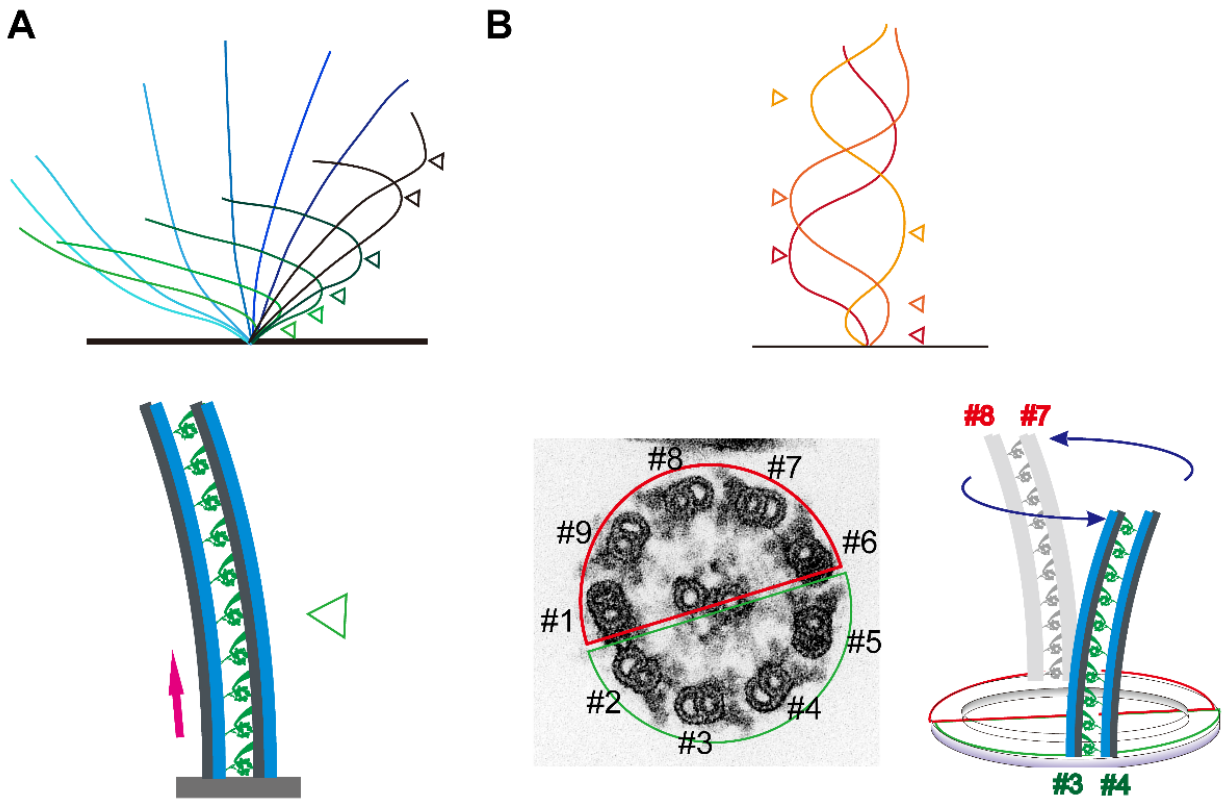

Figure 1.3 **Schematic view of beating mechanisms driven by dyneins**

(A) The sliding between a pair of DMTs driven by dyneins is converted into a bend when the pair of doublets cannot slide at the end of the pair because the microtubules are physically restrained. When the sliding occurs along a whole axoneme, the axoneme forms the effective stroke. When the localized bend is propagated from the base to the tip, the recovery stroke is formed. This mechanism forms the asymmetrical waveform. (B) Since the direction of microtubule active sliding generated by dyneins is unidirectional (base to tip direction), active bending by this sliding is also unidirectional. To generate alternate bending of the flagellum, antagonistic pairs of doublets are needed. In the axoneme, the sliding generated by the pair of doublets #3 and #4 is antagonistic to the sliding generated by the pair of doublets #7 and #8. Among these antagonistic pairs, dynein activity should be well controlled.

Previous theoretical studies suggested that the amount of sliding between adjacent doublets would be regulated temporally and spatially; as a result, a flagellar/ciliary wave is generated (Sugino and Naitoh, 1982). Since the demembranated axoneme maintains the ability to bend, the signal of this coordination in activity should be mechanical. Although several numerical models have been proposed, convincing experimental evidence has not been provided yet owing to the small size of the axonemes, which hampers direct mechanical measurements and manipulation. Therefore, details of the mechanisms of bend formation and propagation have remained unclear. To study the coordination and regulation mechanism of bend formation and propagation of a flagellum, we have used *Chlamydomonas.* The advantage is that it is possible to obtain a large repertoire of mutants showing impaired flagellar motility. Comparative studies of mutant motility and analysis of dyneins *in vitro* have shown each dynein differs greatly in properties (reviewed in Kamiya and Yagi (2014)).

Chlamydomonas flagella normally show an asymmetrical waveform called ciliary beating. When the cell is irradiated by strong light, it suddenly stops and changes its flagellar waveform from asymmetric to symmetric. This response is known as a photophobic reaction (**Figure 1.4**). This waveform change is known to be induced by increasing intracellular calcium ion concentrations (Kamiya and Witman, 1984).

In photophobic reactions of living cells, intense light irradiation causes rapid waveform changes in a moment by the influx of calcium ions. Within a few seconds after irradiation, the waveform returns to ciliary beating. This response is elicited within the flagella since flagellar axonemes isolated from cell bodies retain the ability to respond to changes in Ca^{2+} concentrations. Since demembranated axonemes also show waveform changes coupled with changes in Ca^{2+} concentrations, the signal transduction of this waveform change is mediated by neither membrane potentials nor diffusion of chemical substances (Bessen et al., 1980; Kamiya and Witman, 1984). Therefore, the mechanism in which the axoneme beats in such distinct waveforms using common axonemal structures is worth investigating.

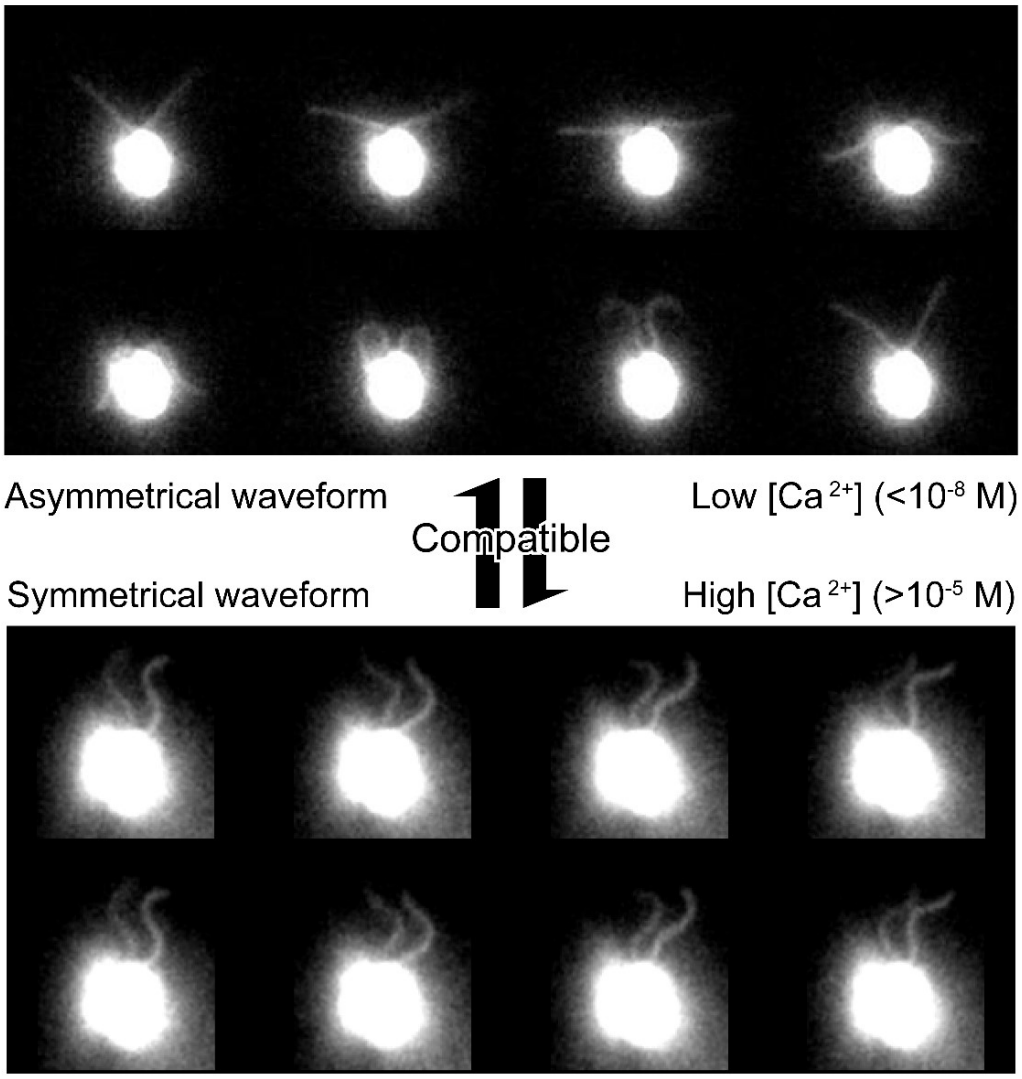

Figure 1.4 **Waveform changes of *Chlamydomonas* flagella in response to intracellular [Ca^{2+}]**

Chlamydomonas flagella normally show an asymmetrical waveform called a ciliary wave under low concentrations of intracellular Ca^{2+} ($<10^{-8}$ M). When *Chlamydomonas* is exposed to intense light, it suddenly changes its waveform to a symmetrical one (called a flagellar wave) with an influx of Ca^{2+} as a photophobic reaction. The threshold concentration of Ca^{2+} is 10^{-5} M.

To solve these unknown mechanisms, extensive theoretical modeling and numerical simulations have been performed. In some models, the amount of shear between doublets was the key to regulation of dynein activity. Active dynein-microtubule cross-bridges are formed and propagated through the axoneme during beating and the load-dependent dissociation of dynein arms from adjacent microtubules is a key regulation factor (Brokaw, 2002, 2014; Lesich et al., 2016; Lindemann, 1994; Riedel-Kruse et al., 2007; Sartori et al., 2016; Sugino and Naitoh, 1982).

In reductionist approaches, researchers dissect the axoneme into its components and characterize the properties of individual components. For instance, *in vitro* motility assays on inner arm dynein subspecies (a to g) have revealed their distinct motile properties (Kagami and Kamiya, 1992). The waveform analysis of mutant flagella is typically performed to investigate the function of components that are lacking in the mutant strain (Brokaw and Kamiya, 1987; Yanagisawa et al., 2014). However, there is less knowledge of the function of dyneins in the axoneme, since dyneins are arranged in arrays and their function is strictly regulated by three-dimensional constraints. To reveal the function of dyneins under structural constraint is important; therefore, using a reactivation system, I aim to identify the essentials for flagellar movement and Ca^{2+}-dependent regulators of waveforms. In this thesis, I report the (1) functional reconstitution of outer arm dyneins into ODA-lacking mutants, which raised the possibility of the existence of small molecules as Ca^{2+}-dependent regulators of waveform, and (2) characterization of putative Ca^{2+} binding protein (flagellar associated protein 85 (FAP85) found through the reconstitution assay). My research has revealed that FAP85 is a microtubule inner protein that potentially stabilizes MTs.

CHAPTER 2

In vitro reconstitution of flagellar waveform changes of *Chlamydomonas* coupled with intracellular calcium ion concentrations

2.1 ABSTRACT

The complexity of the flagellar axoneme is derived from 200-600 types of modular building blocks assembled hierarchically. Among axonemal building blocks, dyneins are indispensable for flagellar motility. They are precisely arranged along doublets and regulated in a coordinated fashion to produce periodic flagellar beating. This beating shows two typical waveforms: symmetric waveform called "flagellar beating," and asymmetric waveform called "ciliary beating." The *Chlamydomonas* flagella usually shows ciliary beating, but at a high intracellular Ca^{2+} level the waveform changes to flagellar beating. Although Ca^{2+} was proven to be the key to this waveform change, the molecular mechanisms are still unknown. Using flagella of *Chlamydomonas* as the model for flagellar motility, we carried out an *in vitro* reconstitution of axonemal structures in a bottom-up manner and compared the mechanical properties of reconstituted axonemes with those of intact ones. Here, we suggest the presence of a regulation factor that is associated with outer dynein arms (ODAs). The axonemes obtained from the outer-armless mutant *oda1* showed slow ciliary beating at low Ca^{2+}, but did not show switching to flagellar beating at high Ca^{2+} (pCa = 4-5). We reconstituted crude ODAs extracted with high salt from wild-type axonemes into *oda1* axonemes. This reconstitution recovers the frequency of the ciliary beating close to the frequency of wild type at low Ca^{2+} and shows waveform switching at high Ca^{2+}. However, when reconstituting ODAs purified by a gel filtration under the presence of high salt into *oda1* axonemes, we observed only ciliary beating with a hint of a reverse bend but not flagellar beating at high Ca^{2+}. These results suggest that there are regulatory factors attached to ODAs and switching the waveform according to Ca^{2+} concentrations. As the result of the peptide mass fingerprinting of some bands from the crude dynein extract, we identified the FAP85 protein, which was predicted to have an EF-hand motif that binds Ca^{2+} ions.

2.2 INTRODUCTION

2.2.1 Structure and force-generating mechanism of dyneins

2.2.1.1 Structural studies on dynein heavy chains

A dynein is a microtubule-based motor that moves on a microtubule toward its minus-end. This motor protein is an essential component for cilia/flagella motility and intracellular transport. Dyneins belong to the AAA+ protein superfamily (ATPases associated with diverse activities) and, like other AAA+ proteins, it has a ring of six AAA+ modules at its motor core. In contrast with conventional AAA+ proteins, six AAA+ modules are concatenated in a heavy chain (Ogura and Wilkinson, 2001). The heavy chain has a molecular mass of typically 500-540 kDa and consists of approximately 4500 amino acid residues. It contains a fundamental motor domain in the C-terminal 320-380 kDa fragment, incorporating sites for both ATP hydrolysis and microtubule binding. The motor domain is composed of six AAA+ modules each of 35-40 kDa (numbered from 1 to 6 from the N-terminus) and three appendages including the microtubule-binding stalk, the buttress/strut, and the linker (Carter, 2013).

The linker connects the AAA1 domain and the tail, and is normally docked onto the head ring. This linker is thought to deliver the power stroke. The tail is formed by the N-terminal one-third of the heavy chain and constitutes an extended structural domain, which mediates dimerization/trimerization of the heavy chains. This tail provides a scaffold for intermediate and light chains and fixes the dynein to the A-tubule of the doublet. The stalk emanating from AAA4 is composed of anti-parallel coiled-coil and the microtubule-binding domain (MTBD) lying at the tip of the coiled-coil. Near its base, the stalk interacts with the buttress/strut that emerges from AAA5 (Carter, 2013).

The crystallographic analyses of the motor domain of *Dictyostelium* dynein (Kon et al., 2012) and that of human dynein 2 (Schmidt et al., 2014) have provided evidence for the structural information pathway between AAA1 and MTBD since the crystal unit contains a whole stalk and two independent motor domains, which adopt different conformations (**Figure 2.1 A**).

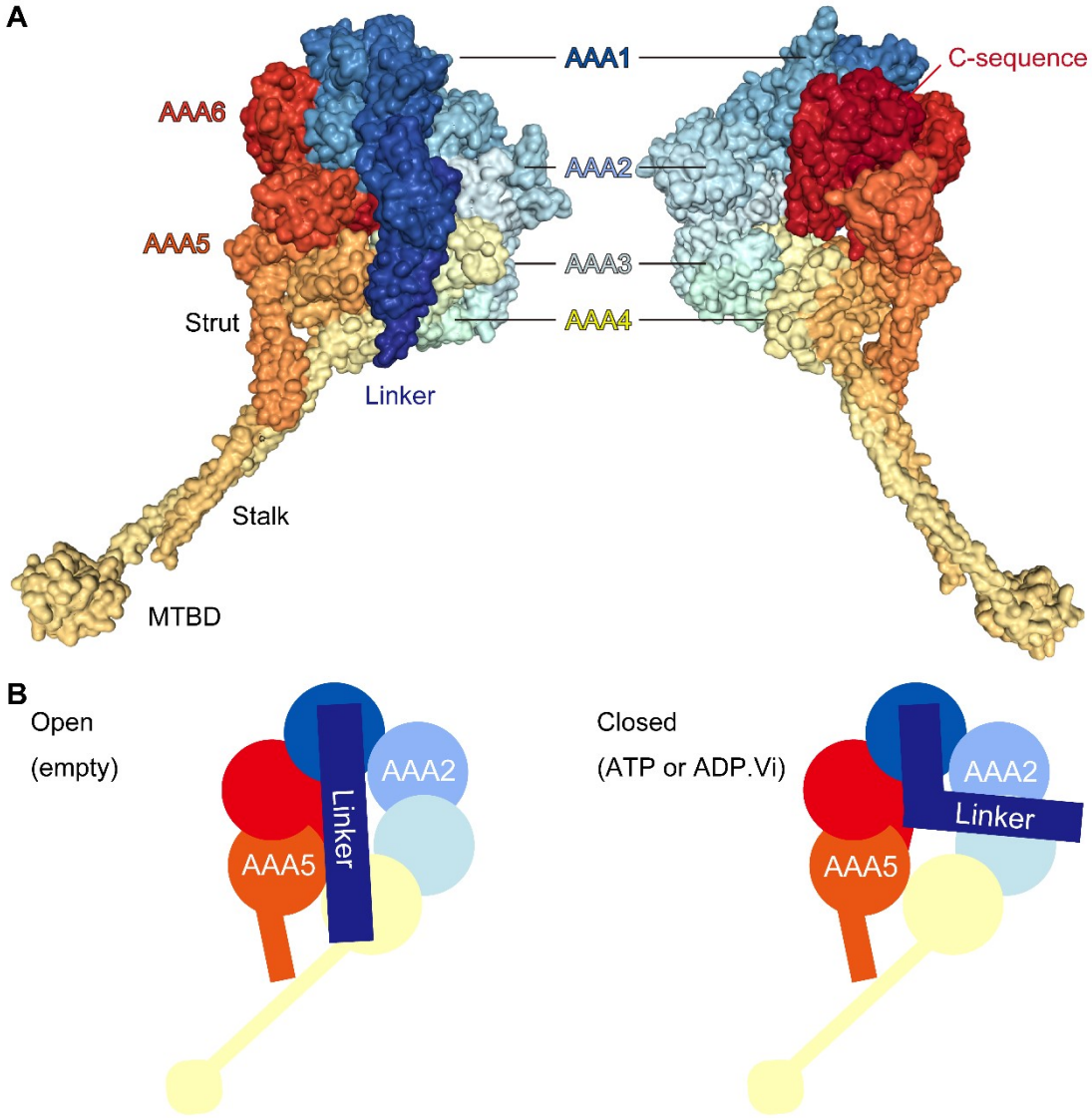

Figure 2.1 **Structure of a dynein**

(A) 3D model of the cytoplasmic dynein of full-length motor domain obtained from the Protein Data Bank (Protein Data Bank ID: 3VKH). (B) The linker bent towards AAA2 when AAA1 binds ATP or ADP-Vi. In the absence of nucleotides, the linker straightens to dock at AAA5.

In the AAA+ ring, four out of six modules (AAA1-AAA4) have functional nucleotide-binding motifs and can bind nucleotides. Previous studies indicate that the primary ATPase site is located at the AAA1, in which ATP is hydrolyzed for dynein motility (Kon et al., 2004). Other ATPase sites in the 2nd to 4th AAA+ modules play regulatory roles in dynein motility. AAA4 has an alpha-helical coiled-coil structure called the stalk (Carter et al., 2008). The carboxyl terminus of AAA5 has a second alpha-helical coiled-coil structure termed "buttress/strut" extending to the base of the stalk. *Dictyostelium* cytoplasmic dyneins have an additional structure following AAA6 named the "C-sequence" (Kon et al., 2012), which is not found in yeast cytoplasmic dyneins.

The linker is the mechanical element of conformational changes in the AAA+ domains (Burgess et al., 2003). Comparison of crystal structures of different nucleotide states suggests the mechanism of the power stroke of dyneins (Carter et al., 2011). The linker is kinked toward AAA2 when AAA1 binds to ATP or ADP-Vi. The release of the hydrolysis product, ADP, makes the linker straight and puts the linker toward the original position. This conformational change is a power stroke. Coupled with the release of inorganic phosphate, the linker straightens and docks on the position on AAA5 (**Figure 2.1 B**).

The stalk is an approximately 15-nm antiparallel coiled-coil formed by a pair of a-helices extending from AAA4 (Carter et al., 2008). The microtubule binding domain (MTBD) is located at the tip of the stalk and has a role in coupling between ATPase and track binding sites, which is essential for motors to move along a track. During the mechanochemical cycle of dynein activity, the two helices of the stalk change their registries. This relative sliding of the alpha-helices changes the conformation of the MTBD and changes its affinity to the microtubule. This is the mechanism that couples the ATPase at the AAA1 site and the microtubule binding activities of the MTBD (Schmidt and Carter, 2016).

The buttress/strut emerges from AAA5 and interacts with the stalk near its base. Kon et al. (2012) performed a functional analysis of a buttress/strut mutant lacking an interaction interface of the strut with the stalk. The mutant showed uncontrolled ATPase rate in the absence or presence of a

microtubule, which suggests the importance of stalk-strut interactions for allosteric communication.

The role of the C-terminal domain was examined by Kon et al. (2012). Their results suggested the H1 helix in the C-terminal domain forms a structural bridge between the AAA1 and AAA6, and the basal portion of the buttress/strut is also crucial for allosteric communication. This study suggested that the stalk, strut, and C-terminal domain are involved in the allosteric communication pathway between MTBD and the AAA1 ATPase site. However, the yeast cytoplasmic dynein does not have the C-terminal domain, but it moves processively on a microtubule. This result has raised questions about the role of the C-terminal domain.

2.2.1.2 Subunits of axonemal dyneins

As mentioned in the previous section, dyneins are classified into axonemal dyneins and cytoplasmic dyneins. From this section forward, I will focus on outer arm dyneins of axonemal dyneins, which is the main target of this thesis.

Axonemal dyneins have heteromeric heavy chains and multiple light and intermediate chains. Outer arm dyneins from most sources consist of two distinct heavy chains, whereas those from *Tetrahymena* and *Chlamydomonas* each contain three distinct heavy chains (Höök and Vallee, 2006). Biochemical and genetic studies on outer arm dyneins of *Chlamydomonas* have revealed that they are composed of distinct heavy chains (HC, α–, β–, and γ–), two intermediate chains of IC1 (IC78, 78 kDa) and IC2 (IC69, 69 kDa), and eleven light chains.

The functions of some light and intermediate chains have been studied; these subunits have been reported to have roles in the functional regulation of axonemal dyneins through Ca^{2+} binding (King and Patel-King, 1995), phosphorylation/dephosphorylation (Yang et al., 2009), and redox poise (Patel-King et al., 1996). The intermediate chains with WD-repeats are expected to be involved in the association of multiple dynein heavy chains. IC78 interacts with α-tubulin in an ATP-insensitive manner indicating that IC78 is involved in binding of outer arm dyneins to the A-tubule (King et al., 1991). The light chains have diverse functions, but most are reported to be related to dynein assembly or modulation of dynein motor activity (Inaba, 2012).

2.2.1.3 Force-generating mechanism of dynein

Quick-frozen deep-etch replica images of *Tetrahymena* and *Chlamydomonas* axonemes showed the compact configuration of outer arm dyneins in the absence of ATP and extended configuration in the presence of ATP-vanadate (Goodenough and Heuser, 1982). In their study, three-headed ODAs were not clearly recognized in electron micrograms because of the spatial resolution of this technique. Thus, the conformational change of the outer dynein arm was decided as conformational changes of whole outer arm. Detailed conformational changes of dynein molecules during force generation were revealed from an isolated axonemal dynein c by EM observations followed by image processing (Burgess et al., 2003). In the ADP-vanadate bound state, the stalk and the tail emerge from the head 10 nm apart; however, without nucleotides they emerge much closer together. Aligning the image of apo and ADP state dyneins by the position of their tail revealed the position of MTBD was moved by approximately 15 nm. These changes clearly indicated a mechanism of dynein power stroke. In the last decade, several models of force generation have been proposed on the basis of the conformational changes of dyneins observed by cryo-EM (Lin et al., 2014; Oda et al., 2007; Ueno et al., 2014; Ueno et al., 2008). However, dynamic properties of mechanosensitivity, conformational changes, and mechanochemical coupling still need to be elucidated.

2.2.1.4 Cooperativity of dynein activity

To evaluate motor protein function, an *in vitro* motility assay has been available since the 1980's. The assay is a system to observe translocation or sliding of filament proteins driven by motor protein bound to a glass surface (Spudich, 1994). In this assay, motor proteins have a random orientation on a glass surface such that sliding of the filament is driven by the force applied only from the motor protein oriented in the same direction as the filament slides. Furuta et al. (2009) conducted a systematic comparison of *in vitro* motile properties of outer arm dyneins using an *in vitro* motility assay. Even though this assay is a powerful tool for functional evaluation of each dynein HC, maximum sliding velocity of microtubule (5.0 μm/sec) was a quarter of the velocity based on microtubule sliding in the axoneme (Kurimoto and Kamiya, 1991 for the velocity of sliding in the

axoneme). Yamada et al. (1998) observed microtubules sliding on rows of dynein arms of sea urchin sperm axonemes exposed to elastase-induced disintegration. Dynein arms on the axoneme preferentially bound microtubules with the same polarity as the axoneme and generated a force to move only one direction with a microtubule sliding velocity of 3.1 ± 2.1 μm/sec (n = 53).

To elucidate why outer arm dynein behaves as a faster motor in the axoneme than in the *in vitro* motility assay, the motile behavior of tightly packed dyneins on the microtubules was examined. Extracted dyneins from *Chlamydomonas* and *Tetrahymena* axonemes bind to microtubules with 24-nm periodicity through their stalk and tail, and cross-bridge microtubules to form bundles (Haimo et al., 1979; Oda et al., 2007; Sakakibara and Nakayama, 1998). The addition of ATP dissociated and slid the dynein-MT bundles with a faster velocity than that of the *in vitro* motility assay; *Tetrahymena* ciliary dynein: ~12 μm/sec (Mimori and Miki-Nomura, 1994), *Chlamydomonas* outer arm dynein: ~30 μm/sec (Aoyama and Kamiya, 2010). These results suggested that higher efficiency could be generated by densely packed dyneins with the same polarity on the tracks.

2.2.1.5 Dynein-related Ca^{2+} binding proteins

Chlamydomonas usually swims with an asymmetrical waveform like the breaststroke, but when *Chlamydomonas* is exposed to intense light, the asymmetrical waveform changes into symmetrical waveform caused by an increase of intracellular Ca^{2+} concentrations (Kamiya and Witman, 1984). Several dynein subunits considered to be involved in waveform changing have been reported. LC4, one of the dynein subunits, directly interacts with γ-HC of *Chlamydomonas* outer arm dynein and alters a conformation of γ-HC in response to Ca^{2+}. EM observations showed that inflection angle between tail region and the motor domain became more flexible in the presence of Ca^{2+} than in the absence of Ca^{2+} (Sakato et al., 2007). In case of sea urchin sperm, calaxin binds to a heavy chain of the outer arm dynein and modulates flagella movement in response to Ca^{2+} (Mizuno et al., 2009; Mizuno et al., 2012). Since there is no mutant lacking LC4 and calaxin, it is unknown what type of phenotype will be induced by the deficiency of these subunits. Therefore, it is still not clear whether modulation of dyneins by these subunits is the mechanism of Ca^{2+}-dependent waveform formation

and switching. To reveal these mechanisms, it is necessary to determine whether modulation of dynein movement is a direct mechanism or another molecular mechanism.

2.2.2 Mechanism of bend formation and propagation of flagella

2.2.2.6 Bend formation and propagation

It has been demonstrated that locally applied ATP by iontophoresis to demembranated sea urchin sperm caused a local sliding between dynein and MTs, which was converted into the bend of both sides of the locally-activated region (Shingyoji et al., 1977) (**Figure 2.2 A**). This phenomenon is thought to be the principle of the bend formation. However, the mechanisms producing oscillatory bending and propagation of bending are unclear. Reconstitution experiments may provide clues to these mechanisms. For instance, Aoyama and Kamiya (2005) showed that a pair of outer doublets can undergo cyclical association/dissociation interactions using spontaneously frayed axonemes. This study proposed the following model of propagation of bending: if the separation of two DMTs was restricted by some elastic links, the sliding force between the two DMTs disrupted the proximal dynein-microtubule cross-bridges and simultaneously produced the sliding in the distal portion of the pair (**Figure 2.2 B**).

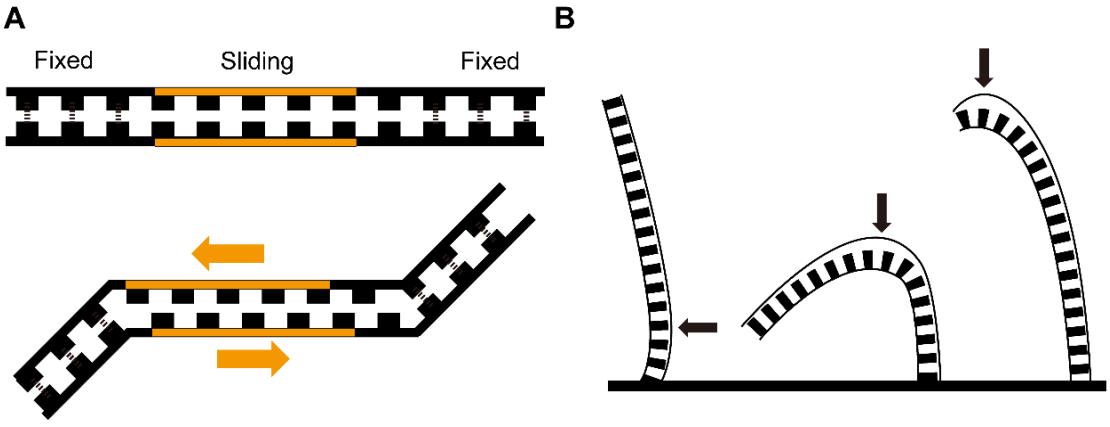

Figure 2.2 **Bend formation in the axoneme**

(A) When sliding locally occurs where both ends are fixed, the sliding is converted into bends. (B) A pair of outer doublets undergo cyclical association/dissociation interaction of dyneins. Dyneins are load-dependently dissociated with the adjacent microtubule by the curvature of bending (indicated by arrows) whereas dyneins on the base side associate with the microtubule and slide it. The association/dissociation interaction propagating from the base to the tip with spatiotemporal regulation results in cyclical bending.

To form a symmetric waveform with bends on both sides, it is necessary to switch active sides where dyneins slide MTs. Previous studies suggest switching active sides is induced by flagellar bending itself (Morita and Shingyoji, 2004; Nakano et al., 2003). This study showed certain dynein arms between DMTs alternate active and inactive in response to experimentally induced bending **(Figure 2.3)**. Although this study raised the possibility of mechanical feedback of dyneins, a detailed mechanism of oscillatory bending remains to be elucidated.

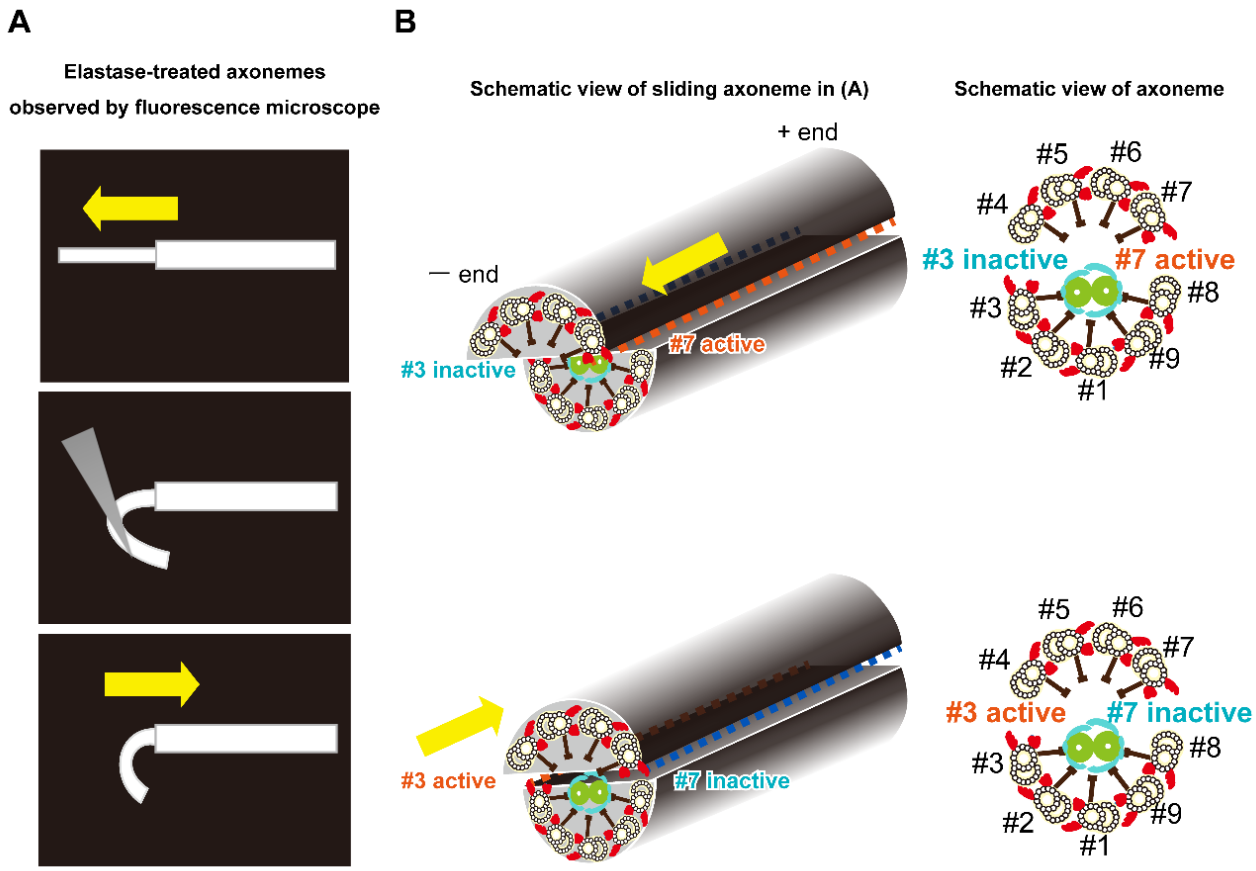

Figure 2.3 **Selective activation of dynein arms by induced bending**

Morita and Shingyoji (2004) suggested that switching active sides is induced by flagellar bending itself. (A) Experimental procedures of elastase-treated axonemes observed by a fluorescence microscope are shown in the figure. A part of the axoneme partly protruded from the elastase-treated axoneme by the addition of small amount of ATP (upper panel). When the part was bent by a glass microneedle (middle panel of (A)), the extruded part slid back into the rest of the axoneme. (B) Schematic views indicating active/inactive dyneins of an elastase-treated axoneme corresponding to the panel in (A).

2.2.3 Self-assembly of axonemal components in vitro

2.2.3.7 Outer arm dynein-docking complex (ODA-DC)

Outer arm dyneins are aligned with 24-nm periodicity on the A-tubule of the DMT. Outer dynein arm-docking complexes (ODA-DCs) periodically bind to microtubules, and provide footholds for ODAs and enable outer arm dyneins to align spontaneously onto MTs (Owa et al., 2014). Although the ODAs themselves can form a regular array with 24-nm periodicity owing to the physical size of the ODA, a recent study showed that DCs strengthen the electrostatic interactions between the ODA and DMT (Oda et al., 2016) and stabilize their interactions.

2.2.3.8 Reconstitution of dynein arms

Haimo et al. (1979) showed that the outer dynein arms bind to microtubules in a cooperative manner. Functional recombination of outer dynein arms with the flagellar axonemes of a mutant lacking outer arms was carried out by Sakakibara and Kamiya (1989). They showed the beating frequency of axonemes was restored by this reconstitution. Smith and Sale (1992b) studied the reconstitution of inner-arm dyneins. Since the dynein arms were re-assembled at correct sites along DMTs in a self-organizing manner, these studies suggest the possibility of reconstituting axonemes in a bottom-up manner with using characterized components.

In contrast, the change in flagellar waveform in response to Ca^{2+} change has not been reported in reconstitution experiments. Poor response to the increase in Ca^{2+} in *Chlamydomonas* mutants lacking outer arm dyneins (Brokaw and Kamiya, 1987) suggests that Ca^{2+} responses are related to the function of outer dynein arms and introduces the possibility of building an assay system for unknown Ca^{2+}- dependent regulatory proteins.

2.3 MATERIALS AND METHODS

2.3.1 Strains

The following two *Chlamydomonas reinhardtii* strains were used: 137c (wild type) and the *oda1* (lacking outer arm dynein).

2.3.2 Preparation of crude dynein extract

Crude dynein extract was obtained according to the method of Witman et al. (1978) with some modifications. *Chlamydomonas reinhardtii* wild type strain (137c mt-) was cultured in 1.2 liter liquid TAP medium under continuous illumination at 20℃ for 4 days with air bubbling. Cells were harvested by centrifugation at 1692 × g (3000 rpm, R10A3 rotor, Himac CR22E) for 6 min, suspended in 40 ml ice-cold HMDS (30 mM HEPES-NaOH, 5 mM $MgSO_4$, 1 mM Dithiothreitol [DTT], 4% Sucrose, pH 7.4) at room temperature. All procedures below were done at 4℃ or on ice unless otherwise stated. The cell suspension was moved to a 50-ml conical centrifuge tube and 1 ml of 100 mM dibucaine HCl (Wako) was added. The suspension was pipetted rapidly in and out of 10-ml Falcon disposable plastic pipettes for 30 sec, then 200 μl of 100 mM EGTA was added and the solution was gently pipetted several times. The cell bodies were removed by centrifugation 1670 × g (3000 rpm, RS-4 rotor, KUBOTA6800) for 6 min, the supernatant was transferred to a new 50-ml conical centrifuge tube and recentrifuged as above. The cell-free supernatant was centrifuged 27720 × g (15,000 rpm, RSR20-2 rotor Himac CR21) for 12 min. The resulting pellet was suspended by 1.5 ml of HMDEK (30 mM HEPES-NaOH, 5 mM $MgSO_4$, 1 mM dithiothreitol [DTT], 1 mM EGTA, 50 mM K-Acetate, pH 7.4) and demembranated by adding 15 μl of 20% Nonidet P-40 (NP-40, Nacalai Tesque). After 5 min, the suspension was centrifuged 21130 × g (15,000 rpm, FA-45-24-11 rotor, Eppendorf 5452R) for 5 min, and resuspended in 1.5 ml HMDEK, this procedure was done again to remove detergent. Axonemes were collected by centrifugation as described above. The pellet was re-suspended with 100 μl of high salt-concentration HMDE (0.6M KCl, 30 mM HEPES-NaOH, 5 mM $MgSO_4$, 1 mM

DTT, 1 mM EGTA) and centrifuged at 21130 ×g (15,000 rpm, FA-45-24-11 rotor, Eppendorf 5452R) for 8 min. The resultant supernatant containing dyneins was collected to a new 0.5-ml Eppendorf tube and the pellet was re-suspended and recentrifuged as described above. Finally, a total of 200 μl of supernatant was collected, referred to as crude dynein extract. The supernatant was desalted by a gel filtration column (Sephadex G-25, GE Healthcare) or dialyzed against HMDEK overnight.

2.3.3 Gel filtration of the crude extract

Putative regulatory proteins were isolated from crude dynein extract with a gel filtration column (Superose 6, GE Healthcare). For the gel filtration, the elution of the proteins was carried out under a high salt condition (0.6 M KCl in HMDE, a flow rate 0.4 ml/min) and a low-salt condition (HMDEK, a flow rate 0.4 ml/min). The elution was fractionated into several fractions.

2.3.4 Reactivation of demembranated axonemes

Axonemes were prepared originally following by the method of Sakakibara and Kamiya (1989) with some modifications. Fifty milliliters of the *oda1* cells (outer armless mutant) in liquid TAP medium were centrifuged 417 × g (1500 rpm, RS-4 rotor, KUBOTA6800) at 20℃ for 6 min, and the pellet was re-suspended in 25 ml S/E solution (1 mM EGTA, 4% Sucrose). The suspension was re-centrifuged as above. The cells were suspended by 1 ml of 0.5% NP-40 in HMDEKP (30 mM HEPES-NaOH, 5 mM $MgSO_4$, 1 mM dithiothreitol [DTT], 1 mM EGTA, 25 mM potassium acetate, 0.5% polyethylene glycol (Mr = 20,000), pH 7.4), the cells were demembranated and some flagella were detached from the cell body during the demembranation. Sakakibara and Kamiya (1989) used this suspension containing cells with flagella as a cell model. In this study, the suspension was centrifuged at 2347 × g (5000 rpm, FA-45-24-11 rotor, Eppendorf 5452R) for 2 min 30 sec, and axonemes were collected for the experiments. Although the total amount of axonemes was smaller than those obtained with the original method, the axonemes were free from the dibucaine shock. These axonemes were

incubated over 60 min with crude dynein extract (final concentration was 100 μg/ml) on ice to reconstruct dyneins into the outer armless axonemes. For evaluating the activity of the gel filtration fractions, equimolar of these fractions were added to the extract. The reconstructed axonemes were mixed with a large volume (>10 times the volume of the axonemes) of 1 mM ATP HMDEKP solution with various Ca^{2+} concentrations calculated by the program "Calcon" (Goldstein, 1979). The reconstituted axonemes were reactivated with Mg-ATP, introduced into a flow chamber, and observed at room temperature with a dark-field microscope (BX-51, Olympus). Movement of the axonemes was recorded with a high speed digital camera (IPX-VGA210-LMCN, IMPERX) at the frame rate of 400 Hz.

2.3.5 Analysis of waveforms of demembranated axonemes

Despite of fast beating of axonemes, the difference in waveforms can be distinguished without detailed analysis when the beating was taken as movies with a high-speed camera. Two types of symmetric waveform and one asymmetric waveform were defined from the observation with a high-speed camera. Even visually, the difference in the curvature of bending of the axonemes was apparent. In some cases where the difference in curvature was too small to be distinguished by sight, the curvature was analyzed using the software Bohboh (Medialand Works, Tokyo, Japan). Images of each axoneme were cropped from the movies of each experiment, and their curvatures were calculated using the method of Baba and Mogami (1985). We followed the procedures of Mizuno et al. (2012). The maximum curvatures of the principal bend (P-bend) and the reverse bend (R-bend) at 5 μm from the base were termed P-$bend_5$ and R-$bend_5$, respectively, and were used to calculate the symmetric index (the ratio of P-$bend_5$ to R-$bend_5$ [P-$bend_5$ / R-$bend_5$]).

2.3.6 Identification of axonemal protein components

Fractions of the gel filtration under high salt conditions were applied to the sodium dodecyl sulfate-

polyacrylamide gel (5-20%) for electrophoresis (SDS-PAGE). Protein bands of interest were excised individually from the gel and sent to Cosmo Bio for MALDI-TOF mass spectrometry. According to the company procedures, the peptides digested by trypsin in the gel were subjected to MALDI-TOF mass spectrometry and FAP85 was identified by PMF analysis (Peptide Mass Fingerprint analysis) using the Mascot search algorithm (http://www.matrixscience.com/).

2.4 RESULTS

2.4.1 Reactivation of mutant axonemes

I carried out the reactivation of demembranated flagellar axonemes of *Chlamydomonas* at the different concentrations of Ca^{2+}. When the wild-type axonemes were reactivated, the reactivation rate was kept within 40% of the wide range of Ca^{2+} concentrations. The ciliary-type beating (asymmetric wave) was observed at low Ca^{2+} concentrations (pCa > 5), while the flagellar-type beating (symmetric wave) was observed at high Ca^{2+} concentrations (pCa ≤ 5) (**Figure 2.4 A**). On the other hand, *oda1* axonemes seem to lose the ability to form a symmetrical wave, i.e. flagellar beating, even in the presence of high Ca^{2+} (pCa < 6) (**Figure 2.4 B**). It has been reported that *oda1* cells can swim only forward by beating flagella with a weak asymmetric waveform but stop swimming when exposed to intense light (Kamiya and Okamoto, 1985). Our data showed the loss of Ca^{2+}-reaction found in *oda1* is derived from the loss of outer arms and/or some factors from the axonemes.

To examine the presence of the missing factors, I used high-salt extract from the *wt* axonemes. Addition of the crude dynein extract of *wt* axonemes desalted by a Sephadex G-25 gel filtration column to *oda1* axonemes restores the beat frequency to the level of the wild type. However, instead of flagellar beating, the axonemes beat in ciliary waveform, even in the presence of high Ca^{2+} (**Figure 2.4 C**).

From these preliminary results, I hypothesized that some factors necessary for the restoration of flagellar beating were lost during preparation of the crude dynein extract. I thought that if I could recombine them properly to *oda1* axonemes, as well as ODAs, symmetric flagellar-type waveform would be restored. Thus, I focused on proteins or peptides with small molecular weights, which were easily lost during the preparation of the crude dynein extract.

To prevent loss of factors during the preparation, the crude high-salt extract was dialyzed with the dialysis membrane with the pore size of MWCO = 0.1-0.5 kDa (Biotech CE). The dialyzed crude extract was used in the reactivation assay as described above. As a result, the addition of the crude

extract restored the asymmetrical waveform under low [Ca^{2+}] (pCa = 8) as well as the symmetrical waveform under high [Ca^{2+}] (pCa = 4). Although the number of experiments performed was so small that we could not assess these data statistically, the results may suggest that some factors with small molecular weights missing in *oda1* are involved in beating with the symmetrical waveform. In addition, utilizing this assay system for evaluating the regulatory factors makes it possible to identify the missing factors from the crude extract.

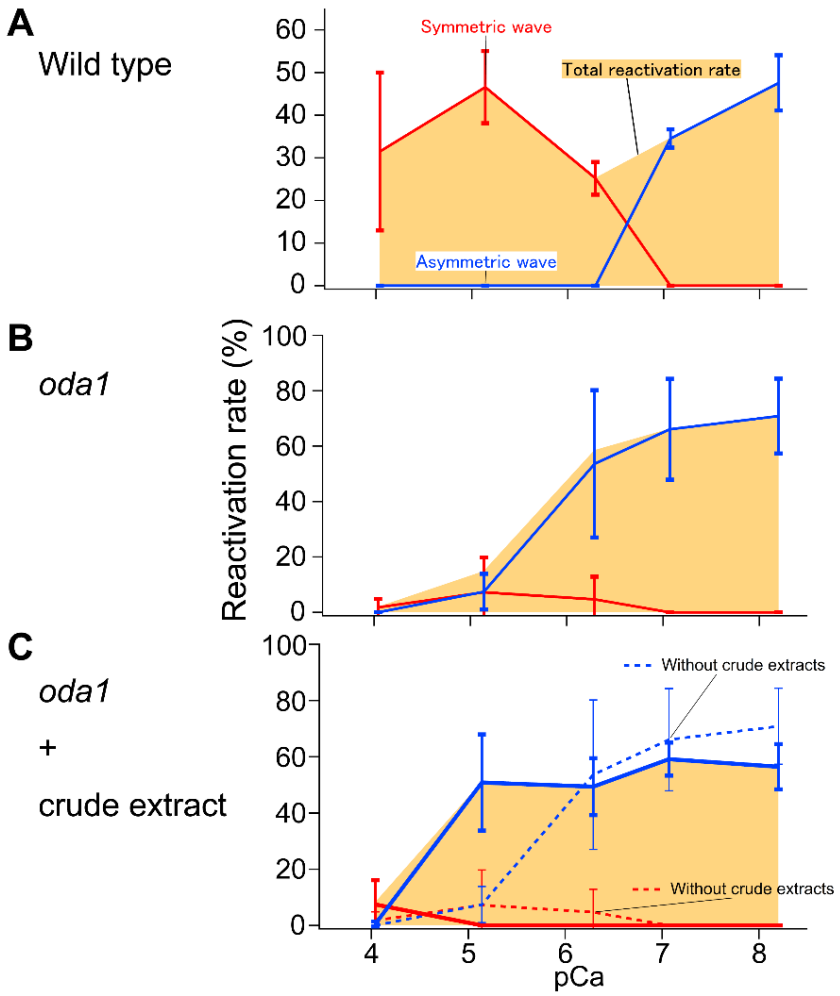

Figure 2.4 **Reactivation rate and ratio of two waveforms of axonemes**

Reactivation rates and the ratio of two waveforms of axonemes obtained from wild type (A), *oda1* (B), and *oda1* treated with crude dynein extract (C). Isolated axonemes from cells are demembranated and reactivated by the addition of ATP. They showed beating with two types of waveforms in a Ca^{2+} dependent manner. (A) Wild type (wt) axonemes beat symmetrically at high Ca^{2+} concentrations, and asymmetrically at low Ca^{2+} concentrations. (B) The outer dynein armless mutant *oda1* axonemes were not able to beat symmetrically, but could asymmetrically at low Ca^{2+} concentrations. (C) After incubating *oda1* axonemes with crude dynein extract (final 90 µg/ml), they showed asymmetric waveform at pCa 5, in which *wt* axonemes beat symmetrically. The dotted line indicates the reactivation rate of *oda1* axonemes shown in (B). The abscissa represents free-Ca^{2+} concentration and the ordinate represents the reactivation rate (the number of reactivated axonemes per the total number of axonemes observed). Error bars represent the standard errors (n = 3).

2.4.2 Analysis of waveforms

To quantify the symmetry of the waveform, I analyzed the waveform of reactivated axonemes with a high-speed camera at the frame rate of 400 Hz (**Figure 2.5**). Images of the waveforms were digitized into the software named Bohboh (Baba and Mogami, 1985). Curvature of the axoneme swimming trajectory was determined by flagellar asymmetry. Flagellar bending consists of a successive and alternating principal-bend (P-bend) and reverse-bend (R-bend). The P-bend is defined as the bend showing the same curve as the swimming circle, while the R-bend is the bend opposite to the P-bend. When those two bends have equal amplitude, axoneme shows a symmetrical waveform. (**Figure 2.5 A**). The image of an axoneme was traced and the curvature along the axoneme was calculated as a function of the distance from the base of the axoneme (**Figure 2.5 B**). The symmetric index was defined as the ratio of absolute values of P-bend$_5$ and R-bend$_5$ (**Figure 2.5 C**). The more symmetric the waveform is, the closer the symmetric index is to unity. This analysis was required since it was difficult to distinguish how symmetric the waveform was. In other cases, the waveform was distinguished visually.

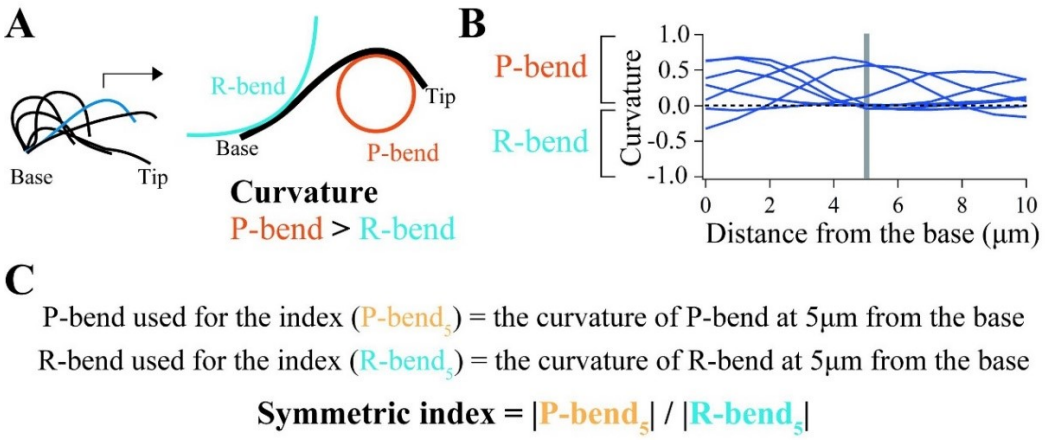

Figure 2.5 **Definition of the parameter for evaluation of symmetry.**

(A, B) The two directions of bending were defined as the principal bend (P-bend) and the reverse bend (R-bend). The curvature of the P-bend is larger than that of the R-bend. (C) The curvatures used for the calculation were 5 μm from the base, which were described as P-bend$_5$ and R-bend$_5$. The symmetric index was the ratio of absolute values of P-bend$_5$ and R-bend$_5$. The more symmetry the waveform has, the closer the symmetric index is to unity.

To evaluate the effects of putative regulatory factors, I first classified the waveforms into three categories: asymmetric waveform, symmetric waveform with a small bias, and symmetric waveform (**Figure 2.6**). The typical asymmetric waveform of wild type reactivated axonemes at low Ca^{2+} concentrations shows a symmetric index larger than unity (**Figure 2.6 A**). In the case of the symmetric waveform with a small bias, the symmetric index calculated at the middle (contour length s = 5 μm) of the axoneme was close to unity. However, at the base of the axoneme, the curvature of P-bend was slightly larger than the R-bend, and at the tip of the axoneme it was reversed (**Figure 2.6 B**). The symmetric waveform was observed only in wild type axonemes (**Figure 2.6 C**). The symmetric waveform with a small bias was often observed in reconstituted *oda1* axonemes in which dynein arms were reconstituted from the crude dynein extract desalted by Sephadex G-25. Since the beat frequency of the reconstituted axonemes recovers to the wild-type level, we considered the symmetric waveform with a slight bias is derived, not from the incompleteness of dynein arm reconstitution, but from missing factors for making the symmetric waveform.

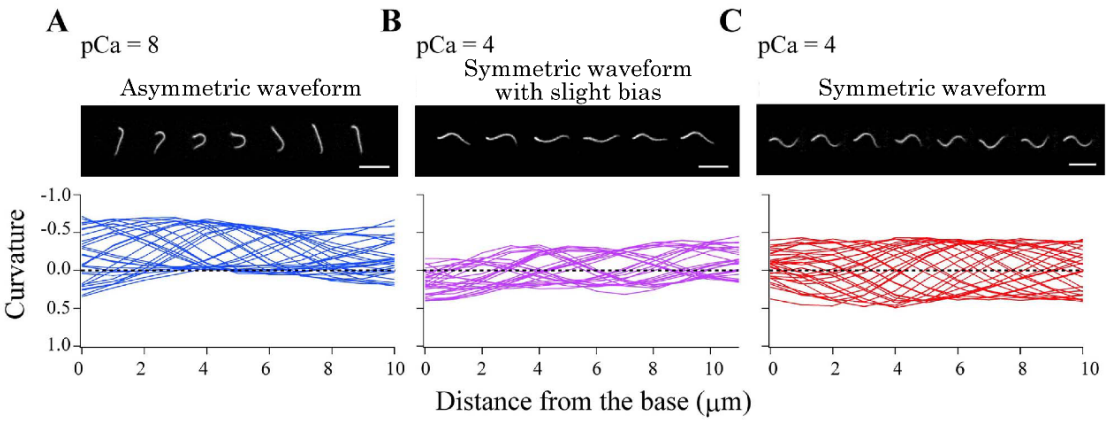

Figure 2.6 **The curvature analysis of waveforms using the software Bohboh**

(A) The typical asymmetric wave of a wild type reactivated axoneme shows highly biased curvature in low Ca^{2+} concentration buffer. (B, C) The symmetric wave was observed in high Ca^{2+} concentration buffer. (B) Symmetric index was close to unity, but the base and the tip of the axoneme were slightly asymmetric. This type was observed in some cases of reactivation axonemes and defined as a symmetric wave. (C) The totally symmetric wave was observed in wild type axonemes and rarely in reactivation axonemes. The time difference of each image is 2.5 msec. Scale bar, 10 μm.

2.4.3 Separation of regulatory factors with gel filtrations under low and high salt conditions

To obtain the putative regulation factors, we carried out a gel filtration column (Superose 6) under low and high salt conditions, followed by a reconstitution and reactivation assay to check for a restoring function of the fractions (**Figure 2.7**). In the case of low salt conditions, elution was divided into seven fractions based on expected MW to obtain OADs and low MW proteins (**Figure 2.7 A**). As a result of the reactivation assay, No. 1 and 2 fractions could restore both asymmetrical and symmetrical waveforms. These fractions were expected to contain OADs, which have ~2000 kDa of three HC because the MW of No.1 and 2 contents were estimated over 670 kDa by molecular weight markers. Furthermore, the addition of the fractions to the G-25 desalted extract could restore both waveforms (**Figure 2.7 B**).

To find regulatory factors, the fractions of gel filtration under high salt conditions were incubated with G-25 desalted extract and evaluated by a reactivation assay (**Figure 2.7 C**). As the result, No. 4, 5, 6, and 7 fractions, which have molecular weights of dozens of kDa, could restore a symmetrical waveform as under low salt conditions (**Figure 2.7 D**). These experiments under high and low salt conditions provide existence of regulatory factors that can attach to OADs and are reconstituted to *oda1* axonemes accompanied with OADs. Because the number of examinations has not been sufficient, the quantitative data cannot be shown here. Additional experiments are needed to confirm the effects of each fraction on the waveforms.

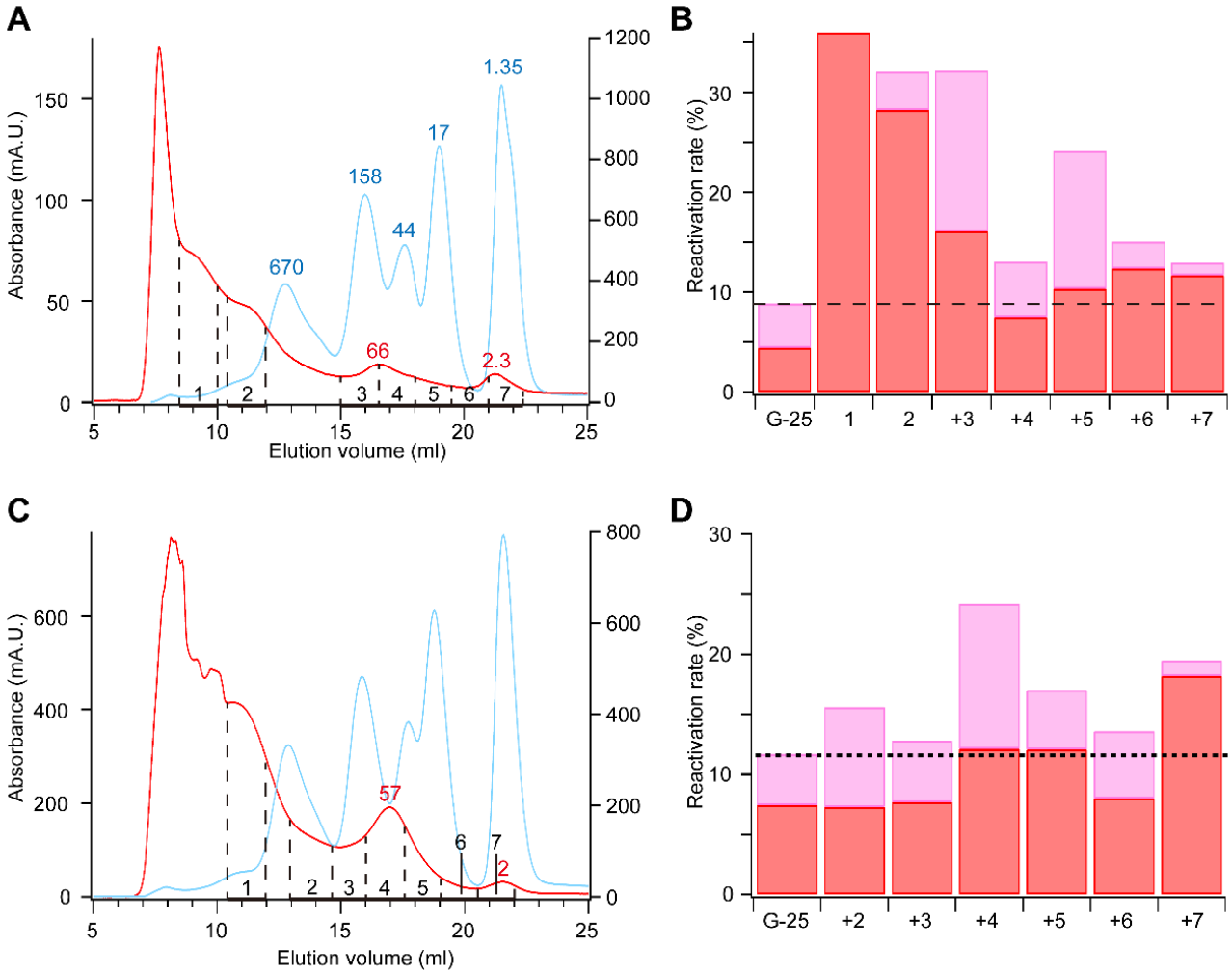

Figure 2.7 **Gel filtration under low and high salt conditions**

Elution patterns of the crude dynein extract under a low salt condition (A) and high salt condition (C) (red curves: crude extract, blue curves: gel filtration standard). The blue characters and red characters indicate the molecular weight of the standard and estimated molecular weight from the standard, respectively. The fractions are numbered 1-7 and written in black. The reactivation rate of symmetrical waveform (red) and symmetrical waveform with bias (purple) is indicated in the bar graph (B: low salt condition, D: high salt condition). (A) Elution was divided into seven fractions. No. 1 and 2 were individually used for the reactivation assay, and No. 3-7 containing dozens of kDa proteins were used with G-25 desalted extract for the assay. (B) The desalting extract by G-25 reactivated less than 10% of demembranated axonemes. However, the fractions No.1 and 2 reactivated them over 30% of the axonemes. The addition of the fractions to the G-25 desalted extract could restore both waveforms. (C) Fractions of No. 2-7 containing proteins of dozens of kDa were used for the experiments as a mixture with the G-25 extract. (D) No. 4, 5, and 7 fractions could restore both waveforms.

2.4.4 Identification of putative regulatory factors by MALDI-TOF-MASS

To analyze contents of fractions, each fraction underwent SDS-PAGE followed by silver-staining (**Figure 2.8 A**). We chose a few well-isolated and intensely stained bands in a small molecular weight region (approximately 10 kDa to 50 kDa) analyzed with MALDI-TOF-MASS. (**Figure 2.8 B**). One of these bands was identified as the novel flagellar associated protein predicted to have an EF-hand motif. This protein was expressed from the gene *FAP85* and was specific for *Chlamydomonas* and its relatives. Since *Chlamydomonas* shows characteristic waveform changes in response to Ca^{2+}, we focused on FAP85. Details are described in Chapter 3.

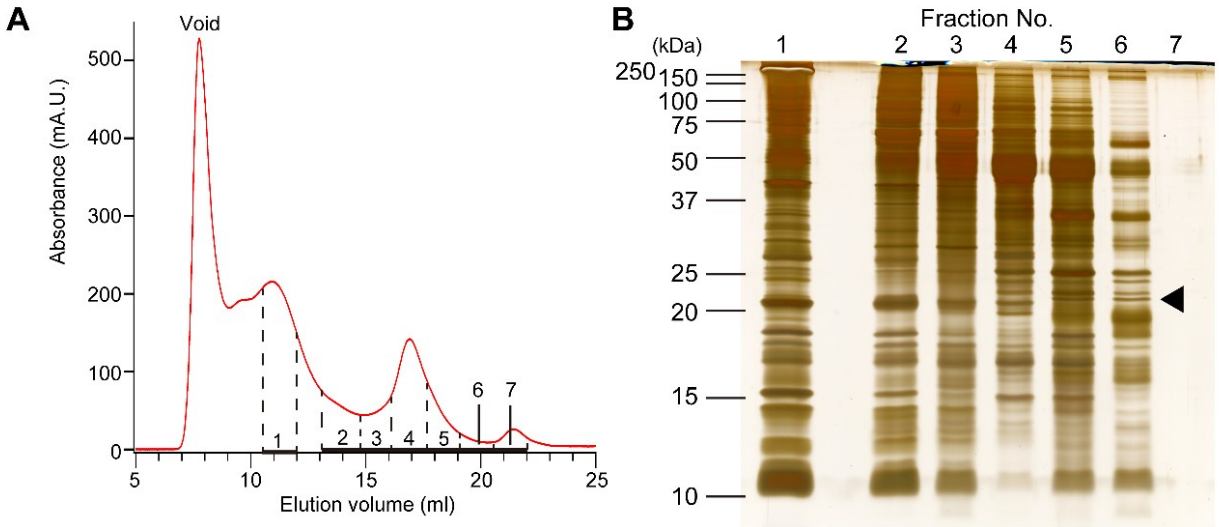

Figure 2.8 **Separation of the crude dynein extract by gel chromatography**

(A) Elution pattern of the crude dynein extract under high salt conditions. Each fraction volume was 0.5 ml, and some were divided into seven fractions. The first peak was regarded as the void region. (B) SDS-PAGE patterns of each collected fraction were analyzed and stained with silver. The gel contained 15% polyacrylamide. An arrow head indicates the band of FAP85, which was excised and used for the MALDI-TOF-MASS.

2.5 DISCUSSION

In this chapter, we demonstrated the possible presence of regulatory factors that are needed to form a symmetrical waveform, in addition to the ODA. The wild type axoneme showed a switching waveform in response to changes in Ca^{2+} concentration. On the other hand, the *oda1* axonemes, ODAs that were reconstituted with G-25 desalted extracts restored only beating frequency with the asymmetrical waveform. However, dialyzed crude extract prepared with a small pour size membrane restored both asymmetrical and symmetrical waveforms of *oda1* mutant axonemes. Thus, we hypothesized that some factors were required in addition to the ODA to form a symmetrical waveform and they was lost during the desalting procedure by G-25.

It is thought that the putative regulatory factors were normally bound to the ODA because restoring the symmetrical waveform was observed in the ODA fraction in gel filtration under low salt conditions. Additionally, other fractions including dozens of kDa proteins incubated with G-25 desalted extract could restore the symmetrical waveform. Furthermore, under high salt conditions, addition of the fractions could restore the symmetrical waveform as with the fractions under low salt conditions. These results suggested the existence of regulatory factors of the symmetrical waveform interacting with ODA.

In this system, it has been shown that the OADs are functionally and structurally reconstituted in the axonemes (Sakakibara and Kamiya, 1989); however, whether they bind to MTs appropriately to generate the symmetrical waveform is unclear. Although the outer arm dynein-docking complex (ODA-DC) is required for periodical binding of ODA onto MTs, Oda et al. (2016) revealed that ODA can bind to MTs with 24-nm periodicity without ODA-DC due to its steric hindrance. The absence of ODA-DC resulted in ODA releasing from MTs at relatively low ionic strength conditions. This suggested that ODA-DC strengthens electrostatic interactions between the ODA and MT. To form a symmetrical waveform, it may be necessary to localize these accessory proteins with the presence of regulatory factors.

2.6 FUTURE DIRECTIONS

With the knowledge accumulated through the experiments described above, flagellar beating could be reconstituted with minimal components. Detailed observations will give us insights on the mechanisms and regulators of waveform change. However, it is too complicated to use an intact flagellum for specification of these components because a flagellum is composed of 200-600 types of proteins. On the other hand, a reconstitution system is made using a small number of well-characterized axonemal components, such as microtubules and dyneins, and some regulatory components. In addition, utilizing the self-organization of axonemal components is vital. For example, I conducted some preliminary studies on a reconstitution system where dynein-docking complexes (DC) were extracted from axonemes and mixed with microtubules. They periodically bind onto microtubules as a foothold for ODAs and enable OADs to align spontaneously onto microtubules. Furthermore, utilizing nanometer-scale processing techniques and surface modification techniques are useful for accuracy in this system. Once a reconstitution system is established, it will help identify the essentials and parameters of periodic movement and verify theoretical models.

We now reach the stage of an integrated science approach including life science, physics, and engineering. Establishment of the synthetic approach leads to identification of the minimum elements in the higher-order structure, especially unknown regulators. This also can contribute to an investigation of ciliopathy. Furthermore, autonomous movement can be sufficiently developed as a micro-machine. In this way, the synthetic biological method greatly contributes to the basic study of flagella movement mechanisms that remain unclear. This is a big challenge, but this could be achieved.

CHAPTER 3

Flagellar-associated protein FAP85 is a microtubule inner protein that potentially stabilizes DMTs

3.1 ABSTRACT

Genomics and proteomics studies in *Chlamydomonas* have revealed that an axoneme is composed of 200-600 types of proteins, including uncharacterized proteins collectively named flagellar-associated proteins (FAPs). Nine FAPs contain the EF-hand motif; however, they have not yet been well characterized. To find components responsible for *Chlamydomonas*-specific waveform changes coupled with intracellular Ca^{2+} concentrations, we focused on FAP85, an EF-hand motif-containing FAP specific to *Chlamydomonas* and its relatives. We cloned the cDNA encoding FAP85, expressed it in *Escherichia coli* cells, and generated a polyclonal antibody against the recombinant protein. Immunoblotting showed that FAP85 was present in every axoneme of several flagellar mutants lacking major axonemal components. Immuno-electron microscopy revealed that anti-FAP85 antibodies were found only on the inner wall of A-tubules of the doublets exposed by *N*-lauroylsarcosine (Sarkosyl) treatment. The zero-length cross-linker 1-ethyl-3-(3-dimethylaminopropyl) carbodiimide (EDC) applied to 0.6 M KCl-extracted axonemes generated a 75-kDa complex containing β-tubulin and FAP85. Further characterization of FAP85 and its effects on microtubule dynamics showed that FAP85 binds to tubulin and stabilized microtubules. According to these results, we conclude that FAP85 is a novel member of microtubule-binding proteins, localizing on the inner wall of the A-tubule and stabilizing microtubules.

3.2 INTRODUCTION

Eukaryotic cilia and flagella are genetically well conserved organelles that play important roles for cell motility, sensing the environment, and generating mucus flow. In humans, cilia and flagella are widely distributed in the body, and disorders of these organelles cause multiple human diseases collectively called ciliopathy (reviewed in Brown and Witman (2014)).

The high homology of axonemal components with those of humans, and the availability of a large repertoire of axonemal mutants have made *Chlamydomonas* a useful model system for investigating the structure and function of eukaryotic cilia and flagella (Silflow and Lefebvre, 2001). Notably, *Chlamydomonas* shows a unique change in waveform between ciliary and flagellar types in response to changes in intracellular calcium concentrations (Kamiya and Witman, 1984). In the ciliary-type waveform, the cell swims forward with its flagella beating asymmetrically with an oar-like effective stroke and a surf-casting-like recovery stroke. In the flagellar-type waveform, the cell moves backward with its flagella beating symmetrically like sinusoidal waves. These *Chlamydomonas*-specific waveform changes led us to examine *Chlamydomonas*-specific flagellar-associated proteins with EF-hand motifs, which are putative calcium-binding proteins. Several important studies on calcium-mediated regulation of flagellar beating have been performed (DiPetrillo and Smith, 2010; Sakato et al., 2007; Smith and Lefebvre, 1997; Wakabayashi et al., 1997; Yang et al., 2001); however, nine types of flagellar-associated proteins (FAPs) containing EF-hand motifs in *Chlamydomonas* (FAP85, FAP183, FAP200, FAP225, FAP252, FAP268, FAP272, FAP288, and FAP290) remain uncharacterized.

3.2.1 Axonemal components on the DMTs

The cilia/flagella's scaffold is called an axoneme. Its characteristic structure consists of nine peripheral DMTs surrounding two singlet MTs. In addition, several hundred types of proteins compose functional protein complexes creating the structural and functional complexity of axoneme (Merchant et al., 2007). These various proteins form functionally distinct axonemal components

known as the inner dynein arm (IDA), outer dynein arm (ODA), radial spoke (RS), and nexin-dynein regulatory complexes (N-DRC), which are essential to generate cilia/flagella beating (Bui et al., 2008; Heuser et al., 2009; Pigino et al., 2011). In addition to the major axonemal proteins, proteomics and genomics have revealed the presence of FAPs in the axoneme; the latter have not been functionally characterized to date (Pazour et al., 2005)

For normal function, each protein complex is aligned on the DMTs with specific periodicity repeating at 96 nm. Some studies reported that several proteins periodically bind to the DMT as a mechanism of periodical binding of axonemal components. For example, the ODA-docking complex is composed of three proteins (DC1, 2, and 3) and generates a 24-nm long space for regular arrangement of the ODA (Owa et al., 2014). In another case, FAP59 and FAP172 form a 96-nm long complex, which works as a molecular ruler of 96-nm periodicity of the IDA, RS, and N-DRC in the axoneme (Oda et al., 2014). All these complexes are aligned onto one side of the DMT.

3.2.2 Composition of the DMT

The DMT is composed of A-tubules and B-tubules (**Figure 3.1**). The A-tubule is a scaffold of all axonemal components and consists of 13 protofilaments (PFs) of α- and β-tubulin heterodimers. The B-tubule consists of 10 PFs forms a C-shape tubule binding to the A -tubule and becomes an interaction destination of dyneins. There could be many important roles for axonemes; however, little is known about how DMTs are built, what proteins make CO shape architecture, why axonemal components can localize on one side of the DMTs, and specific protofilaments.

3.2.3 Microtubule inner proteins (MIPs)

Recent progress of observation techniques, such as Cryo-EM tomography and single particle analysis, has revealed that DMTs are very complex, composed of several structures beside the microtubule and located within the microtubules. These structures are called the microtubule inner proteins (MIPs [**Figure 3.1**]).

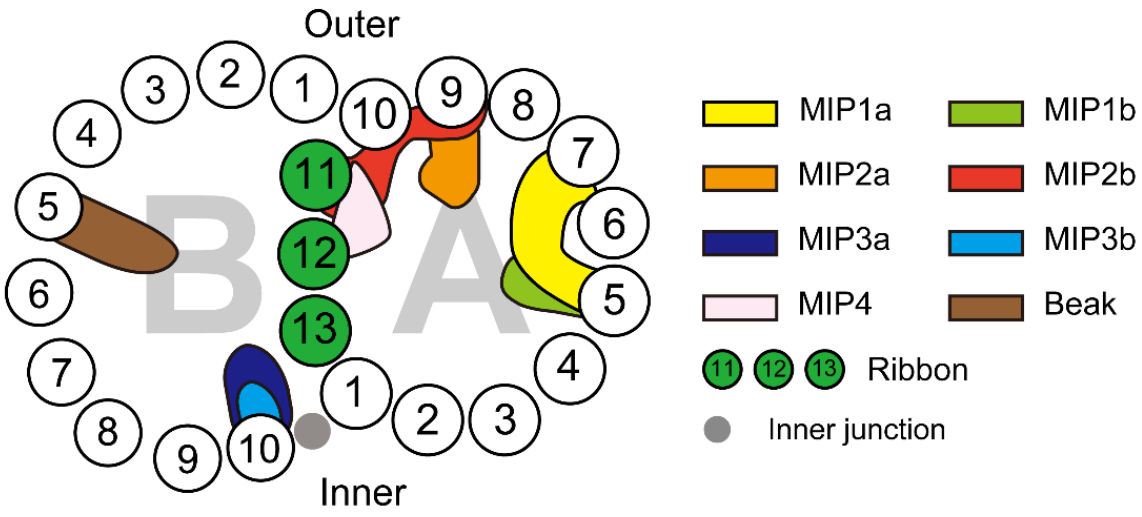

Figure 3.1 **Schematic representation of the arrangement of MIPs.**

Several types of MIPs of *Chlamydomonas* flagella have been reported. Light gray letters indicate A-tubule and B-tubule of a DMT. Modified after Pigino et al., (2012)

MIPs are proteins that are periodically attached to the inner surface of DMTs, and initially reported by two independent studies in 2006 (Nicastro et al., 2006; Sui and Downing, 2006). In their studies, MIPs were classified to three components (MIP1, MIP2, and MIP3). In 2011, a detailed DMT structure was solved by cryo-electron tomography (Nicastro et al., 2011) and gave more information on MIPs. This study showed that the MIPs were more complex than previously thought and were composed of alternating small and large subunits with a periodicity of 16 and/or 48 nm. Each subunit of MIP1, 2, and 3 was classified as "-a" and "-b," and additional shallow densities per 48 nm were named MIP4 (**Figure 3.1**). This study also revealed that B-tubules contained exactly ten PFs. Also, the inner junction (IJ) and outer junction between the A-tubule and B-tubule were different structures.

IJ consisted of an axially periodic ladder-like structure, whereas the outer junction appeared to be formed by interactions between the tubulin subunits of the three PFs.

Comparative structural analysis revealed these molecular architectures were common among the axonemes of *Tetrahymena* cilia, sea urchin sperm, and *Chlamydomonas* flagella, and were very similar structures with several differences (Pigino et al., 2012). This result can be the basis for future correlations between structural diversities and different waveforms.

Maheshwari et al. (2015) reported a detailed three-dimensional structure of *Tetrahymena* DMT at ~19 Å resolution by single particle cryo-EM and the presence of additional MIPs. MIP4 was classified as MIP4a, MIP4b, and MIP4c, and two more structures named MIP5 and MIP6 were identified. Subsequently, Ichikawa et al. (2017) performed single particle cryo-EM combining assignment of α- and β-tubulin in DMT, which demonstrated further diversity of MIPs and interaction between MIPs and tubulin dimers at subnanometre-resolutions. They reported the presence of sixteen types of MIPs including subtypes. There were eleven types of MIPs in the A-tubule (MIP1a, 1b, MIP2a, 2b, 2c, MIP4a, 4b, 4c, 4d, MIP6a, and 6b), five types in the B-tubule (MIP3a, 3b, MIP5a, 5b, and MIP7), and eleven types of filamentous structures longitudinally running in-between PFs named filamentous MIPs (fMIPs). There are four fMIPs in the A-tubule and seven fMIPs in the B-tubule. At the present time, a total 27 of MIPs have been identified in *Tetrahymena* cilia (Ichikawa et al., 2017). This study suggested the roles of MIPs in the assembly process of DMT because of the localization and interaction of MIPs on MTs. It was also suggested that there must be cooperation in the assembly of MIPs and outside proteins, such as ODA and RS.

Only one study to the best of our knowledge about the proteins constituting of DMT has been published and it showed that FAP20 constituting IJ of DMT is essential for both the stability of the flagella and the planar asymmetrical waveform in *Chlamydomonas* (Yanagisawa et al., 2014).

The development of observation technologies, such as EM tomography, makes it possible to identify new MIPs as additional structures, and to provide clues as to their functions important not only for assembly of DMT and other axonemal components, also to determination of the waveforms

of beating. Although the structures of MIPs have been described at subnanometre resolutions, the identification of proteins constituting MIPs and individual functions of MIPs remains to be revealed.

3.2.4 FAP85 is our target protein

In this chapter, we report that FAP85, one of the flagella associated proteins (FAPs) is identified as one of the MIPs and FAP85 has a function to stabilize MTs. We originally screened FAP85 through the reactivation assay from the viewpoints in which FAP has an EF-hand motif common in Ca^{2+} binding proteins, and its function is unknown and unique to *Chlamydomonas*. These viewpoints were based on the idea that unique waveform changing of *Chlamydomonas* is regulated by calcium ion concentrations, that is, calcium binding proteins in *Chlamydomonas* flagella could be involved in a mechanism of waveform changing.

We first cloned FAP85 from cDNA prepared from mRNA of *Chlamydomonas,* and expressed it in *E coli* cells as a ProS2 conjugated protein. By using the expressed protein as an antigen, polyclonal antibody was prepared. The antibody recognized the native FAP85 in the residual axoneme subjected to 0.6 M-KCl extraction. Immuno-electron microscopy showed the anti-FAP85 antibody localized on the inner wall of the A tubules of DMTs. Although no significant effect of FAP 85 on flagellar waveform was observed, FAP85 modified microtubule dynamics and facilitated polymerization of tubulins into microtubules. These observations identify the FAP85 as one of the microtubule inner proteins (MIPs) that may function in the structural assembly of the axoneme.

3.3 MATERIALS AND METHODS

3.3.1 Strains and culture

The following strains of *Chlamydomonas reinhardtii* were used: *137c* (wild type); *oda1*, *oda2,* both lacking the outer arm dynein; *ida1*, lacking the inner arm dynein I1; *ida5*, lacking four inner arm dynein subspecies a, c, d, and e; *ida7*, lacking the intermediate chain of the inner arm dynein I1/f, IC140; *pf2*, exhibiting failure to assemble five of the seven dynein regulatory complex (DRC)-associated subunits; *pf3*, lacking DRC1 and dynein e; *pf14* lacking radial spokes and missing a set of 17 spoke-associated polypeptides, and *pf18* lacking the central apparatus; and *mbo1*, lacking beak-like structures. Cells were grown according to procedures described by Gorman and Levine (1965), in Tris-acetic acid-phosphate (TAP) medium with aeration and continuous illumination at 25°C for four days.

3.3.2 Preparation of axonemes

Cells were harvested by centrifugation at 3,000 rpm (1,692 × *g*, R10A3 rotor, Himac CR22E) for 6 min at 27 ± 2°C, suspended in 40 ml of ice-cold HMDS solution (30 mM HEPES-NaOH, 5 mM $MgSO_4$, 1 mM dithiothreitol (DTT), 4% Sucrose, pH 7.4). All subsequent procedures were carried out at 4°C or on ice.

Chlamydomonas flagella were isolated using the dibucaine method (Witman et al., 1978). In brief, dibucaine HCl (Wako, Japan) was added to the cell suspension at a final concentration of 2.5 mM. Shear was applied by repetitive pipetting. Deflagellated cells were removed by centrifugation at 3,000 rpm (1670 × *g*, RS-4 rotor, KUBOTA6800) for 6 min, and then the supernatant containing flagella was collected. The flagella were spun down at 15,000 rpm (27,720 × *g*, RSR20-2 rotor, Himac CR21) for 12 min. Resultant flagella were suspended and demembranated with HMDEK solution (30 mM HEPES, 5 mM $MgSO_4$, 1 mM DTT, 1 mM EGTA, and 50 mM potassium acetate, pH 7.4) containing 0.2% Nonidet P-40 (NP-40, Nacalai Tesque).

The demembranated flagella suspension was centrifuged at 15,000 rpm (21,130 × *g*, FA-45-24-11 rotor, Eppendorf 5452R) for 5 min. The resulting pellet was suspended in 1.5 ml of HMDEK solution. The suspension was re-centrifuged for 5 min, and the resultant pellet was re-suspended in 1.5 ml of HMDEK. This procedure was repeated several times in order to remove the detergent completely.

To obtain the axonemes without components soluble in 0.6 M KCl, the demembranated axonemes were suspended in high-salt-HMDE solution (0.6 M KCl or 0.6 M KI, 30 mM HEPES-NaOH, 5 mM $MgSO_4$, 1 mM DTT, 1 mM EGTA) for 15 min and centrifuged at 15,000 rpm for 8 min. The high-salt extraction was repeated twice; residual axonemes after high-salt extraction were obtained as the pellet and used for immunoblotting experiments and the Sarkosyl treatment experiments (see below).

3.3.3 Sequencing of the 25-kDa FAP85 by MALDI-TOF Mass Spectrometry

The relevant protein bands were excised from the gel and sent to Cosmo Bio for MALDI-TOF mass spectrometry. According to the company procedures, the peptides digested by trypsin in the gel were subjected to MALDI-TOF mass spectrometry.

3.3.4 Cloning of cDNA encoding FAP85 and expression of FAP85 as a ProS2-conjugate

The DNA encoding FAP85 was amplified from a *Chlamydomonas* cDNA library by PCR. The primers used were: FAP85-F, 5’ TCG AAG GTA GGC ATA TG ATG TCG TTC TTC GGG CTC 3′; and FAP85-R, 5′ CGA CAA GCT TGA ATT CTT ACC CCA GGA AGT GGC CGT 3′. The FAP85 cDNA was inserted into the NdeI/EcoRI-digested pCold-ProS2 vector (Takara Bio, Kusatsu, Japan), originating the ProS2-FAP85 plasmid: this plasmid expressed FAP85 N-terminally fused with a polyhistidine tag followed by the ProS2 tag protein, consisting of the tandem N-terminal domain of Protein S from *Myxococcus xanthus,* which increases solubility of expressed proteins. For MT

binding assays, the Orange Nano-lantern (ONL) (Takai et al., 2015) was cloned and inserted in N-terminal of FAP85 plasmid to obtain the orange luminescent protein, ONL-FAP85 (migrating as 85 kDa by SDS-PAGE). The ProS2-FAP85, pCold-ProS2 and ONL-FAP85 plasmids were transformed into BL21 Star (DE3) chemically competent cells (ThermoFisher Scientific, Waltham, MA, USA) and the recombinant proteins they encoded for were expressed according to conventional methods.

3.3.5 Purification of ProS2-FAP85

E. coli cells were first grown at 37°C in 50 ml of LB medium (1%, w/v) Bacto-Tryptone (DIFCO; 0.5%, w/v) Bacto Yeast Extract (BD DIFCO; 1%, w/v) NaCl (Wako)) with 50 μg/ml ampicillin overnight, and then poured into 1 L of LB medium with ampicillin and cultured at 37°C until the absorbance at 600 nm was 0.6. The *E. coli* cells were incubated on ice for 5 min. Isopropyl β-*D*-1-thiogalactopyranoside (0.1 mM) was added to the cells and were incubated at 15°C. After 24 hours, the cells were harvested by centrifugation at 5,000 rpm (4,500 × g, R10A3 rotor, Himac CR22E) for 10 min at 4 °C followed by suspension in distilled water. The suspension was centrifuged at 4,800 rpm (4275 × g, RS-4 rotor, KUBOTA6800) for 10 min at 4 °C and the pellet was frozen in liquid nitrogen to weaken the cell wall. The thawed cells were suspended in lysis buffer (20 mM Tris-HCl, 250 mM NaCl, 1 mM dithiothreitol, and 10 mM imidazole, pH 7.5) and in the presence of a protease inhibitor mixture (Nacalai Tesque); then, the cells were sonicated and spun down. The supernatant was loaded onto a column containing Ni-immobilized metal ion affinity chromatography resin (Bio-Rad) and His-tagged proteins were eluted with elution buffer (20 mM Tris-HCl, 250 mM NaCl, 1 mM dithiothreitol, and 250 mM imidazole, pH 7.5).

3.3.6 Purification and preparation of Ca^{2+} free ProS2-FAP85 and ProS2

To examine thermodynamic properties of FAP85 with the isothermal titration calorimetry (ITC),

we prepared Ca^{2+}-free FAP85. The ProS2-FAP85 was dissolved in HED solution (30 mM HEPES-NaOH, 1 mM EGTA, 1 mM DTT, pH7.4), loaded onto the MonoQ column (GE Healthcare), and then eluted with a linear gradient of 0 mM to 1 M KCl in HED buffer. To assess the binding of Mg^{2+} ion to the EF-hand motif, we prepared ProS2-FAP85 in the Mg^{2+}-free solution. Resultant ProS2-FAP85 solution was divided into two fractions and they were dialyzed against the HK solution (30 mM HEPES-NaOH, 100 mM KCl, pH 7.4) and the HKM solution (30 mM HEPES-NaOH, 100 mM KCl, 5 mM MgSO4, pH 7.4), respectively. All glassware was washed with 1 mM EGTA solution and rinsed with ultra-pure water before preparation of the buffers used for the calorimetry. The ProS2 was prepared in the similar way to the ProS2-FAP85 with some modifications. The ProS2 sample was eluted from the MonoQ column (GE Healthcare) with a linear gradient of 0 mM to 2 M KCl in HED buffer. The fraction containing ProS2 was dialyzed as described for ProS2-FAP85.

3.3.7 Isothermal titration calorimetry (ITC)

The ITC was carried out using a MicroCal PEAQ-ITC (Malvern Instruments Limited). The protein concentrations of ProS2-FAP85 were determined with the Bradford method using BSA as the standard. The ProS2-FAP85 at 1 μM in the HKM (HK) solutions was titrated with the 300 μM $CaCl_2$ in HKM (HK) solution, respectively. For the reference data of ProS2, Ca^{2+}-free ProS2 was used under the same condition as ProS2-FAP85. The concentrations of ProS2 were measured with the UV absorbance (ε = 7460 $M^{-1}cm^{-1}$, at 280 nm).

3.3.8 Preparation of anti-FAP85 antibody

One milligram of ProS2-FAP85 was prepared and used as the antigen. The rabbit serum was obtained by the Eurofins Genomics (Tokyo, Japan), according to company procedures. For further purification of antibody from the serum, ProS2-FAP85-affinity column chromatography and ProS2-affinity chromatography were performed in order to exclude undesirable antibodies against ProS2

and other contaminants. The antibody titer was examined by ELISA against ProS2-FAP85 and found to be > 10^5.

3.3.9 Immunoblotting

Flagella, KCl extract, KI extract, and residual axonemes were loaded on to a 4-15% SDS-polyacrylamide gel and separated by electrophoresis. The molecular weight marker proteins (Bio-Rad, CA, USA) containing 250-, 150-, 100-, 75-, 50-, 37-, 25-, 20-, 15-, and 10-kDa proteins were run alongside samples to estimate molecular weight. The resulting protein bands were then transferred onto a PVDF membrane using a Bio-Rad mini-gel transfer apparatus (Bio-Rad, Richmond, CA), followed by incubation with a blocking buffer (3% skim milk in phosphate-buffered saline with Tween 20) for an hour at 20-25℃. The PVDF membrane was incubated for 45 min with anti-FAP85 antibody. After washing three times with the blocking buffer, the membrane was incubated for 45 min with the secondary antibody, alkaline phosphatase goat anti-rabbit IgG (Vector laboratories) for Sarkosyl experiments and anti-rabbit IgG, horseradish peroxidase-linked whole Ab donkey (GE Healthcare) for other experiments. The membrane was then washed three times with blocking buffer and stained with the BCIP/NBT phosphatase substrate system (Sera Care Life Sciences, Inc.) or ECL substrate (Clarity Wester ECL Substrate, Bio-Rad).

3.3.10 Immunofluorescence microscopy of Chlamydomonas axonemes

Immunofluorescence microscopy was performed according to procedures described by Sanders and Salisbury (1995) with some modifications. First, the coverslips (18 mm×18 mm, Matsunami, Japan) were cleaned with a non-ionic, non-phosphoric detergent, rinsed with running deionized distilled water, and soaked into 5 mM EGTA for 10 min. A droplet of 0.1% poly-*L*-lysine was placed onto the center of the coverslip; after a 30-sec incubation, the coverslip was rinsed with deionized water and air-dried. Freshly prepared *Chlamydomonas* cells were placed onto the poly-*L*-lysine-

coated coverslip and incubated for 10 min, allowing the cells to settle on the glass surface. Immediately after the removal of excess suspension by blotting, the cells were fixed with fixative solution (50 mM HEPES-NaOH, 3 mM EGTA, 1 mM $MgSO_4$, 25 mM KCl, pH 6.8, with 3% formaldehyde and 0.1% glutaraldehyde) for 30 min at room temperature. In order to quench the fixatives, we washed the specimen with MTSB-NH_4Cl buffer (50 mM HEPES-NaOH, 3 mM EGTA, 1 mM $MgSO_4$, 25 mM KCl, 50 mM NH_4Cl, pH 6.8), and MTSB buffer (50 mM HEPES-NaOH, 3 mM EGTA, 1 mM $MgSO_4$, 25 mM KCl, pH 6.8) three times. The MTSB buffer was exchanged with Na-PBS, pH 7.2, through a series of increasing ratios of Na-PBS buffer to the MTSB buffer (33%, 66%, and 100% Na-PBS). The specimen was finally incubated in blocking buffer (3% bovine serum albumin (BSA), 5% glycerol, 20% fish gelatin in PBS, pH 7.2) for 30 min at room temperature. The primary antibodies were anti-FAP85, non-immune normal rabbit IgG (148-09551, Wako, Japan) and rabbit anti-IC140 antibody (Yang and Sale, 1998). These primary antibodies, which were diluted in blocking buffer, were placed onto the Parafilm M® as a droplet. The coverslip was placed upon the droplet and incubated for 2 hours at 37°C in a moist chamber. The primary antibody was then washed three times by Na-PBS buffer. The coverslips were then incubated in blocking buffer containing the secondary antibody (the goat anti-rabbit IgG cross-absorbed secondary antibody Cy3-conjugated (cat. #A10520, Thermo Fisher Scientific). After two hours of incubation, the secondary antibody was washed out using the same procedure as that for the primary antibody. The resulting specimens were observed in mounting buffer (0.109 mg/ml glucose oxidase, 0.04 mg/ml catalase, 43 mM glucose in Na-PBS, pH 7.2) with a fluorescence microscope (BX-51, Nikon, Japan) equipped with a 100 ×/1.35 NA oil-immersion objective lens and EM-CCD digital camera C9100 (Hamamatsu, Japan).

3.3.11 N-lauroylsarcosine (Sarkosyl) treatment of DMTs

To prepare A- and B-tubules of DMTs separately, the axoneme were suspended in 0.2, 0.3, 0.4, and 0.7% *N*-lauroylsarcosine (Sarkosyl) in 10 mM Tris-NaCl, pH 7.8, was incubated for an hour and one of the samples with 0.7% Sarkosyl was treated overnight in order to dissolve all DMTs. After

treatment, the axonemes were collected as pellets with a Beckman TLA100.1 angle rotor at 53,000 rpm (~100,000 × *g*) for an hour. Supernatants containing the dissolved portions of DMTs were also collected. The pellets containing residual parts of DMTs were re-suspended in 1 ml of Tris-NaCl and spun down again. Both supernatants and pellets were analyzed with 4-15% SDS-polyacrylamide gel, followed by immunoblotting analysis. The pellet obtained by treatment with 0.3% Sarkosyl was used for immuno-gold electron microscopy, as described below.

3.3.12 Immuno-gold electron microscopy of DMTs

Immuno-gold electron microscopy of DMTs was performed according to Ikeda et al. (2003) with some modifications. All procedures were performed at room temperature and solution exchange was carried out by replacing grids onto the drop of another solution. Carbon-coated, collodion nickel EM grids were placed onto the droplet of 0.1% poly-L-lysine for 5 min, and washed with distilled water. Sarkosyl-treated DMTs were placed onto the grids and incubated for 10 min. The grids were rinsed with a blocking solution (1% bovine serum albumin in PBS, pH 7.4) and incubated for an hour with anti-FAP85 antibody diluted 10 times in the blocking buffer. The grids were then washed with the blocking buffer for six times. The 10 nm-gold-conjugated goat anti-rabbit IgG antibody (G7402-.4ML, SIGMA) was applied to the grid, incubated for an hour, and washed out with the blocking buffer. Finally, grids were washed with PBS and distilled water, and the specimens were negatively stained with 1% uranyl acetate. The specimens were observed with a transmission electron microscope (JEM 2000, JEOL, Japan).

3.3.13 Cross-linking of FAP85 with zero-length cross-linker EDC

Sarkosyl treatment of the DMTs yielded the A-tubule-rich fraction. These A-tubule fractions were further treated with 0-10 mM 1-ethyl-3-(3-dimethylaminopropyl) carbodiimide hydrochloride (EDC, Thermo-Fisher) according to King et al. (1991). The pellet of A-tubules was suspended in HMDEK

to 1 mg/ml, and an equal volume of 0-20 mM EDC in HMDEK was added to final concentrations of 0-10 mM EDC. This treatment was performed for 1 hour at room temperature, followed by addition of 2-mercaptoethanol for 50 mM in order to terminate the reaction. The samples were prepared for electrophoresis by the addition of SDS-PAGE sample buffer. FAP85 was detected by immunoblotting with anti-FAP85 antibody.

3.3.14 Immunoprecipitation of FAP85 co-precipitation and tubulin binding analysis

Immunoprecipitation of FAP85 was carried out using Dynabeads (Thermo Fisher Scientific) in accordance with the supplier's instructions. In brief, Dynabeads conjugated with protein G were incubated for 10 min with 2 μg of mouse anti-ProS2 monoclonal antibody (M200, Takara, Japan) and anti-FAP85 antibody diluted in PBS-T buffer (10 mM Na-PBS, pH 7.4, with 0.02% Tweenr-20). The beads were washed and suspended in PBS-T buffer. A small aliquot of the sample containing the antigen was added and incubated while gently mixing for 15 min. After washing with PBS-T, collected beads were boiled with the SDS sample buffer for electrophoresis and the immunoblotting.

For co-precipitation, the axoneme isolated from 20 L of culture of the wild type *Chlamydomonas* was demembraned, extracted with high salt-concentration HMDE solution and treated with 0.7% Sarkosyl overnight. The supernatant was diluted 10 times with Tris-HCl, pH 7.8, followed by dialysis against PBS to remove Sarkosyl from the sample. This sample was used for the antigen sample of co-precipitation. For tubulin binding analysis, tubulin purified from the porcine brain according to the method of Castoldi and Popov (2003) and ProS2-FAP85 was incubated at a 10: 1 weight ratio for 30 min at 4℃, as performed with the antigen sample.

3.3.15 Microtubule-binding assay

The affinity of FAP85 to microtubules was measured by the assays in which the amount of FAP85 co-sedimenting with microtubules was quantified by SDS-PAGE (Butner and Kirschner, 1991). Tubulin solution and ONL-FAP85 solution were centrifuged with the Beckman TLA 120.2 angle rotor at 100,000 rpm, for 10min at 4°C to remove undesirable aggregates. Tubulin was polymerized at 37°C for 30 min at the concentration of 10 mg/ml in the BRB80 buffer (80mM PIPES-KOH, 1 mM $MgCl_2$ and 1 mM EGTA, pH6.8) with 1 mM GTP, and stabilized with 10 μM taxol. The polymerized microtubules were loaded over the sucrose cushions (25% sucrose in BRB80, 10 μM taxol) and centrifuged with Beckman TLA 120.2 angle rotor at 75,000 rpm, for 15 min at 25°C. The pellet was suspended in BRB80 containing 1 mM GTP and 10 μM taxol. The resultant suspension of microtubules was diluted with BRB80 containing 1 mM GTP and 10 μM taxol to obtain a series of solutions containing 1, 2, 5, 10, and 20 μM tubulin. These microtubule solutions were incubated for 60 min with 0.77 μM of ONL-FAP85 and 100 μg/mg BSA. The mixtures were then centrifuged. Supernatants were carefully collected and the remaining supernatant was removed from the pellet. The pellets were re-suspended by addition of 4× SDS sample buffer (250 mM Tris-HCl, 40% Glycerol, 5% SDS, 5% BPB, 5% 2-mercaptoethanol). These samples were boiled and the equal amounts of the samples were loaded onto 4-15% mini protean stain-free gel (Bio-Rad, CA, USA). The gel was scanned and quantified with using ChemiDoc (Bio-Rad, CA, USA).

For co-polymerization experiments, 5, 10, 20 and 30 μM tubulin and ONL-FAP85 were co-polymerized in BRB80 with 1mM GTP, 100 μg/ml BSA at 37°C for 30 min and resultant microtubules were stabilized with 100 μM taxol. The mixtures were centrifuged in Beckman TLA120.2 angle rotor at 100,000 rpm for 10min. The supernatants and the pellets were loaded onto the gel and quantified as the same way for the co-sedimentation assay.

The amount of proteins was quantified by densitometry. The percentages of ONL-FAP85 bound to the microtubules were calculated as ratios to the total density of ONL-FAP85 bands in the supernatant and the pellet. Binding curves were fitted to the experimental data with Igor Pro with the equation:

$$B = Bmax\ T / (Kd + T),$$

where B represents the percentage of bound FAP85, T is the concentration of tubulin used in the experiment, $Bmax$ is the maximum percentage of FAP85 can bind to the microtubules and Kd is the dissociation constant.

3.3.16 In vitro assembly and disassembly of microtubules

Tubulin polymerization was monitored as turbidity at 350 nm, using a Synergy H1 (Biotek Japan) microplate reader. The solution obtained was added into a 384-well black glass bottom plate (Thermo Scientific). The change in the absorbance at 350 nm was measured at 37℃ for 120 min; this duration was sufficient for polymerization of most of the tubulin without evaporation of the solution. The total volume of the solution was 50 µl. The various concentrations of tubulin (5-35 µM) in BRB80 and 1 mM GTP were incubated for 5 min on ice. This was followed by the addition of 2 µl of 70 µM FAP85 in 250 mM KCl in HMDE (the final concentrations were 2.8 µM of FAP85 and 10 mM KCl), or of 250 mM KCl in HMDE (final concentration, 10 mM KCl), and incubation for 5 min. Measurement was started immediately after all solutions were added to the wells.

For the kinetics of depolymerization, turbidity of pre-polymerized microtubules was monitored at 350 nm using a DU 800 spectrophotometer (Beckman Coulter). Hundred micro liters of 30 µM tubulin, with and without 2.8 µM FAP85, were polymerized at 37℃ for 30 min. MTs were immediately moved to the cuvette; then, depolymerization was induced by cooling the water-jacketed cell holder to 15℃ using an F25 Refrigerated circulator (JULABO), and monitored for 5 min. First, absorbance at 350 nm (Abs_{350nm}) was stable within 1 min; subsequently, this absorbance linearly decreased, which indicated that MTs underwent depolymerization during this period. The range of Abs_{350nm}, which linearly decreased, was fitted to a linear equation. The inclination, which was defined as time (sec) versus ΔAbs_{350nm}, represented the depolymerization rate (Johnson and Borisy, 1977).

3.4 RESULTS

3.4.1 Expression of FAB85 in E coli cells

FAP85 has previously been identified by proteomics studies of *Chlamydomonas* flagella (Pazour et al., 2005), and included in the National Center for Biotechnology Information (NCBI: https://www.ncbi.nlm.nih.gov/) database. FAP85 is predicted to be 197 amino acids in length and has a molecular mass of 22.2 kDa. InterPro annotation shows that FAP85 has an EF-hand motif near its center, which is characteristic of calcium-binding proteins (**Figure 3.2**). BLAST searches showed that FAP85 homologs of unknown function, including hypothetical proteins are present in *Volvocine* algae such as *Volvox*, and *Gonium* (E value < 1 e^{-105}), and also found in *Micromonas* (E value < $2e^{-21}$) and *Monoraphidium* (E value < $2e^{-13}$).

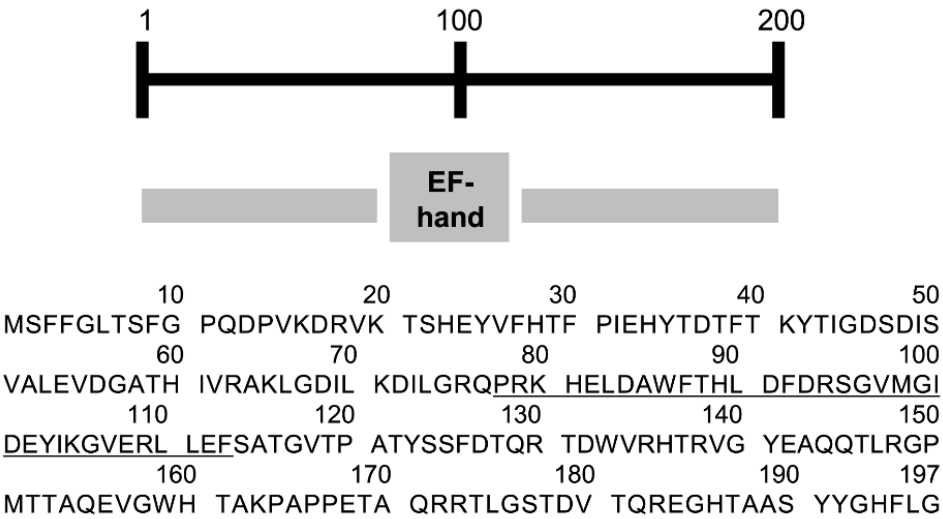

Figure 3.2 **The amino-acid sequence of FAP85 and predicted EF-hand motif of FAP85**

InterPro identified one EF-hand motif in the middle of the polypeptide (underlined). No coiled-coil regions were predicted. The scale indicates the positions of amino acid residues.

The cDNA corresponding to the 22-kDa polypeptide was cloned and sequenced, and we confirmed that it is identical to the sequence recorded as FAP85 in GenBankTM/EBI (accession number, XM_001695284). To increase the solubility of the protein, the cDNA of FAP85 was conjugated with the ProS2 sequence, which increases the solubility of expressed polypeptides. Protease treatment of the recombinant protein liberated FAP85 that was insoluble and formed aggregates. Consequently, we used recombinant FAP85 as a ProS2-conjugate. The fraction extracted with anion exchange column after Ni-column elution contained ProS2-FAP85 alone. **(Figure 3.3)** The recombinant protein was used as an antigen mixed with an adjuvant to generate polyclonal antibodies in rabbits.

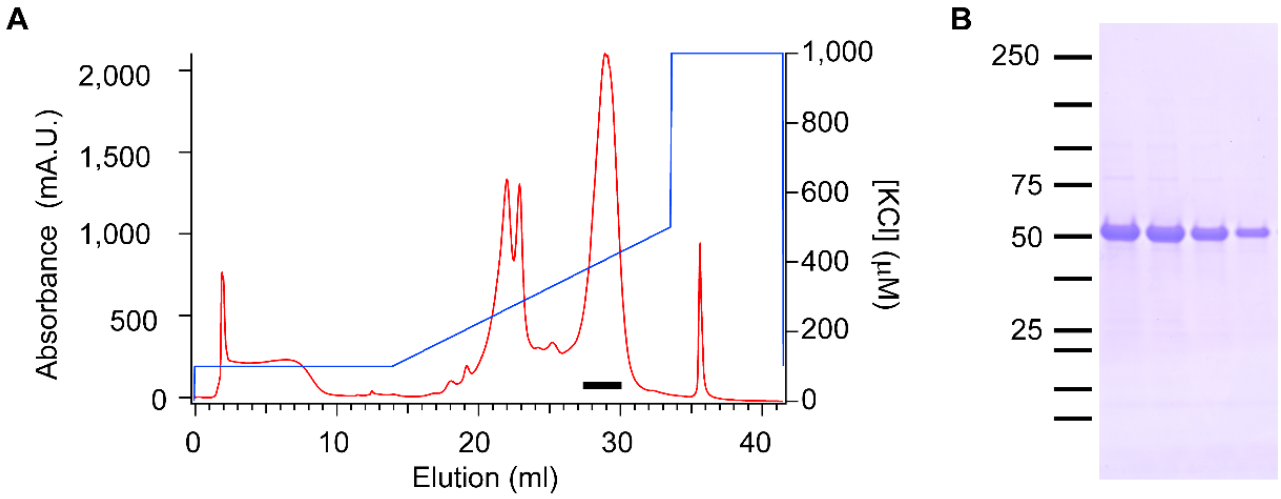

Figure 3.3 **Purification of ProS2-FAP85**

(A) Ni-column elute was subjected to anion exchange column (MonoQ) and eluded with a linear gradient of 0 mM to 1 M KCl buffer (red line: absorbance of λ = 280 nm, blue line: concentration of KCl in elution buffer). The fractions used for experiments were indicated by a bar in the graph. (B) The fractions indicated by a bar in (A) were subjected to the SDS-PAGE. These fractions contained ProS2-FAP85 alone.

The association of calcium with this recombinant ProS2-FAP85 was examined using isothermal titration calorimetry (**Figure 3.4).** The ITC supports that FAP85 has a single EF-hand motif. As ProS2 has two Ca^{2+} binding sites, recombinant ProS2-FAP85 possesses a total of three Ca^{2+}-binding sites. By analyzing data, including ProS2 data, we estimated the K_d of the Ca^{2+}-binding site of FAP85 to be $1 – 8 \times 10^{-8}$ M. The K_d was far from the range of Ca^{2+} concentrations that occur during the waveform changes (pCa4 - pCa5). The results suggest that FAP85 is bound to Ca^{2+} under physiological conditions and may not be directly involved in the waveform changes.

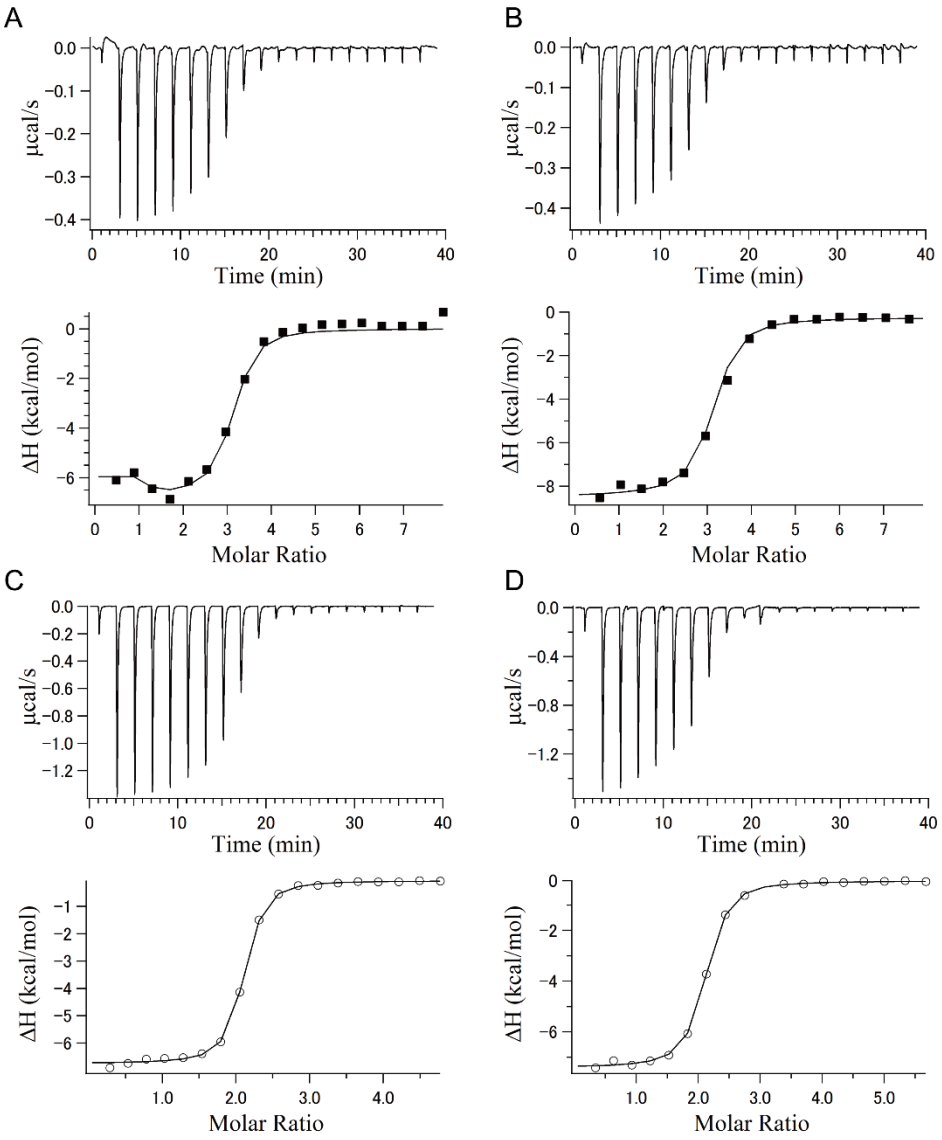

Figure 3.4 **Isothermal titration calorimetry data of ProS2-FAP85 and ProS2.**

(A) and (B). The ProS2-FAP85 at 1 µM in the HK (A) and HKM (B) solutions were titrated with the 300 µM $CaCl_2$ in HK and in HKM solutions, respectively. (C) and (D). The ProS2 under the same condition as ProS2-FAP85 was measured as the reference data of ProS2. The ProS2 was in the HK (C) and HKM (D) solutions. ProS2 had two Ca^{2+} binding site: $K_d = 5.1\times10^{-7}$ (M), ΔH = -7.36 (kcal/mol) in HKM buffer and $K_d = 3.3\times10^{-7}$ (M), ΔH = -6.69 (kcal/mol) in HK buffer, and did not exhibit any thermal reactions with titration of $MgSO_4$ (data were not shown here). ProS2-FAP85 was analyzed including ProS2 data, and estimated one Ca^{2+} binding site: $K_d = 8.2\times10^{-8}$ (M), ΔH = -7.69 (kcal/mol) in HKM buffer and $K_d = 9.6\times10^{-9}$ (M), ΔH = -6.57 (kcal/mol) in HK buffer.

3.4.2 Poly-clonal rabbit antibody against ProS2-FAP85 recognizes native FAP85

After extraction of dynein arms with 0.6M KCl, the residual pellet of wild-type axonemes was analyzed by SDS-PAGE followed by immunoblotting. The anti-ProS2-FAP85 antibody (whose generation is described in Materials and Methods) detected a single band of the expected size (~25 kDa) (**Figure 3.5**). Immune-precipitates obtained using the anti-ProS2-FAP85 antibody were subjected to peptide mass fingerprinting by MALDI-TOF mass spectrometry, which identified the single band detected by the anti-ProS2-FAP85 antibody as FAP85. Thus, we concluded that the anti-ProS2-FAP85 antibody we generated was capable of recognizing the native FAP85 protein (hereinafter, the anti-ProS2-FAP85 antibody is referred to as the anti-FAP85 antibody).

When the axonemes were treated with 0.6 M KCl, a small amount of the FAP85 could be extracted; however, this amount was too small to be detected by the anti-FAP85 antibody. After centrifugation, the pellet of 0.6 M-KCl extract was then subjected to extraction with 0.6 M KI. The resulting extract and residual axonemes were examined by immunoblotting with the anti-FAP85 antibody. The results showed that FAP85 was solubilized with KI from the axonemes in the extract. These results suggest that FAP85 is resistant to 0.6 M KCl extraction and tightly attached to axonemes.

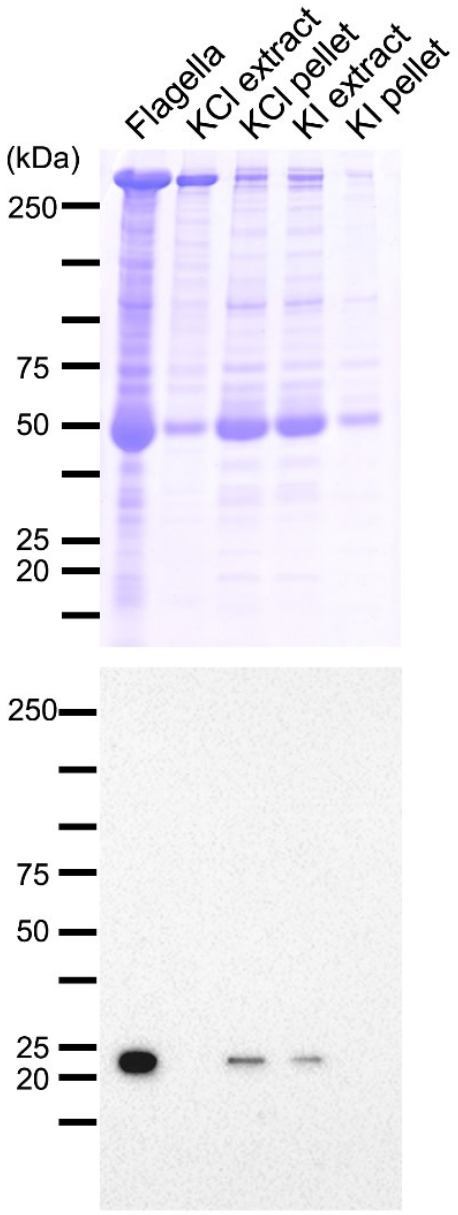

Figure 3.5 **SDS-PAGE (the upper panel) and immunoblot (the lower panel, lanes blotted from the SDS-PAGE lanes) of flagella and their extracts**

Anti-FAP85 antibody detected a single band with the expected molecular weight of FAP85. An FAP85 band was not detected in the 0.6 M KCl extract; however, this was observed in the residual axonemes. The treatment of the axonemes with 0.6M KI resulted in complete extraction of FAP85 in the supernatant.

3.4.3 FAP85 is present even in mutant axonemes lacking major axonemal components

The presence and localization of the FAP85 in the axoneme were examined with anti-FAP85 antibody in various mutants missing major axonemal components. The mutants used were *oda1* and *oda2*; both of which lack the entire outer arm: *ida1* lacks the heavy chain of the inner arm dynein I1/f; *ida5*, lacks four inner arm dynein subspecies, a, c, d, and e; *ida7* lacks the intermediate chain, IC140, of dynein I1/f which leads to the total loss of dynein I1/f, IC140; *pf2* fails to assemble five of the seven dynein regulatory complex (DRC)-associated subunits; *pf3* lacks DRC1 and dynein e; *pf14*, lacking radial spokes as well as a set of 17 spoke-associated polypeptides; *pf18* lacks a central pair; *mbo1* lacks beak-like structures in the DMTs (**Table I**).

Strains	Missing Structure/ Components	References
oda1	outer arm dyneins/ODA-DC	(Kamiya and Okamoto, 1985)
oda2	outer arm dyneins	(Mitchell and Rosenbaum, 1985)
ida1	dynein f (dynein I1)	(Kamiya et al., 1991; Myster et al., 1997)
ida5	dynein a, c, d, e	(Kato-Minoura et al., 1997; Kato et al., 1993)
ida7	dynein I1/f	(Perrone et al., 1998)
pf2	dynein b, e (reduced), DRC	(Rupp and Porter, 2003)
pf3 (wild type for CNK11)	dynein e, DRC	(Lin et al., 2015)
pf14	radial spokes	(Piperno et al., 1977)
pf18	central pair	(Adams et al., 1981)
mbo1	beak-like projection #5,6	(Segal et al., 1984)

Table I. The list of *Chlamydomonas* mutants used in this study

First, we treated the demembraned axonemes with 0.6M KCl to remove soluble components from the axonemes. The residual axonemes were then analyzed by SDS-PAGE and subjected to immunoblotting. Immunoblotting data demonstrated that the anti-FAP85 antibody recognizes a prominent band of 23-kDa in each mutant axoneme. Although quantification of protein abundance by immunoblotting is difficult because of the poor linearity to protein content and large variation of transfer efficiency, no significant difference in the amount of the FAP85 with respect to the amount of tubulin was observed between these axonemes. As FAP85 was found in the residual axonemes of each mutant examined, this protein is likely to be localized on DMTs (**Figure 3.6**).

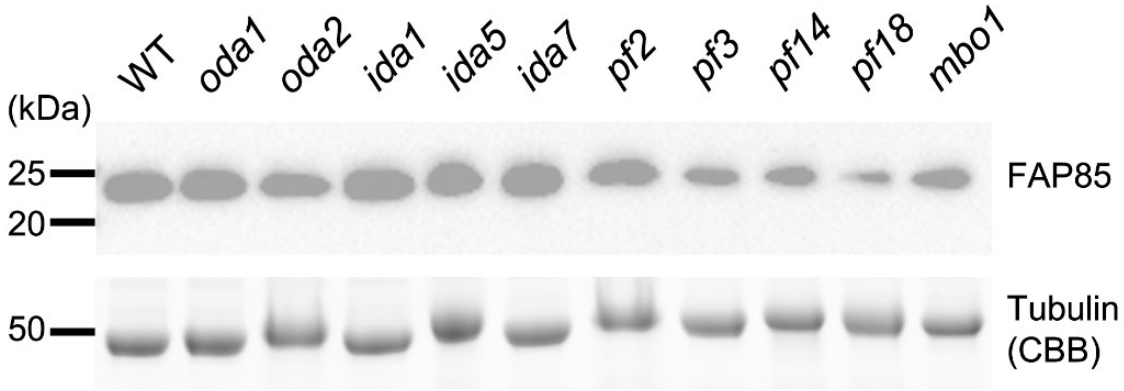

Figure 3.6 **FAP85 was present in various types of flagellar mutants lacking major axonemal components.**

FAP85 was present in various types of flagellar mutants lacking major axonemal components. Prior to electrophoresis, flagella from each mutant were demembraned and extracted with 0.6 M KCl. Protein loading was standardized based on tubulin concentrations determined using densitometry of the CBB staining. Relatively lower content of FAP85 in *pf18* axonemes was due to the variation of the transfer efficiency of the blotting.

3.4.4 Observation of FAP85 in an axoneme by immunofluorescence microscopy

Immunofluorescence microscopy was carried out in *Chlamydomonas* cells; however, the antibody did not show significant immunoreactivity to the axonemes of wild-type cells (**Figure 3.7**). Compared with the antibody against IC140 (the intermediate chain of inner arm dynein I1/f), which showed strong immuno-reactivity along the entire flagellum, the anti-FAP85 antibody did not indicate any significant fluorescence signals, which were comparable to those of the non-immune rabbit IgG. These fluorescence signals observed on the axonemes were probably due to non-specific interactions of the antibody with the flagella. The anti-FAP85 antibody rarely labels axonemes, indicating that the epitopes of FAP85s in the intact axonemes are inaccessible to the antibodies.

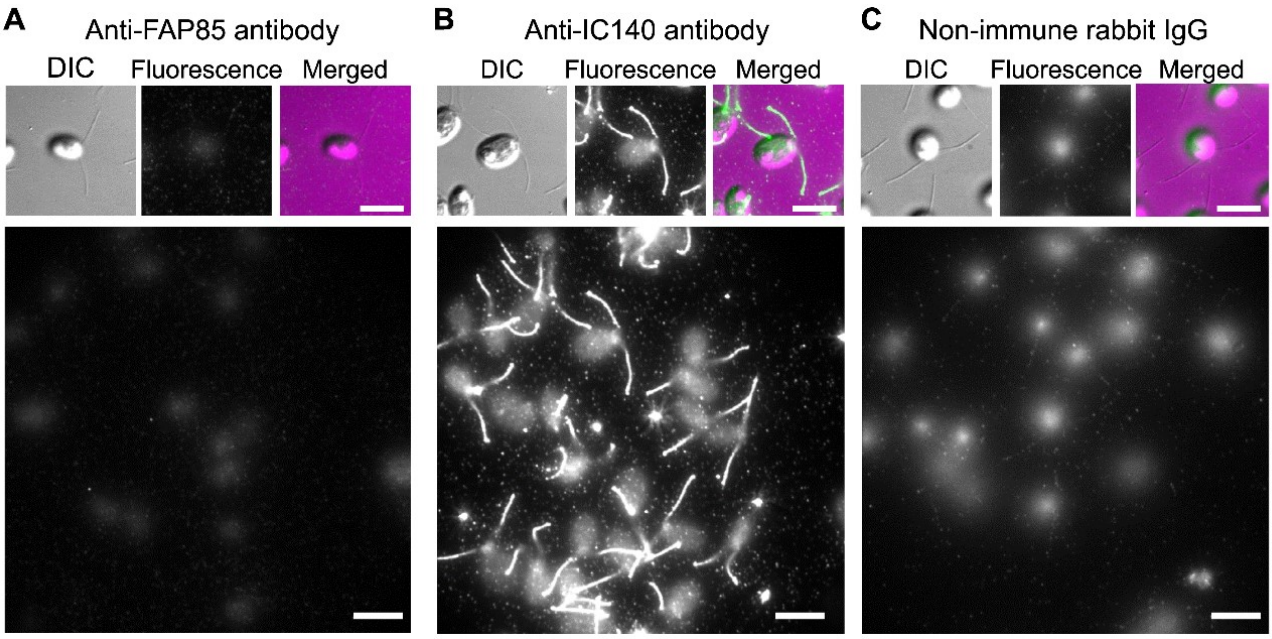

Figure 3.7 **Immunofluorescence microscopy of the wild-type cells**

(A) The cells were incubated with anti-FAP85 antibody followed by labeling with Cy3-conjugated anti-rabbit IgG antibody. The flagella were so weakly stained that the signal was not detected under this condition. (B) The cells were incubated with the anti-IC140 antibody instead of the specific antibody to FAP85 as the positive control. Fluorescence was observed specifically along the length of the axonemes. (C) The cells were treated with non-immune rabbit IgG instead of the specific antibody to FAP85 as the negative control. IgG was present on the cell body and flagella; however, the intensity of the signal was so faint that the fluorescence signals were considered to be derived from nonspecifically-bound IgG. Three small panels on each large panel (images of the entire field of view) represent enlarged views of single cells: differential interference contrast images (the left panels), fluorescence images (the middle panels), merged images (the right panels); scale bars, 10 μm in all panels.

3.4.5 Solubilizing DMTs with Sarkosyl

Immunoblotting analysis of mutant flagella and immunofluorescence microscopy suggested that FAP85 is located in a region of the DMTs where the antibody is unable to interact with epitopes. To expose the epitopes of FAP85 and determine the localization of FAP85 on DMTs, we extensively solubilized axonemes of *pf14* (the mutant missing the radial-spokes) with Sarkosyl. This allowed us to observe protofilaments of DMTs in detail. The demembraned axonemes of *pf14* were pre-treated with 0.6 KCl to remove soluble components from the doublets. At certain concentrations of Sarkosyl (>0.3%), most B-tubules are dissolved while the A-tubules remained almost intact. Thus, the resulting DMTs may be separated by centrifugation into B-tubules, which are dissolved in the supernatant, and A-tubules, which remain in the pellet (Witman et al., 1972).

Treatment of axonemes with 0.2% Sarkosyl showed that proteins over 250 kDa were dissolved in the supernatant; however, most of the tubulin and FAP85 protein remained in the pellet (**Figure 3.8**). Increasing the Sarkosyl concentration to 0.3% resulted in partial dissolution of the DMTs; however, most of the FAP85 remained in the pellet. The supernatants of 0.4%- and 0.7%-Sarkosyl-treated axonemes contained proteins similar to those found in the supernatant of 0.3%-Sarkosyl-treated axonemes. When the concentration of Sarkosyl was increased to 0.7%, DMTs and FAP85 were completely dissolved in the supernatant following overnight treatment.

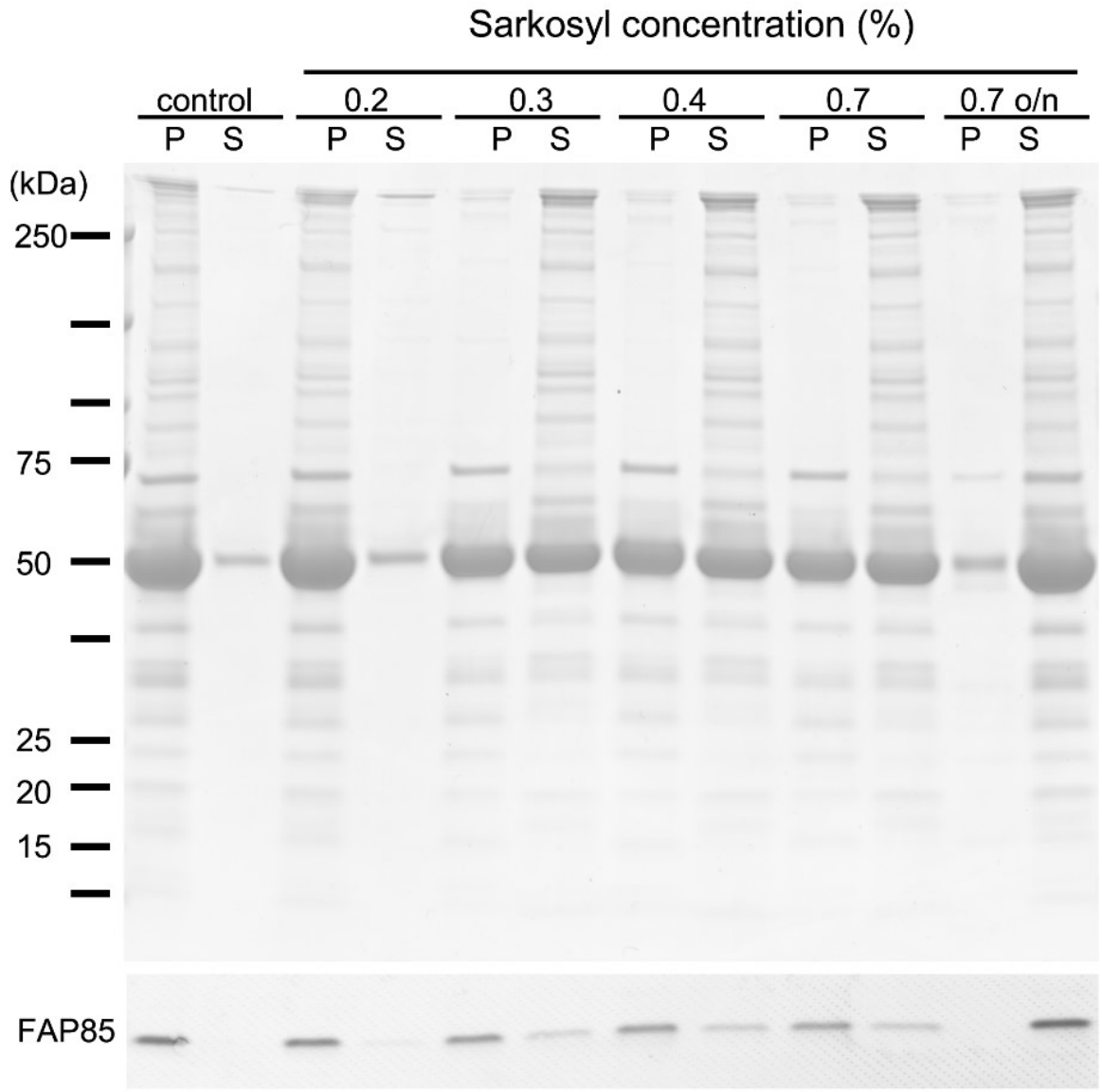

Figure 3.8 **Extraction of FAP85 from the DMTs via treatment with 0.2-0.7% Sarkosyl**

FAP85 was extracted from axonemes of the mutant *pf14* that lacks radial spokes at the various concentration of Sarkosyl. Without Sarkosyl treatment, FAP85 was detected only in the pellet. Increasing concentrations of Sarkosyl facilitated solubility of FAP85 in the supernatant as well as in the pellet. Overnight treatment with 0.7% Sarkosyl (indicated as 0.7 o/n in the figure) resulted in complete dissolution of FAP85 in the supernatant.

To examine the morphology of DMTs in the pellet as a function of the concentrations of Sarkosyl, we dispersed and stained the pellet with uranyl-acetate and observed the pellet using an electron microscope (**Figure 3.9**).

In the presence of 0.2% Sarkosyl, the pellet contained a significant amount of DMTs. Increasing the Sarkosyl concentration to 3% resulted in dissolution of the B-tubules; however, the singlet A-tubules remained (doublets (A- and B-tubules): A-tubule =24:76). The electron microscopic observations showed that the pellets of 0.4%- and 0.7%-Sarkosyl-treated axonemes contained numerous singlet A-tubules without B-tubules. Furthermore, none of the B-tubules were observed following treatment with > 0.5% Sarkosyl, and A-tubules were cleaved into the ribbon structure (Norrander et al., 2000).

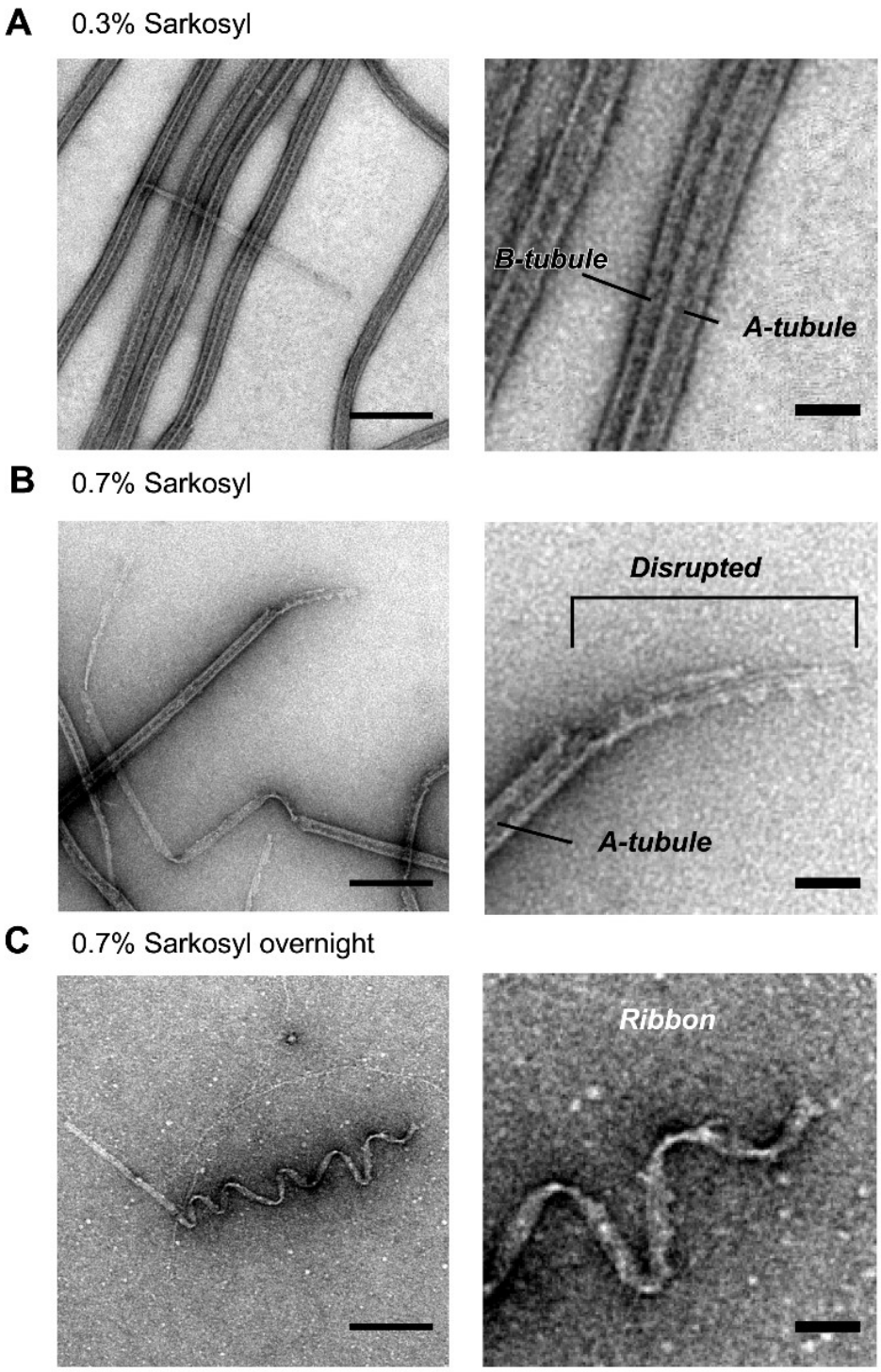

Figure 3.9 **Negatively stained DMTs in the pellet samples of Sarkosyl-treated axonemes**

Negatively stained DMTs in the pellet samples of Sarkosyl-treated axonemes were observed by transmission electron microscopy (bars: the left panels, 200 nm; right panels, 50 nm). (A) Treatment with 0.3% Sarkosyl partially dissolved the DMTs. (B) In the case of 0.7%-Sarkosyl treatment, the B-tubules were completely dissolved but the A-tubules were partially dissolved; the inner wall of the A-tubules were exposed in some regions and protofilaments were partially disrupted. (C) Overnight treatment with 0.7% Sarkosyl resulted in the formation of Sarkosyl-insoluble "ribbon" structures.

The ribbon structures even within the A-tubule were easily identified via their characteristic features, by negative staining; these structures were thick filaments composed of three protofilaments, but were so poorly stained that the details of the protofilaments could not be clearly observed in the structures. Extensive long-term treatment of the axonemes with 0.7% Sarkosyl dissolved the doublets and yielded three protein bands in the pellet sample: tubulin and two proteins with molecular weights of ~70 kDa and ~50 kDa; the latter was distinct from tubulin. According to a previous study (Ikeda et al., 2003), the ~70k-Da protein was Rib72, and the ~50-kDa protein Rib43. Electron microscopic observations of these axoneme samples showed that only ribbon structures were present in the pellet. Under this long-term 0.7% Sarkosyl treatment, FAP85 was found in the supernatant but not in the pellet.

Comparison between the immunoblotting of FAP85 and electron microscopic observations of Sarkosyl-treated axonemes showed that FAP85 emerged in the supernatant concomitantly with the disassembly of A-tubules, but not with B-tubules (**Figure 3.10**). This relationship suggested that FAP85 was associated tightly with the A-tubules. Furthermore, the treatment of axonemes with 0.6 M KCl followed by 0.3-0.7%-Sarkosyl treatment removed almost all of axonemal proteins from DMTs. Even under these conditions, FAP85 was detected in the pellet containing A-tubules. Therefore, the emergence of FAP85 in the supernatant coincided with the disassembly of A-tubules. These observations additionally suggest that the binding of FAP85 to the DMTs was independent of axonemal components such as dyneins, radial spokes, and the central apparatus.

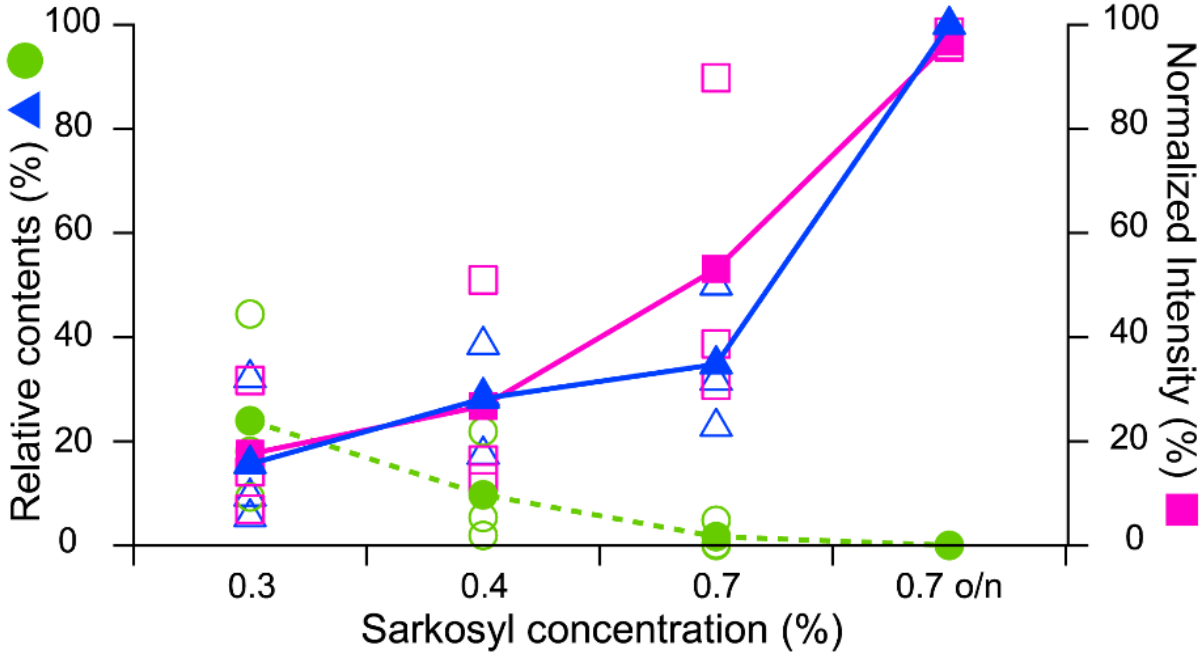

Figure 3.10 **Comparison between the immunoblotting of FAP85 and electron microscopic observations of Sarkosyl-treated axonemes**

The line plots summarize the electron microscopic observations of the fractions of disrupted A-tubules (▲: mean of three experiments; △: individual experiments), B-tubules (●: mean of three experiments; ○: individual experiments) and the amount of FAP85 detected in the supernatant by immunoblotting (■: mean of three experiments; □: individual experiments). The increase in the amount of dissolved FAP85 corresponded to the increase in the proportion of disrupted A-tubules. The observation that FAP85 in the supernatant was concomitant with the disassembly of A-tubules, but not with that of B-tubules, suggested that FAP85 was tightly associated with the A-tubules.

3.4.6 Immuno-gold electron microscopy of FAP85 on DMTs

In order to investigate the presence of FAP85 on the A-tubules, we carried out immuno-gold electron microscopy of the axonemes. Intact DMTs did not show significant immunoreactivity against anti-FAP85 antibody (data not shown). Thus, we focused on the Sarkosyl-treated axonemes. These were first incubated with anti-FAP85 as a primary antibody, and subsequently treated with 10 nm-gold-conjugated anti-rabbit IgG antibody as a secondary antibody. Rabbit IgG obtained from the serum of a non-immunized animal was used as a negative control.

In the presence of 0.3% Sarkosyl, gold particles were found in the partially dissolved axoneme samples only on regions where the inner wall of the A-tubules was exposed (**Figure 3.11 A**). The A-tubules with exposed inner wall were defined according to the width of the tubule: in the negatively stained samples, an inner-wall-exposed A-tubule is wider than an intact one, and a larger number of protofilaments may be recognized in the A-tubule than in an intact one (**Figure 3.11 B, C, D**).

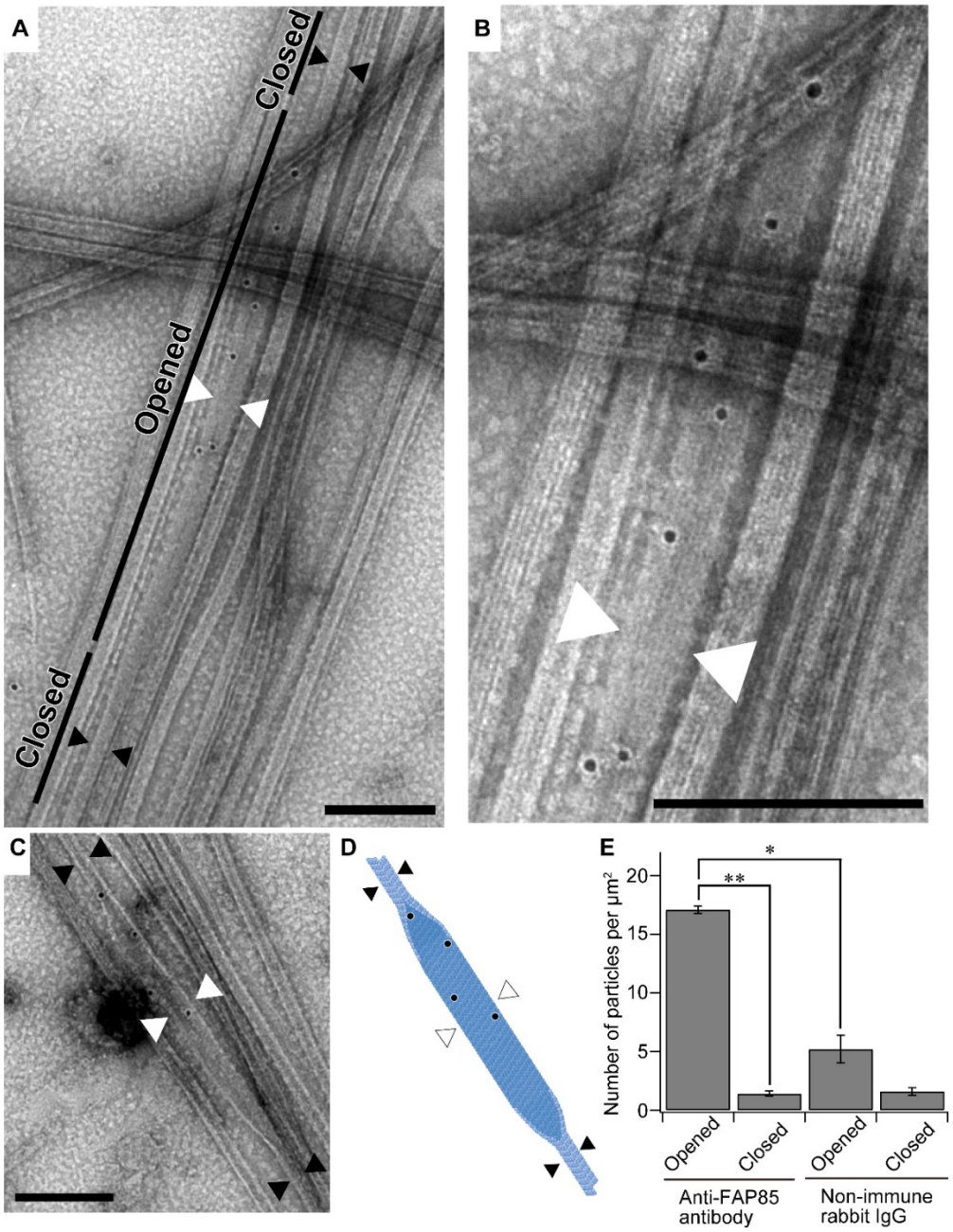

Figure 3.11 **Immunogold electron microscopy of 0.3% Sarkosyl-treated axonemes**

The anti-FAP85 antibody did not frequently label intact A-tubules; however, A-tubules with loss of structural integrity (white arrowhead) were labeled: gold particles were found only where the inner wall of the A-tubule was exposed. (A) A-tubule of DMTs showed both closed and opened parts along the long axis (black and white arrowhead, respectively). (B) A magnified image of the DMTs, with the inner walls were exposed (indicated as "opened"). The gold particles were often found on the exposed portion. (C) Another field of the view showed in (A), confirming that the gold particles were frequently found on the exposed inner wall of the A-tubules. (D) A schematic drawing of the positions of gold particles and the doublet MT exposing the inner walls of the A-tubule shown in (C); bar in (A-C) = 200 nm. (E) The number of gold particles in the opened region per unit area was significantly higher than that in the closed regions and that in the opened region treated with IgG isolated from non-immunized rabbits (**: $p < 0.01$, *:$p<0.05$, χ^2 -test).

The number of gold particles in the exposed region per unit area was significantly higher than that in the intact regions (**Figure 3.11E, Table II**). These results suggest that FAP85 is localized only on the inner wall of the A-tubules.

	Number of particles per μm^2 (Total number of particles)						Un-assigned	Total
	On axonemes				Background			
	Opened region		Closed region					
Anti-FAP85	17.1$^{**, *}$	(542)	1.4	(268)	1.1	(598)	87	1495
Non-immune rabbit IgG	5.2	(108)	1.6	(193)	0.5	(289)	30	620

** compared to the number of gold particles per μm^2 in the closed region ($p < 0.01$ by χ^2-test).

* compared to the number of non-immunized-gold particles per μm^2 in the opened region ($p < 0.05$ by χ^2-test).

Table II. Statistics of immuno-electron microscopy of Sarkosyl-treated DMTs

The gold particles observed on the specimens were categorized into four groups: particles within a distance of 23 nm (the expected distance occupied by primary and secondary antibody complexes) from the edge of the DMTs, further divided into opened and closed groups; particles farther than 23 nm were defined as background, and particles positioned near the edge of the field of view or over unrecognizable materials were unassigned. The number of gold particles per unit length in the exposed region was significantly higher than that in the intact regions ($p < 0.01$, by χ^2 test) and in the exposed region of samples treated with control antibody from non-immunized rabbits ($p < 0.05$, by χ^2 test). The total number of gold particles in the anti-FAP85 sample was also higher than that in normal rabbit IgG samples. The total number of particles were determined in three independent experiments.

However, treatment with 0.7% Sarkosyl resulted in fully dissolved axonemes containing the ribbon structures and individual protofilaments, which were easily identified with negative staining. The immuno-gold particles were rarely observed on the ribbon structures; however, these particles occurred on protofilaments juxtaposed with the ribbon structure. Since the gold particles conjugated to the secondary antibody exhibited various angles of binding to the antigen, these particles were distributed within a circle of 23-nm radius around a fixed point (Norrander et al., 2000), on which the antigen presumably exists. Thus, the precise position and periodicity of the FAP85 antigen could not be determined. However, a line could be drawn wherein we minimized the sum of the squared distances between the gold particles and the given line to as small a value as possible (the best-fit least square line in **Figure 3.12**).

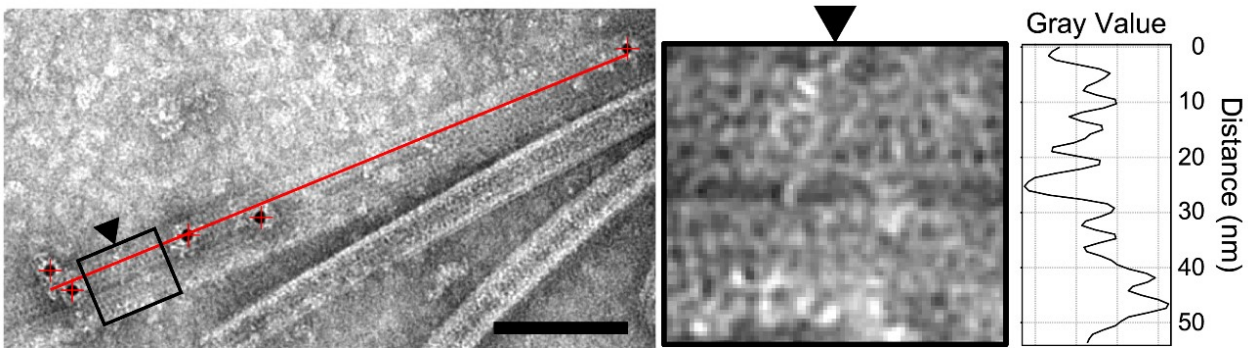

Figure 3.12 **Gold particles on the exposed inner wall of DMTs were found to be aligned along a protofilament.**

Gold particles on the exposed inner wall of DMTs were found to be aligned along a protofilament. The best-fit least square line (red line) was parallel to the protofilament. Since the "Ribbon" structure is identified as the protofilament bundle without showing the details in the bundle, the protofilament number to which the regression lines running parallel can be determined by using the grey scale plot. The enlarged view of the ROI (middle panel) and the plot of the gray value obtained from the ROI (right panel).

Since this line was almost parallel to the protofilament in A-tubule, we considered FAP85 to be attached to the inner wall of A-tubule along a protofilament. Furthermore, the pairwise distance measured between each possible pair of particles was distributed as a multimodal distribution with peaks at integral multiples of ~50 nm (**Figure 3.13**).

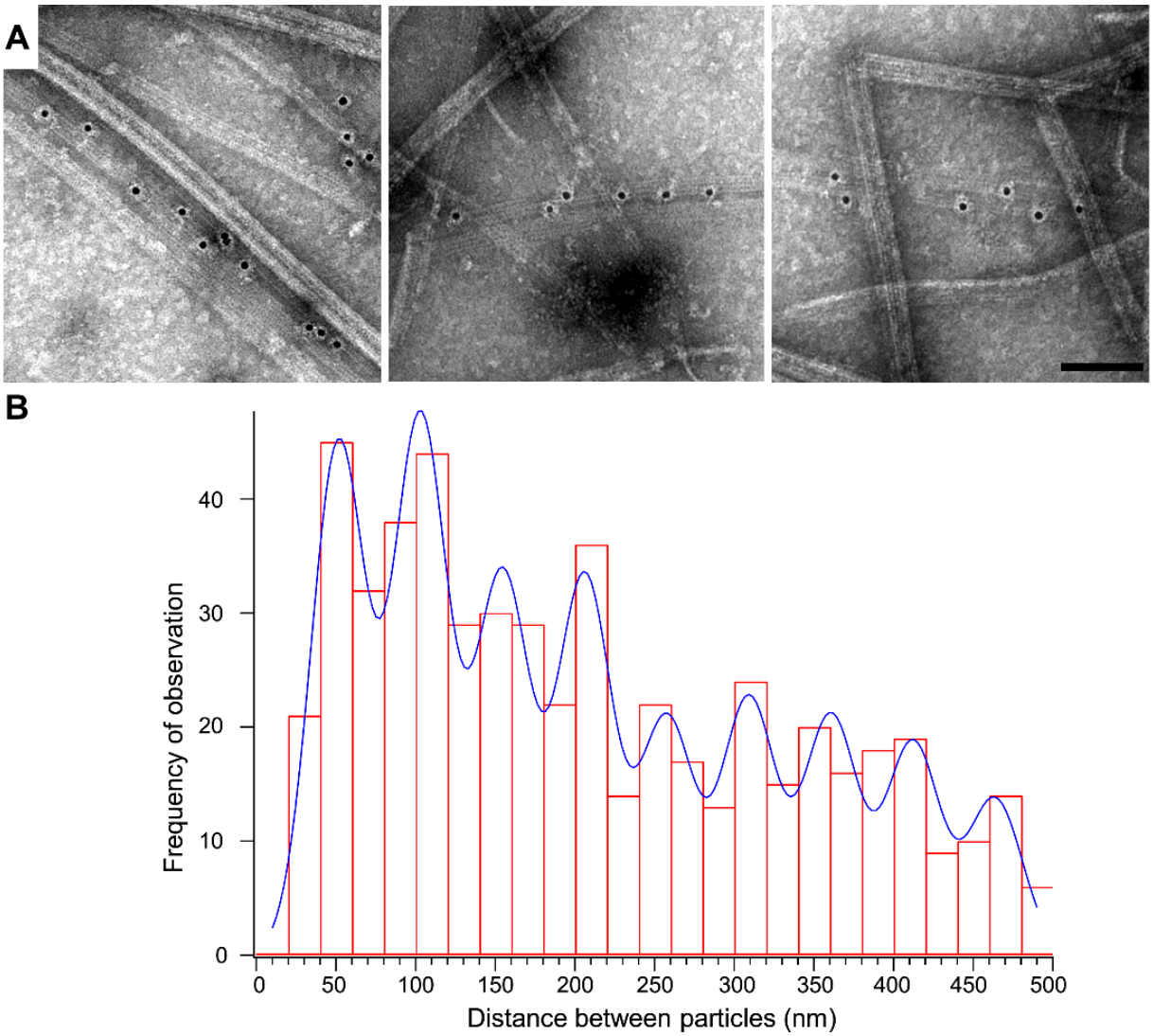

Figure 3.13 **The gold particles on inner-wall-exposed microtubules appeared to have a certain periodicity.**

(A) The gold particles on inner-wall-exposed microtubules appeared to have a certain periodicity. Bar = 100 nm (B) In order to determine the periodicity of FAP85, the distance between the gold particles for all possible pairs (n = 650) were measured. The pairwise distance distribution of the gold particles was a multimodal distribution with peaks emerging at the integral multiples of ~50 nm.

Recombinant FAP85 was examined with negative-staining electron microscopy followed by single-particle analysis. Although numerous aggregates were observed, dispersed non-aggregated particles had non-filamentous but globular molecular shapes (data not shown). In addition, the sequence of FAP85 does not predict the presence of coiled-coil structure. Therefore, we speculate that FAP85 localizes periodically on the inner-wall of A-tubules along a protofilament as a globular structure.

In some cases of partially dissolved axonemes, nine DMTs originating from the same axoneme were found. In this case, immuno-gold particles were found to be labeled on all nine DMTs with exposed inner walls of A-tubules (**Figure 3.14**). The results indicate that FAP85 does not localize in any specific doublets.

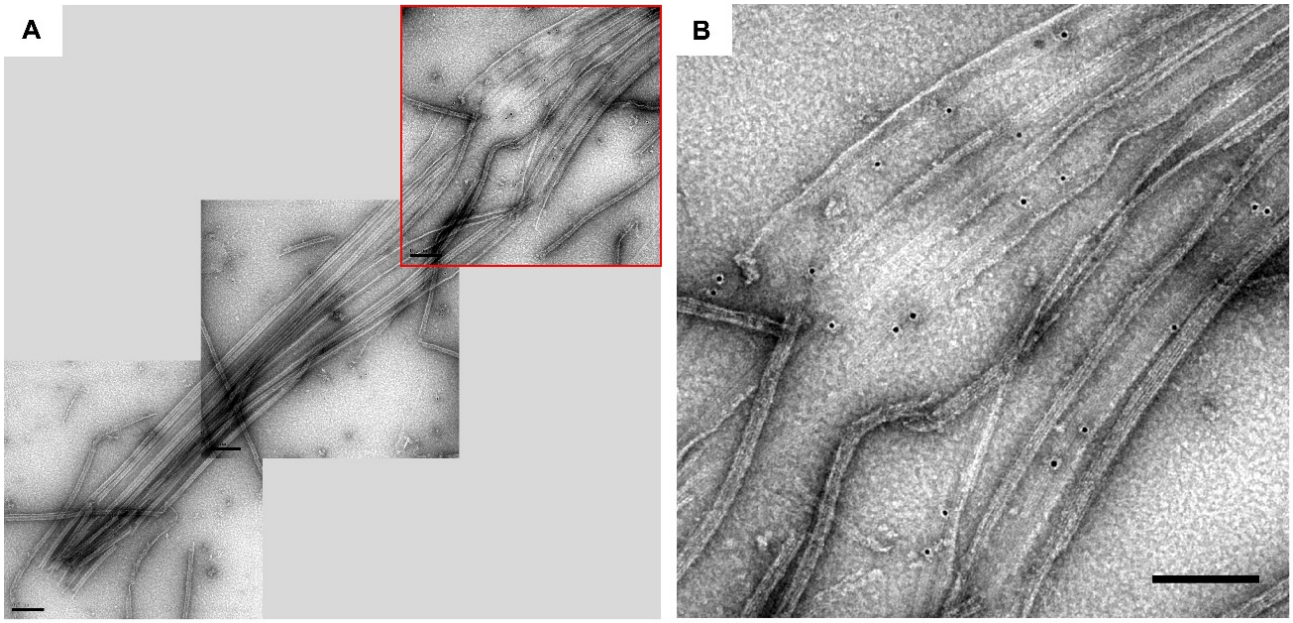

Figure 3.14 **FAP85 is not found in a particular DMT in an axoneme.**

(A) When partially-dissolved axonemes were observed as shown in the tiled three electron micrographs, nine DMTs were easily identified as those originated from the same axoneme. The image enclosed in a red square was enlarged and shown in (B). (B) Gold particles were found to be labeled on all the DMTs exposing the inner walls of A-tubules. This electron micrograph suggests that FAP85 was present in all nine DMTs in an axoneme.

3.4.7 Immunoprecipitation and covalent cross-linking confirmed direct interaction of FAP85 with tubulin

To examine whether native FAP85 directly binds to tubulin or other proteins, we carried out immunoprecipitation of Sarkosyl-treated axonemes with anti-FAP85 antibody (**Figure 3.15**). First, the axonemes were completely dissolved by 0.7% Sarkosyl-treatment overnight and dialyzed against PBS for removal of Sarkosyl from solubilized proteins. The dialysis was additionally expected to facilitate re-binding of FAP85 to the binding partners. The complexes containing FAP85 were precipitated by anti-FAP85 antibody. The precipitated sample contained ~25- kDa and ~50- kDa proteins. The 25-kDa and 50-kDa bands were identified as FAP85 and β-tubulin, respectively, through MALDI-TOF mass spectrometry. No significant trace of the α-tubulin fragments was found in the MALDI-TOF mass spectra. This result suggests that FAP85 is capable of directly binding to β-tubulin in the A-tubules.

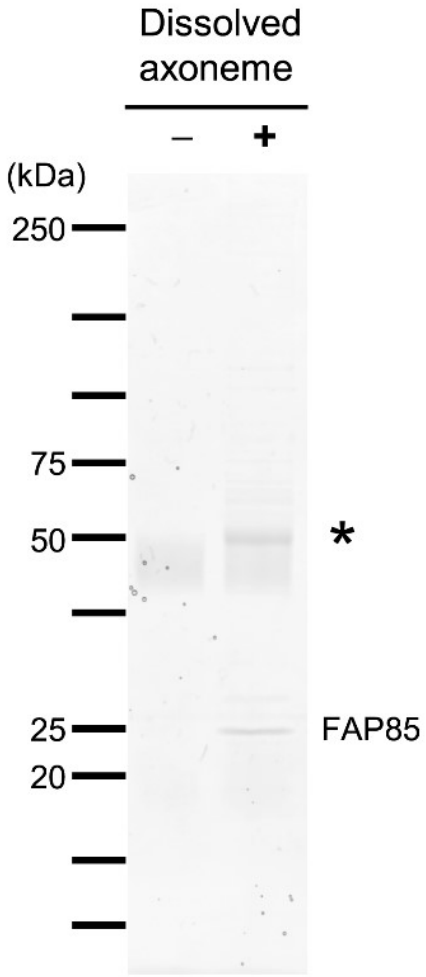

Figure 3.15 **Immunoprecipitation of 0.7% Sarkosyl-dissolved axonemes with the anti-FAP85 antibody**

Immunoprecipitation of 0.7% Sarkosyl-dissolved axonemes with the anti-FAP85 antibody demonstrated that FAP85 bound to a protein of ~50 kDa in size (star), which was identified as β-tubulin by MALDI-TOF MASS.

To examine the interaction of the expressed ProS2-FAP85 with tubulin, we performed immunoprecipitation with anti-ProS2 antibody. Anti-ProS2 antibody was used as this antibody was expected to bind to ProS2-FAP85 without interfering with the interaction between FAP85 and microtubules. The beads with anti-ProS2 antibody were incubated with three samples: tubulin alone, ProS2-FAP85 alone, ProS2-FAP85 with tubulin. The resulting precipitates were analyzed by electrophoresis and immunoblotting with anti-FAP85 antibody (**Figure 3.16**). The bands of anti-ProS2 antibody appeared at around 50 kDa and 25 kDa (**Figure 3.16 lane 1**). ProS2-FAP85 was detected as a protein band around 50 kDa (**Figure 3.16 lane 3**). The immunoprecipitated specimen of the tubulin-ProS2-FAP85 mixture generated a band just above that corresponding to the anti-ProS2 antibody (**Figure 3.16 lane 4**). The band was distinguishable from the band of the anti-ProS2 antibody, and was not seen in other lanes. The position of the additional band was the same as that of the tubulin band (**Figure 3.16 lanes 5 and 6**). Immunoblotting with anti-FAP85 antibody clearly showed that the bands appearing in lanes 3 and 4 corresponded to ProS2-FAP85. These results showed that recombinant ProS2-FAP85 interacts with microtubules.

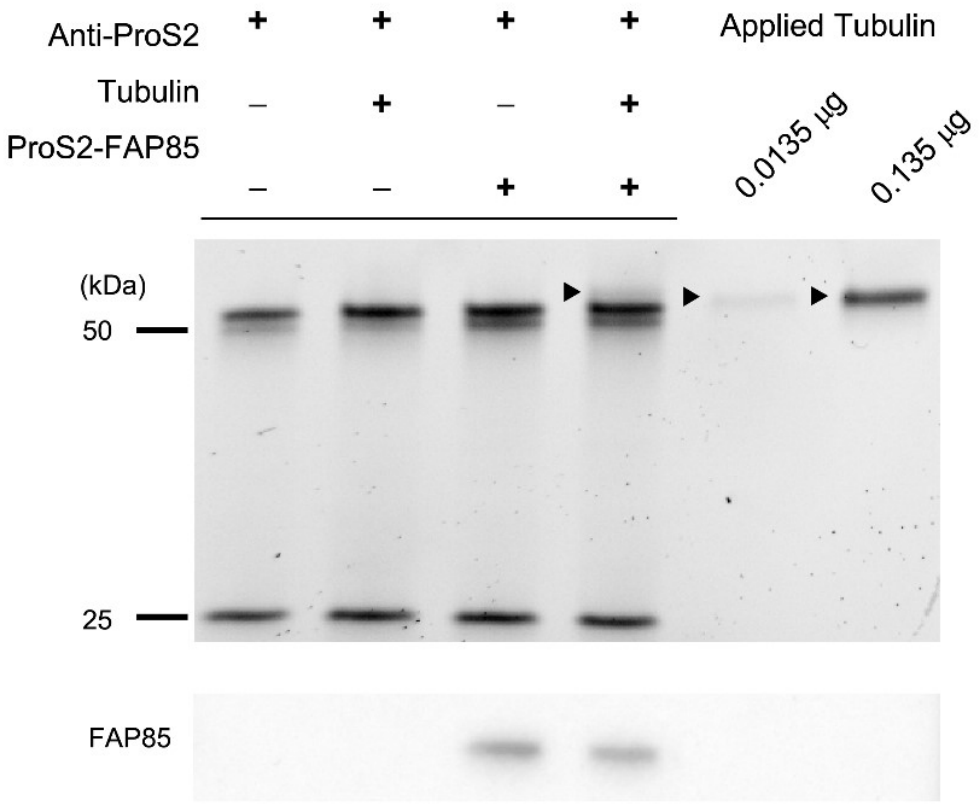

Figure 3.16 **Immunoprecipitation of recombinant FAP85 and porcine brain tubulin with anti-ProS2 antibody**

After the reactions, all samples were subjected to the SDS-PAGE and immunoblotting with anti-FAP85 antibody. Two protein bands of ~25 kDa and ~50 kDa derived from the antibodies were shown in lane 1 and detected in all lanes. The addition of tubulin did not yield any other protein bands. ProS2-FAP85 (~50 kDa) overlapped with the ~50 kDa band, resulting in the appearance of a band thicker than that in lane 1. Binding of ProS2-FAP85 to the anti-ProS2 antibody was confirmed by immunoblotting of anti-FAP85 antibody, as shown in the lower panel. Addition of ProS2-FAP85 and the tubulin mixture yielded an additional protein band that was detected as a ~50-kDa band of antibodies in lane 4. The position of the additional band was the same as that of the tubulin band (lane 5, 6).

3.4.8 l-ethyl-3-(3-dimethylaminopropyl) carbodiimide (EDC) crosslink experiments

Chemical crosslinking provides a direct method for identifying both transient and stable interactions of FAP85 with binding partner proteins. The heterobifunctional, water-soluble, zero-length carbodiimide crosslinker, 1-ethyl-3-(3-dimethylaminopropyl) carbodiimide hydrochloride (EDC) was used to couple FAP85 and its binding partners. If FAP85 physically interacts with binding partners *in vivo*, they may be covalently cross-linked by EDC. The formation of crosslinks between FAP85 and proteins is direct and convincing evidence of their close proximity.

Sarkosyl-treated A-tubules were cross-linked with EDC. The reaction was terminated by addition of several molar excess of 2-mercaptoethanol. The EDC-treated proteins were electrophoresed, and cross-linked FAP85 was detected by immunoblotting with anti-FAP85 antibody (**Figure 3.17**). The untreated sample showed a single band corresponding to the FAP85 (**Figure 3.17 lane 1**). With the increase of the EDC concentrations, two bands (~75 kDa, ~150 kDa) emerged in addition to that of FAP85. The stained protein bands, corresponding to the partner proteins, were excised and analyzed by MALDI-TOF mass spectrometry. As a result, the 150-kDa band contained peptides derived from β-tubulin 2, and the 75-kDa band contained peptides derived from FAP85. This result, combined with immunoblotting data, was consistent with the results from immunoprecipitation, and indicated that the ~75-kDa band was formed by crosslinking of β-tubulin 2 (~50 k Da) and FAP85 (~22 kDa); the ~150-kDa band was formed by crosslinking of two β-tubulin-FAP85 complexes that were in close proximity *in situ*. Although no significant trace of the α-tubulin fragments was found in the MALDI-TOF mass spectra, but we could not exclude the possibilities that the ~150-kDa complex was composed of α-tubulin, β-tubulin, and FAP85 or composed of two β-tubulin and FAP85.

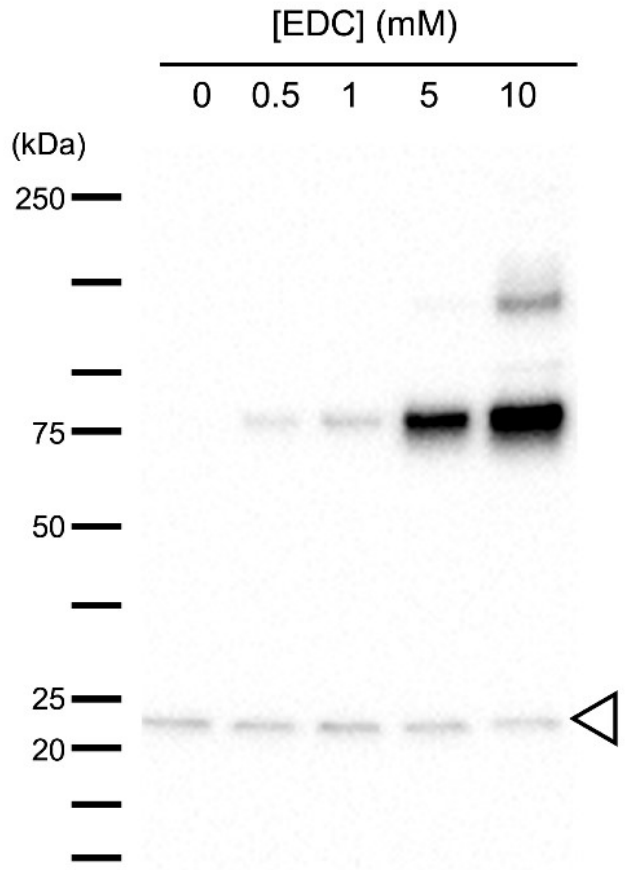

Figure 3.17 **The zero-length chemical crosslinker, EDC, used for the Sarkosyl treated axonemes**

The zero-length chemical crosslinker, EDC, used for the Sarkosyl treated axonemes yielded ~75-kDa and ~150-kDa protein bands detected by immunoblotting against the anti-FAP85 antibody, in addition to the FAP85 bands (white arrowhead). These two bands were identified as β-tubulin-FAP85 complexes by MALDI-TOF-MASS, suggesting that FAP85 was localized quite close to β-tubulin in the axoneme.

3.4.9 Binding affinity of FAP85 to microtubules in vitro

The *in vitro* interactions of FAP85 with tubulin and/or MTs were examined using recombinant ONL-FAP85 and tubulin purified from porcine brains. As both ProS2-FAP85 (~50kDa) and tubulin (~55kDa) have similar molecular weights, they could not be distinguished using SDS-PAGE. Therefore, we used ONL-FAP85 (85 kDa) instead of ProS2-FAP85. Taxol-stabilized microtubules and ONL-FAP85 at various mixing ratios were incubated for 30 min at room temperature (27 ± 2°C), and then spun down at 10,000 rpm for 10 min followed by SDS-PAGE. The density of ONL-FAP85 bands were quantified and the ratio of the amount of bound FAP85 was calculated (**Figure 3.18A, B**). The same procedure was applied to the solution containing only ONL-FAP85, and a small amount of ONL-FAP85 precipitate (~ 5% of the total amount of ONL-FAP85) was generated. Therefore, we concluded that FAP85 directly binds the MTs.

To determine the binding affinity of FAP85, we analyzed the amount of ONL-FAP85 (0.77 μM) depleted from the supernatant with increasing concentrations of stabilized microtubules in co-sedimentation assays **(Figure 3.18C)**. The dissociation constant (K_d) of FAP85 was estimated to be 14.2 ± 3.5 μM (n = 3). Strikingly, in co-polymerization experiments in which tubulin was polymerized in the presence of FAP85, we observed rapid depletion of FAP85 even at concentrations just above the critical concentration of tubulin, indicating that, during tubulin polymerization, FAP85 interacts with the binding sites of the inner wall of MTs (K_d = 4.3 ± 0.6 μM, **Figure 3.18B, C**).

According to the parameters determined by the fit, the stoichiometry of FAP85 to tubulin was about 1:31 in co-polymerization experiments. Assuming that the number of protofilaments in the A-tubule is thirteen, the stoichiometry suggests that two~three tubulin dimers (16~24 nm) interact with one FAP85, which is consistent to a 16nm-structural repeat of MIP1a (Ichikawa et al., 2017).

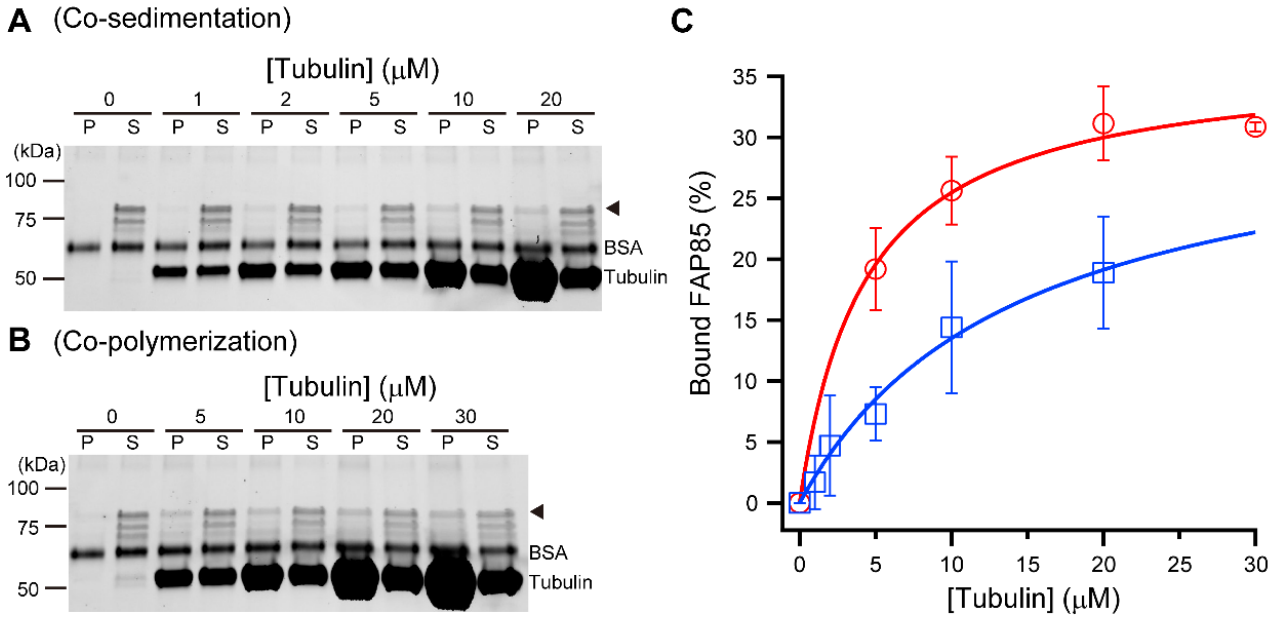

Figure 3.18 **Microtubule-binding assay of FAP85.**

(A) Co-sedimentation of ONL-FAP85 and taxol-stabilized MTs at various concentrations of MTs. ONL-FAP85 (~85 kDa) is indicated by the arrowhead. The band just below ONL-FAP85, which might indicate the degradation/cleavage of ONL-FAP85. (B) Co-polymerization of tubulin with ONL-FAP85. Tubulin at various concentrations was polymerized in the presence of ONL-FAP85. At higher tubulin concentrations, a significant amount of ONL-FAP co-precipitated with the MTs. To indicate the FAP85 bands clearly, the contrast of the gel images was linearly enhanced in (A) and (B). The images of tubulin bands were thus saturated due to the large difference in concentrations between tubulin and FAP85. (C) Percentages of ONL-FAP85 bound to MTs plotted against the tubulin concentrations. The equation, $B = B_{max}\ T / (Kd + T)$ was used to fit the data. Error bars represent the standard deviation (S.D., n = 3). The red curve is the best fit for the data from co-polymerization experiments. Below the critical concentration of tubulin (< 5 μM), no pellet was found after the centrifugation. The blue curve is the best fit for the data from the co-sedimentation experiments. For co-polymerization experiments, B_{max} = 36.4 ± 1.4, K_d = 4.3 ± 0.6 μM and for co-sedimentation experiments, B_{max} = 32.7 ± 4.3 and K_d = 14.2 ± 3.5 μM.

3.4.10 Binding of FAP85 to microtubules altered their dynamics

To examine the effects of FAP85 on microtubule dynamics, we assembled and disassembled microtubules *in vitro*, with or without FAP85, and monitored the turbidity of the microtubule solution at 350 nm **(Figure 3.19)**. Microtubules initiated disassembly when exposed low temperatures: polymerized microtubules were chilled at 15 ± 0.5℃ in the presence or the absence of FAP85, and the change in turbidity was monitored for 5 min. The microtubules without FAP85 were depolymerized almost completely within the observation period. However, the turbidity of microtubules with FAP85 decreased about 0.7 times as slowly as that without FAP85, and remained at a higher level than without FAP85, even after prolonged cold incubation. The depolymerization rates measured were 0.11 ± 0.01 ΔAbs_{350nm}/min (only tubulin) and 0.07 ± 0.01 ΔAbs_{350nm}/min (tubulin with FAP85). The results indicated that FAP85 functions to stabilize microtubules against cold-induced disassembly (**Figure 3.19A**).

On the other hand, polymerization of tubulin was initiated by incubation at 37℃ (**Figure 3.19B**). Within the range of tubulin concentrations (5 to 25 μM), the addition of FAP85 (2.8 μM) resulted in substantially faster polymerization of tubulin into microtubules than without addition of FAP85 (**Figure 3.19C**). At higher concentrations of 30 and 35 μM tubulin, polymerization was so rapid that the acceleration of the polymerization by FAP85 was not obvious. The initial delay in increasing absorbance, however, became shorter in samples with FAP85 than those without FAP85 (**Figure 3.19 D**). To verify MT formation, we observed the resulting solutions with dark-field microscopy and negative staining electron microscopy and confirmed the formation of MTs but no formation of significant bundles in the presence of FAP85 (data not shown) .

These *in vitro* results suggest that FAP85 plays a role in microtubule dynamics by reducing critical concentrations for tubulin polymerization. The critical concentration was calculated from the plot of absorbance at 350 nm, 120 min following initiation of polymerization, as the function of tubulin concentrations (**Figure 3.19E**). The linear fits to the data for 20 to 35 μM tubulin concentrations provided the critical concentrations with or without FAP85; these were 14.3 ± 1.3 μM (n = 3), and 11.4 ± 1.8 μM (n = 3), respectively **(Figure 3.19F)**.

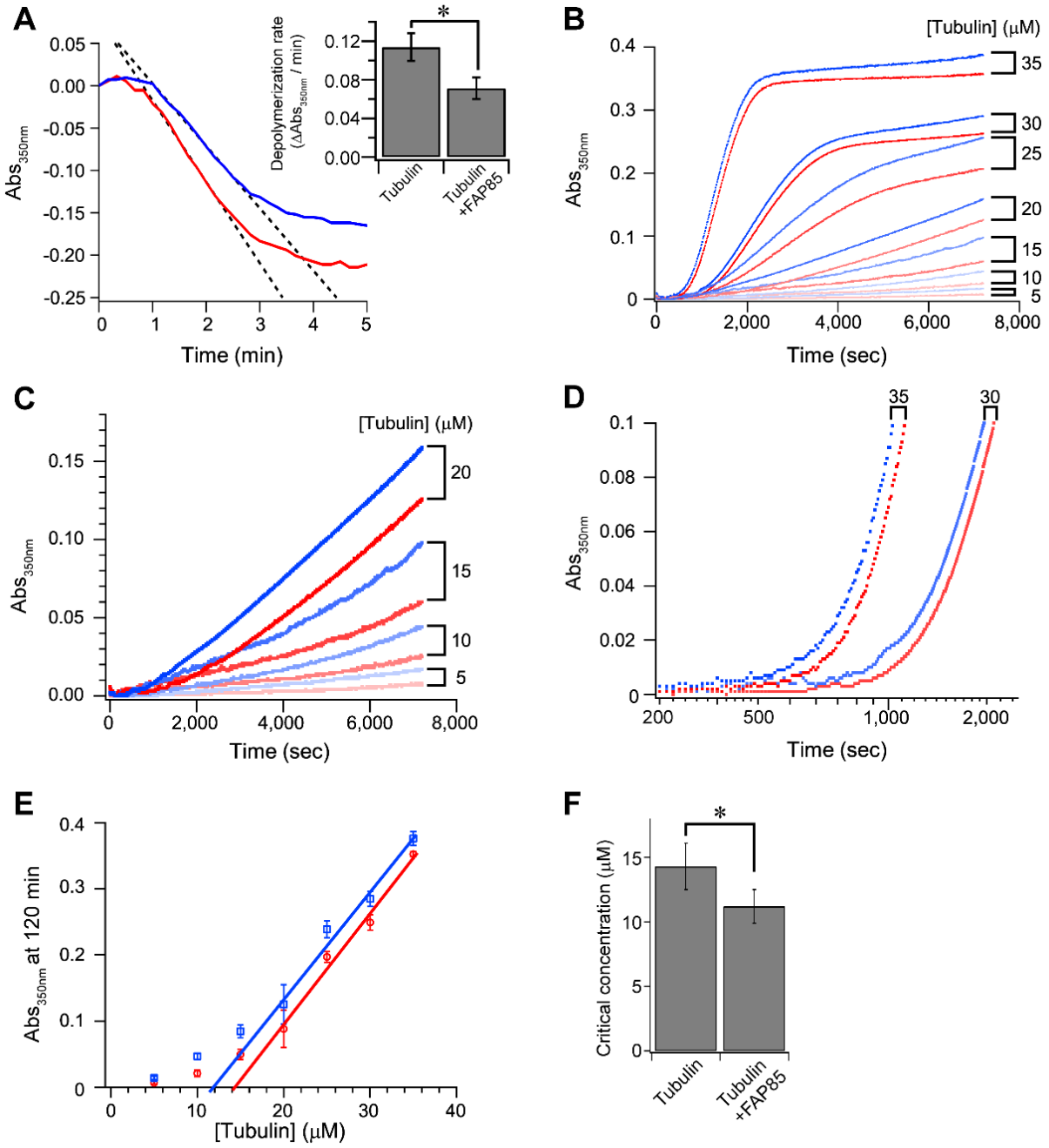

Figure 3.19 **Effects of FAP85 on polymerization and depolymerization kinetic of tubulin**

Tubulin polymerization and depolymerization were monitored as the change in turbidity at 350 nm (Abs_{350nm}). (A) The depolymerization rate (ΔAbs_{350nm}/min) was calculated in the range in which the turbidity decreased linearly (dotted lines). The bar graph indicated the depolymerization rates with (blue line) and without (red line) FAP85, which were 0.071 ± 0.011 min^{-1} and 0.113 ± 0.014 min^{-1}, respectively (n=3, *: $p < 0.05$, Student's t-test). (B) Polymerization of tubulin at various concentrations in the presence (blue lines) or the absence (red lines) of FAP85. The polymerization was initiated by heating the tubulin solution in the micro-plate to 37°C and was monitored for 120 min. (C) Within the range of tubulin concentrations from 5 to 25 μM, the addition of FAP85 resulted in faster polymerization of tubulin into MTs (blue lines compared to red ones).

(D) At concentrations of 30 and 35 μM tubulin, polymerization occurred too rapidly to identify FAP85 effect. However, the initial delay in the increasing absorbance was shorter in the presence of FAP85 (blue lines) than without (red lines). (E and F) The critical concentration of tubulin polymerization was calculated from the plot of Abs_{350nm} at 120 min after the initiation of polymerization. The linear fits to the data obtained for 20, 25, 30, and 35 μM tubulin provide the critical concentrations of tubulin in the presence or absence of FAP85, which were 11.2 ± 1.8 μM and 14.3 ± 1.3 μM, respectively (mean ± the standard deviation [S.D.], n = 3, *: $p < 0.05$, Student's t-test).

3.5 DISCUSSION

In this study, we cloned cDNA of FAP85 and expressed this protein as a ProS2-FAP85 conjugate in *E. coli* cells. The prepared antibody against ProS2-FAP85 recognized native FAP85 with high specificity; therefore, we performed localization and biochemical characterization of FAP85 using this antibody as a probe. Biochemical studies of FAP85 showed that the protein binds directly to microtubules, stabilizing these structures. Immuno-electron microscopy showed that FAP85 localizes on the inner wall of the A-tubule of DMTs. Therefore, we concluded that FAP85 specific to *Chlamydomonas* is an MIP. We additionally showed that FAP85 plays a role in microtubule dynamics by stabilizing microtubules and slight enhancement of the polymerization of tubulins by reducing the critical concentrations of tubulin polymerization.

The original aim of this study was to identify protein components strongly associated with waveform changes coupled with intracellular calcium concentration. *C. reinhardtii* beats two flagella synchronously, with asymmetric effective and recovery strokes. When the intracellular calcium concentration increases, the waveform changes to symmetric type and symmetric bending waves are cyclically produced. This waveform change is observed specifically in *Chlamydomonas*. Thus, we hypothesized that the diversity of flagella-associated proteins found in *Chlamydomonas* contributes to the changes in the bending pattern. Consequently, we focused on FAP85, a putative calcium-binding protein specific to *Chlamydomonas*. We were unable to obtain direct evidence to support the idea that FAP85 is the key component of the waveform changes coupled with Ca^{2+} concentration; however, we established that FAP85 is a MIPs that plays a role in stabilizing DMTs.

3.5.1 FAP85 is a Chlamydomonas-specific component of MIP1a

Advanced electron microscopy, particularly cryo-electron microscopy and cryo-electron tomography, have revealed structures associated with the inner wall of DMTs; filamentous tektin runs along the ribbon structure of the doublets and other globular or filamentous proteins periodically arranged on the inner wall of the DMTs (Linck et al., 2014). These proteins are now known as MIPs

(Heuser et al., 2012; Ichikawa et al., 2017; Maheshwari et al., 2015; Nicastro et al., 2011; Nicastro et al., 2006; Pigino et al., 2012; Sui and Downing, 2006). Recently, Ichikawa and his colleagues performed cryo-electron microscopy, combined with single particle analysis, of *Tetrahymena* cilia, and demonstrated the presence of various types of MIPs and their interactions with tubulin dimers at sub-nanometer-resolutions (Ichikawa et al., 2017). Eleven types of filamentous MIPs running along the PFs were described as filamentous MIPs (fMIPs): there are four fMIPs in the A-tubule and seven fMIPs in the B-tubule. On the basis of the localization of MIPs on the protofilaments, the authors claimed that these proteins play important roles in building DMTs and are involved in their assembly.

Comparison of the axonemes from various types of organisms has enabled the categorization of MIPs into several species; MIP1a, MIP1b, MIP2a, MIP2b, MIP3a, MIP3b, MIP4, and beak (Pigino et al., 2012). Numerous MIPs are well conserved in these organisms; further, *Chlamydomonas*-specific MIPs have also been reported. The axonemal components are arranged on DMTs as axial repeats that are multiples of the 8-nm tubulin-dimer repeat. Major axonemal components, such as dynein arms and radial spokes, have 96-nm structural repeats that represent the fundamental functional unit (Bui et al., 2008; Toba et al., 2015). Previous studies have shown that MIPs possess such structural repeats: MIP1a and MIP1b make an array alternatingly and possess repeats with 16-nm spacing; those of MIP2a exhibit 16- and 32-nm spacing; those of MIP2b, 48-nm spacing; those of MIP3a and MIP3b, 16-nm spacing; and those of MIP4, 48-nm spacing.

Immuno-gold particles of anti-FAP85 antibodies were found along a line parallel to a protofilament in the A-tubule (**Figure 3.12**). The pairwise distance between gold particles was measured and the distribution of the distance was examined. A broad distribution with multimodal peaks, which emerged at integral multiples of ~50 nm, was observed (**Figure 3.13**). As our electron microscopic data strongly indicated that FAP85 is a non-filamentous protein (data not shown), this protein is putatively located along a protofilament as isolated patches.

Furthermore, the location of FAP85 in the A-tubule was estimated by immunoelectron microscopy. The typical example was shown in **(Figure 3.20)**. The gold particles were not found on the ribbon structure, but on or near the protofilaments juxtaposed five to seven protofilaments away from the edge of the ribbon (**Figure 3.20 and Figure 3.12**). This observation suggests that FAP85 is located closer to protofilaments 5th to 7th of the A-tubule (in this paper, we follow the numbering of protofilaments used in Ichikawa et al., 2017).

MIP1 is composed of a large unit, MIP1a, and a small unit, MIP1b, each of which has a periodicity of 16 nm. In addition, MIP1a of *Chlamydomonas* flagella has three slightly different structures that repeat with a 48-nm periodicity (Pigino et al., 2012). This feature has also been observed in sea urchin sperm, but not in *Tetrahymena*. The stoichiometry of FAP85 to tubulin we biochemically determined suggests that two~three tubulin dimers (16~24 nm) interact with one FAP85, which is consistent with a 16-nm structural repeat of MIP1a. A 50-nm structural repeat of FAP85 revealed by immunoelectron microscopy is explained by the triplet MIP1a complex, which could occupy two adjacent binding sites of FAP85 but not the rest where the FAP85 can bind. Three slightly different structures of MIP1a with a 48-nm periodicity would reflect ~50-nm structural repeat of FAP85 *in situ*.

In addition, MIP1a of *Chlamydomonas* was found to be larger than that of sea urchin sperm, and had an obvious structure bridging protofilaments 5th to 7th of A-tubules (these correspond to protofilaments 10th to 8th in the study from Pigino and colleagues [Pigino et al., 2012]). Therefore, comparing the localization and the periodicity of FAP85 on the A-tubule with that of the previously described MIP1a, we concluded that FAP85 is a component of MIP1a.

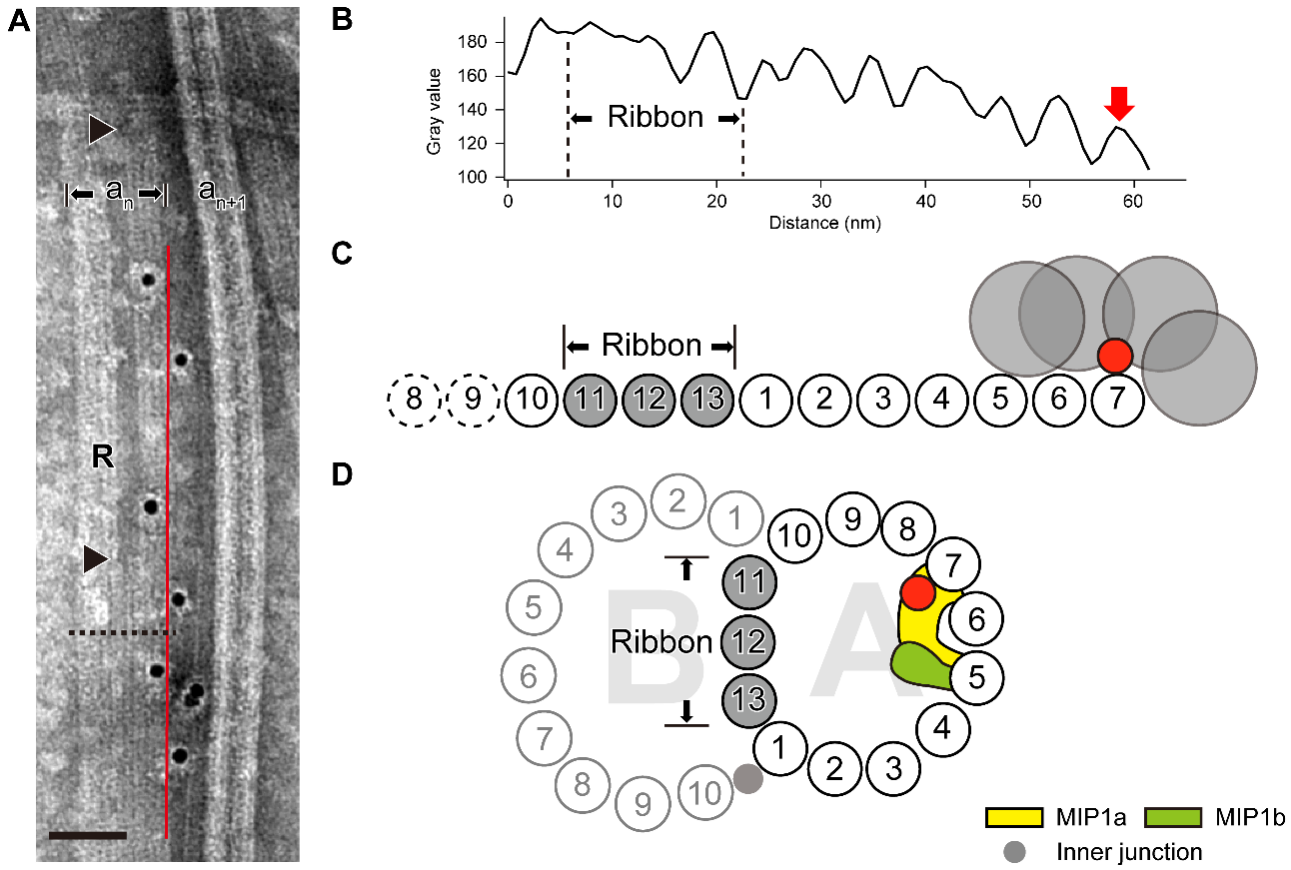

Figure 3.20 **Localization of FAP85 on the A-tubule of Sarkosyl-treated doublet microtubules.**

(A) Immuno-gold labeling of the MT disrupted by Sarkosyl treatment and protofilament ribbons (R) that have been negatively stained with uranyl acetate. The least square method applied on the gold-particle positions provided the line (red line), on which FAP85 molecules were presumably located. The line was almost parallel to the protofilament and there were at least seven protofilaments between the line and the edge of the ribbon structure. The A-tubule was opened (a_n) and partially dissolved indicated by arrows. The opened A-tubule was wider than intact A-tubule (a_{n+1}). Scale bar, 50 nm. (B) Intensity profile of the disrupted A-tubule along the dashed-line in (A). Each peak corresponded to a protofilament. The ribbon corresponded to the region with large gray values with few details. In this electron micrograph (A), the least square line was located on the 7th protofilament (arrow). (C) Diagram illustrating the assignment of numbers to the thirteen protofilaments of the A-tubule of the DMT and localization of FAP85 on the basis of electron microgram (A). The protofilament numbering was done according to Witman et al. (1972) and Linck et al. (2014), assuming that the 8th protofilament was first dissolved by Sarkosyl treatment and the A-tubule was cleft between 7th and 9th protofilaments. The stable ribbon corresponds to the protofilaments 11th -12th -13th, according to Ichikawa et al. (2017). In the electron micrograph (A), immune-gold particles were localized around the antigen (red circle). (D) Diagram illustrating the localization of FAP85 (red circle) in a DMT. On the basis of the observation on the Sarkosyl-treated A-tubule in (A), the position of FAP85 overlapped with MIP1a (the yellow blob) but not MIP1b (the green blob). Modified after (Pigino et al., 2012).

3.5.2 FAP85 is a putative stabilizer of DMTs

Although MIPs have been reported to represent the protein components of DMTs, their composition, biochemical properties, and functions have not been characterized to date. FAP85 is therefore the first MIP to be biochemically characterized. Previous studies suggest that MIPs may contribute to the stability of the DMTs, as the doublets do not fragment even when cilia/flagella beat with a frequency of dozens of hertz. Schaedel et al. (2015) used polymerized MTs and a microfluidic device, and showed that the stiffness of MTs decreased each time they were folded by flow. These findings are similar to other cases of material fatigue; the concentration of mechanical stress on pre-existing defects further decreases microtubule stiffness. Although this study showed that damaged microtubules were recovered by recruiting new tubulin dimers into their lattice *in vitro*, this is not considered to occur in the axoneme as recovery takes tens of seconds. Therefore, the stability of tubulin-tubulin interaction is important in axonemes to prevent microtubule breakage caused by beating. The observed effects of FAP85 on tubulin polymerization and depolymerization imply that this protein plays roles in stabilization of the microtubules.

3.5.3 Doublet microtubule associated proteins contribute to the waveform

. There are several studies that axonemal components associated with DMTs are important to form cilia/flagella waveform. Yanagisawa et al. (2014) showed that FAP20 is the protein constituting inner junction (IJ) where B-tubule and A-tubule are bridged by nontubulin proteins, and FAP20 is essential for the planar asymmetric ciliary-type waveform. In addition to FAP20, the beak-like structure found within the B-tubule of outer doublet 1st, 5th and 6th are supposed to have a role in forming the asymmetrical ciliary-type waveform, because several mutant termed *mbo* lacking the beak-like structure exhibit only a symmetrical flagellar-type waveform (Segal et al., 1984). Furthermore, the beak-like structure exists only in *Chlamydomonas* and was not found in *Tetrahymena* and sea urchin.

Various types of MIPs have been described in a variety of organisms, and divergence of molecular

architecture of MIPs as well as structural similarities have been reported in these organisms. The divergence of these MIPs may lead to various waveform change of the organisms (Pigino et al., 2012). FAP85, which is expected to be one of MIP1a, may contribute to such differences by altering stiffness or other mechanical properties of DMTs. In order to elucidate the precise roles of FAP85, further experiments on flagellar mechanics and structure are needed.

3.6 CONCLUSIONS

Among the EF-hand motif proteins which have not been well characterized in *Chlamydomonas* flagella, I focused on FAP85, specific to *Chlamydomonas* and its relatives. Biochemical and electron microscopic characterizations of FAP85 showed that FAP85 localized on the inner wall of the doublet microtubules *in vivo* and had ability to stabilize microtubules through co-polymerization. According to the results, I conclude that FAP85 is a novel member of microtubule-binding proteins that localizes on the inner wall of the A-tubule and potentially enhances the strength and stability of DMTs as a lining on their inner walls. This study does not directly address the function of FAP85 in *Chlamydomonas* flagella. However, the carefully-performed experiments and scholarly study on the inner axonemal protein FAP85, which is one of a large set of proteins of unknown function in the flagella are likely to help understand flagellar structure and assembly in a range of organisms, while this particular protein appears to be specific to *Chlamydomonas* and its close relatives.

REFERENCES

Adams, G.M., Huang, B., Piperno, G., and Luck, D.J. (1981). Central-pair microtubular complex of *Chlamydomonas* flagella: polypeptide composition as revealed by analysis of mutants. *J. Cell Biol.* **91**, 69-76.

Aoyama, S., and Kamiya, R. (2005). Cyclical interactions between two outer doublet microtubules in split flagellar axonemes. *Biophys. J.* **89**, 3261-3268.

Aoyama, S., and Kamiya, R. (2010). Strikingly fast microtubule sliding in bundles formed by *Chlamydomonas* axonemal dynein. *Cytoskeleton* **67**, 365-372.

Baba, S.A., and Mogami, Y. (1985). An approach to digital image analysis of bending shapes of eukaryotic flagella and cilia. *Cell Motil.* **5**, 475-489.

Bessen, M., Fay, R.B., and Witman, G.B. (1980). Calcium control of waveform in isolated flagellar axonemes of *Chlamydomonas*. *J. Cell Biol.* **86**, 446-455.

Brokaw, C.J. (2002). Computer simulation of flagellar movement VIII: coordination of dynein by local curvature control can generate helical bending waves. *Cell Motil. Cytoskeleton* **53**, 103-124.

Brokaw, C.J. (2014). Computer simulation of flagellar movement X: Doublet pair splitting and bend propagation modeled using stochastic dynein kinetics. *Cytoskeleton* **71**, 273-284.

Brokaw, C.J., and Kamiya, R. (1987). Bending patterns of *Chlamydomonas* flagella: IV. Mutants with defects in inner and outer dynein arms indicate differences in dynein arm function. *Cell Motil. Cytoskeleton* **8**, 68-75.

Brown, J.M., and Witman, G.B. (2014). Cilia and diseases. *Bioscience* **64**, 1126-1137.

Bui, K.H., Sakakibara, H., Movassagh, T., Oiwa, K., and Ishikawa, T. (2008). Molecular architecture of inner dynein arms *in situ* in *Chlamydomonas reinhardtii* flagella. *J. Cell Biol.* **183**, 923-932.

Bui, K.H., Yagi, T., Yamamoto, R., Kamiya, R., and Ishikawa, T. (2012). Polarity and asymmetry in the arrangement of dynein and related structures in the *Chlamydomonas* axoneme. *J. Cell Biol.* **198**, 913-925.

Burgess, S.A., Walker, M.L., Sakakibara, H., Knight, P.J., and Oiwa, K. (2003). Dynein structure and power stroke. *Nature* **421**, 715-718.

Butner, K.A., and Kirschner, M.W. (1991). Tau protein binds to microtubules through a flexible array of distributed weak sites. *J. Cell Biol.* **115**, 717-730.

Carter, A.P., Cho, C., Jin, L., and Vale, R.D. (2011). Crystal structure of the dynein motor domain. *Science* **331**, 1159-1165.

Carter, A.P. (2013). Crystal clear insights into how the dynein motor moves. *J. Cell Sci.* **126**, 705-713.

Carter, A.P., Garbarino, J.E., Wilson-Kubalek, E.M., Shipley, W.E., Cho, C., Milligan, R.A., Vale, R.D., and Gibbons, I.R. (2008). Structure and functional role of dynein's microtubule-binding domain. *Science* **322**, 1691-1695.

Castoldi, M., and Popov, A.V. (2003). Purification of brain tubulin through two cycles of

polymerization–depolymerization in a high-molarity buffer. *Protein Expr. Purif.* **32**, 83-88.

DiPetrillo, C.G., and Smith, E.F. (2010). Pcdp1 is a central apparatus protein that binds Ca^{2+}-calmodulin and regulates ciliary motility. *J. Cell Biol.* **189**, 601-612.

Dutcher, S.K. (1995). Flagellar assembly in two hundred and fifty easy-to-follow steps. *Trends Genet.* **11**, 398-404.

Furuta, A., Yagi, T., Yanagisawa, H., Higuchi, H., and Kamiya, R. (2009). Systematic comparison of *in vitro* motile properties between *Chlamydomonas* wild-type and mutant outer arm dyneins each lacking one of the three heavy chains. *J. Biol. Chem.* **284**, 5927-5935.

Goldstein, D.A. (1979). Calculation of the concentrations of free cations and cation-ligand complexes in solutions containing multiple divalent cations and ligands. *Biophys. J.* **26**, 235-242.

Goodenough, U.W., and Heuser, J.E. (1982). Substructure of the outer dynein arm. *J. Cell Biol.* **95**, 798-815.

Gorman, D.S., and Levine, R. (1965). Cytochrome f and plastocyanin: their sequence in the photosynthetic electron transport chain of *Chlamydomonas reinhardtii*. *Proc. Natl. Acad. Sci. U.S.A.* **54**, 1665-1669.

Haimo, L.T., Telzer, B.R., and Rosenbaum, J.L. (1979). Dynein binds to and crossbridges cytoplasmic microtubules. *Proc. Natl. Acad. Sci. U.S.A.* **76**, 5759-5763.

Heuser, T., Barber, C.F., Lin, J., Krell, J., Rebesco, M., Porter, M.E., and Nicastro, D. (2012). Cryoelectron tomography reveals doublet-specific structures and unique interactions in the I1 dynein. *Proc. Natl. Acad. Sci. U.S.A.* **109**, E2067-E2076.

Heuser, T., Raytchev, M., Krell, J., Porter, M.E., and Nicastro, D. (2009). The dynein regulatory complex is the nexin link and a major regulatory node in cilia and flagella. *J. Cell Biol.* **187**, 921-933.

Hirakawa, E., Higuchi, H., and Toyoshima, Y.Y. (2000). Processive movement of single 22S dynein molecules occurs only at low ATP concentrations. *Proc. Natl. Acad. Sci. U.S.A.* **97**, 2533-2537.

Höök, P., and Vallee, R.B. (2006). The dynein family at a glance. *J. Cell Sci.* **119**, 4369-4371.

Ichikawa, M., Liu, D., Kastritis, P.L., Basu, K., Hsu, T.C., Yang, S., and Bui, K.H. (2017). Subnanometre-resolution structure of the doublet microtubule reveals new classes of microtubule-associated proteins. *Nat. Commun.* **8**, 15035.

Ikeda, K., Brown, J.A., Yagi, T., Norrander, J.M., Hirono, M., Eccleston, E., Kamiya, R., and Linck, R.W. (2003). Rib72, a conserved protein associated with the ribbon compartment of flagellar A-microtubules and potentially involved in the linkage between outer doublet microtubules. *J. Biol. Chem.* **278**, 7725-7734.

Inaba, K. (2012). Regulatory subunits of axonemal dynein. In Handbook of dynein, Keiko Hirose and Linda Amos, ed. (Temasek Boulevard, Singapore: Pan Stanford Publishing Pte. Ltd.), pp.303-324.

Ishikawa, T. (2012). 3D Structures of axonemes. In Handbook of dynein, Keiko Hirose and Linda Amos, ed. (Temasek Boulevard, Singapore: Pan Stanford Publishing Pte. Ltd.), pp. 245-266.

Ishikawa, T., Sakakibara, H., and Oiwa, K. (2007). The architecture of outer dynein arms *in situ*. *J. Mol. Biol.* **368**, 1249-1258

Johnson, K.A., and Borisy, G.G. (1977). Kinetic analysis of microtubule self-assembly *in vitro*. *J. Mol. Biol.* **117**, 1-31.

Kagami, O., and Kamiya, R. (1992). Translocation and rotation of microtubules caused by multiple species of *Chlamydomonas* inner-arm dynein. *J. Cell Sci.* **103**, 653-664.

Kamiya, R., Kurimoto, E., and Muto, E. (1991). Two types of *Chlamydomonas* flagellar mutants missing different components of inner-arm dynein. *J. Cell Biol.* **112**, 441-447.

Kamiya, R., and Okamoto, M. (1985). A mutant of *Chlamydomonas reinhardtii* that lacks the flagellar outer dynein arm but can swim. *J. Cell Sci.* **74**, 181-191.

Kamiya, R., and Witman, G.B. (1984). Submicromolar levels of calcium control the balance of beating between the two flagella in demembranated models of *Chlamydomonas*. *J. Cell Biol.* **98**, 97-107.

Kamiya, R., and Yagi, T. (2014). Functional diversity of axonemal dyneins as assessed by *in vitro* and *in vivo* motility assays of *Chlamydomonas* mutants. *Zoolog. Sci.* **31**, 633-644.

Kato, T., Kagami, O., Yagi, T., and Kamiya, R. (1993). Isolation of two species of *Chlamydomonas reinhardtii* flagellar mutants, *ida*5 and *ida*6, that lack a newly identified heavy chain of the inner dynein arm. *Cell Struct. Funct.* **18**, 371-377.

Kato-Minoura, T., Hirono, M., and Kamiya, R. (1997). *Chlamydomonas* inner-arm dynein mutant, *ida*5, has a mutation in an actin-encoding gene. *J. Cell Biol.* **137**, 649-656.

King, S.M., Wilkerson, C.G., and Witman, G.B. (1991). The M_r 78,000 intermediate chain of *Chlamydomonas* outer arm dynein interacts with alpha-tubulin *in situ*. *J. Biol. Chem.* **266**, 8401-8407.

King, S.M., and Patel-King, R.S. (1995). Identification of a Ca^{2+}-binding light chain within *Chlamydomonas* outer arm dynein. *J. Cell Sci.* **108**, 3757-3764.

Kon, T., Imamula, K., Roberts, A.J., Ohkura, R., Knight, P.J., Gibbons, I.R., Burgess, S.A., and Sutoh, K. (2009). Helix sliding in the stalk coiled coil of dynein couples ATPase and microtubule binding. *Nat. Struct. Mol. Biol.* **16**, 325-333.

Kon, T., Nishiura, M., Ohkura, R., Toyoshima, Y.Y., and Sutoh, K. (2004). Distinct functions of nucleotide-binding/hydrolysis sites in the four AAA Modules of cytoplasmic dynein. *Biochemistry* **43**, 11266-11274.

Kon, T., Oyama, T., Shimo-Kon, R., Imamula, K., Shima, T., Sutoh, K., and Kurisu, G. (2012). The 2.8 Å crystal structure of the dynein motor domain. *Nature* **484**, 345-350.

Kurimoto, E., and Kamiya, R. (1991). Microtubule sliding in flagellar axonemes of *Chlamydomonas* mutants missing inner- or outer-arm dynein: Velocity measurements on new types of mutants by an improved method. *Cell Motil. Cytoskeleton* **19**, 275-281.

Lesich, K.A., dePinho, T.G., Pelle, D.W., and Lindemann, C.B. (2016). Mechanics of the eukaryotic flagellar axoneme: Evidence for structural distortion during bending. *Cytoskeleton* **73**, 233-245.

Lin, H., Zhang, Z., Guo, S., Chen, F., Kessler, J.M., Wang, Y.M., and Dutcher, S.K. (2015). A NIMA-related kinase suppresses the flagellar instability associated with the loss of multiple axonemal structures. *PLoS Genet.* **11**, e1005508.

Lin, J., Okada, K., Raytchev, M., Smith, M.C., and Nicastro, D. (2014). Structural mechanism of the dynein power stroke. *Nat. Cell Biol.* **16**, 479-485.

Linck, R., Fu, X., Lin, J., Ouch, C., Schefter, A., Steffen, W., Warren, P., and Nicastro, D. (2014). Insights into the structure and function of ciliary and flagellar doublet microtubules: tektins, Ca^{2+}-binding proteins, and stable protofilaments. *J. Biol. Chem.* **289**, 17427-17444.

Lindemann, C.B. (1994). A "Geometric clutch" hypothesis to explain oscillations of the axoneme of cilia and flagella. *J. Theor. Biol.* **168**, 175-189.

Maheshwari, A., Obbineni, J M., Bui, K.H., Shibata, K., Toyoshima, Y.Y., and Ishikawa, T. (2015). α- and β-tubulin lattice of the axonemal microtubule doublet and binding proteins revealed by single particle cryo-electron microscopy and tomography. *Structure* **23**, 1584-1595.

Merchant, S.S., Prochnik, S.E., Vallon, O., Harris, E.H., Karpowicz, S.J., Witman, G.B., Terry, A., Salamov, A., Fritz-Laylin, L.K., Maréchal-Drouard, L., Marshall, W.F., Qu, L.-H., Nelson, D.R., Sanderfoot, A.A., Spalding, M.H., Kapitonov, V.V., Ren, Q., Ferris, P., Lindquist, E., Shapiro, H., Lucas, S.M., Grimwood, J., Schmutz, J., Cardol, P., Cerutti, H., Chanfreau, G., Chen, C.-L., Cognat, V., Croft, M.T., Dent, R., Dutcher, S., Fernández, E., Fukuzawa, H., González-Ballester, D., González-Halphen, D., Hallmann, A., Hanikenne, M., Hippler, M., Inwood, W., Jabbari, K., Kalanon, M., Kuras, R., Lefebvre, P.A., Lemaire, S.D., Lobanov, A.V., Lohr, M., Manuell, A., Meier, I., Mets, L., Mittag, M., Mittelmeier, T., Moroney, J.V., Moseley, J., Napoli, C., Nedelcu, A.M., Niyogi, K., Novoselov, S.V., Paulsen, I.T., Pazour, G., Purton, S., Ral, J.-P., Riaño-Pachón, D.M., Riekhof, W., Rymarquis, L., Schroda, M., Stern, D., Umen, J., Willows, R., Wilson, N., Zimmer, S.L., Allmer, J., Balk, J., Bisova, K., Chen, C.-J., Elias, M., Gendler, K., Hauser, C., Lamb, M.R., Ledford, H., Long, J.C., Minagawa, J., Page, M.D., Pan, J., Pootakham, W., Roje, S., Rose, A., Stahlberg, E., Terauchi, A.M., Yang, P., Ball, S., Bowler, C., Dieckmann, C.L., Gladyshev, V.N., Green, P., Jorgensen, R., Mayfield, S., Mueller-Roeber, B., Rajamani, S., Sayre, R.T., Brokstein, P., Dubchak, I., Goodstein, D., Hornick, L., Huang, Y.W., Jhaveri, J., Luo, Y., Martínez, D., Ngau, W.C.A., Otillar, B., Poliakov, A., Porter, A., Szajkowski, L., Werner, G., Zhou, K., Grigoriev, I.V., Rokhsar, D.S. and Grossman, A.R. (2007). The *Chlamydomonas* genome reveals the evolution of key animal and plant functions. *Science* **318**, 245-250.

Mimori, Y., and Miki-Nomura, T. (1994). ATP-induced sliding of microtubules on tracks of 22S dynein molecules aligned with the same polarity. *Cell Motil. Cytoskeleton* **27**, 180-191.

Mitchell, D.R., and Rosenbaum, J.L. (1985). A motile *Chlamydomonas* flagellar mutant that lacks outer dynein arms. *J. Cell Biol.* **100**, 1228-1234.

Mitchison, T.J., and Mitchison, H.M. (2010). Cell biology: How cilia beat. *Nature* **463**, 308-309.

Mizuno, K., Padma, P., Konno, A., Satouh, Y., Ogawa, K., and Inaba, K. (2009). A novel neuronal calcium sensor family protein, calaxin, is a potential Ca^{2+}-dependent regulator for the outer arm dynein of metazoan cilia and flagella. *Biol. Cell* **101**, 91-103.

Mizuno, K., Shiba, K., Okai, M., Takahashi, Y., Shitaka, Y., Oiwa, K., Tanokura, M., and Inaba, K. (2012). Calaxin drives sperm chemotaxis by Ca^{2+}-mediated direct modulation of a dynein motor. *Proc. Natl. Acad. Sci. U.S.A.* **109**, 20497-20502.

Morita, Y., and Shingyoji, C. (2004). Effects of imposed bending on microtubule sliding in sperm flagella. *Curr. Biol.* **14**, 2113-2118.

Myster, S.H., Knott, J.A., O'Toole, E., and Porter, M.E. (1997). The *Chlamydomonas* Dhc1 gene encodes a dynein heavy chain subunit required for assembly of the I1 inner arm complex. *Mol. Biol. Cell* **8**, 607-620.

Nakano, I., Kobayashi, T., Yoshimura, M., and Shingyoji, C. (2003). Central-pair-linked regulation of microtubule sliding by calcium in flagellar axonemes. *J. Cell Sci.* **116**, 1627-1636.

Nicastro, D., Fu, X., Heuser, T., Tso, A., Porter, M.E., and Linck, R.W. (2011). Cryo-electron tomography reveals conserved features of doublet microtubules in flagella. *Proc. Natl. Acad. Sci. U.S.A.* **108**, E845-E853.

Nicastro, D., Schwartz, C., Pierson, J., Gaudette, R., Porter, M.E., and McIntosh, J.R. (2006). The molecular architecture of axonemes revealed by cryoelectron tomography. *Science* **313**, 944-948.

Norrander, J.M., deCathelineau, A.M., Brown, J.A., Porter, M.E., and Linck, R.W. (2000). The Rib43a protein is associated with forming the specialized protofilament ribbons of flagellar microtubules in *Chlamydomonas*. *Mol. Biol. Cell* **11**, 201-215.

Oda, T., Abe, T., Yanagisawa, H., and Kikkawa, M. (2016). Docking-complex-independent alignment of *Chlamydomonas* outer dynein arms with 24-nm periodicity *in vitro*. *J. Cell Sci.* **129**, 1547-1551.

Oda, T., Hirokawa, N., and Kikkawa, M. (2007). Three-dimensional structures of the flagellar dynein-microtubule complex by cryoelectron microscopy. *J. Cell Biol.* **177**, 243-252.

Oda, T., Yanagisawa, H., Kamiya, R., and Kikkawa, M. (2014). A molecular ruler determines the repeat length in eukaryotic cilia and flagella. *Science* **346**, 857-860.

Ogura, T., and Wilkinson, A.J. (2001). AAA+ superfamily ATPases: common structure–diverse function. *Genes Cells* **6**, 575-597.

Owa, M., Furuta, A., Usukura, J., Arisaka, F., King, S.M., Witman, G.B., Kamiya, R., and Wakabayashi, K. (2014). Cooperative binding of the outer arm-docking complex underlies the regular arrangement of outer arm dynein in the axoneme. *Proc. Natl. Acad. Sci. U.S.A.* **111**, 9461-9466.

Patel-King, R.S., Benashski, S.E., Harrison, A., and King, S.M. (1996). Two functional thioredoxins containing redox-sensitive vicinal dithiols from the *Chlamydomonas* outer dynein arm. *J. Biol. Chem.* **271**, 6283-6291.

Pazour, G.J., Agrin, N., Leszyk, J., and Witman, G.B. (2005). Proteomic analysis of a eukaryotic cilium. *J. Cell Biol.* **170**, 103-113.

Perrone, C.A., Yang, P., O'Toole, E., Sale, W.S., and Porter, M.E. (1998). The *Chlamydomonas* IDA7 locus encodes a 140-kDa dynein intermediate chain required to assemble the I1 inner arm complex. *Mol. Biol. Cell* **9**, 3351-3365.

Pigino, G., Bui, K.H., Maheshwari, A., Lupetti, P., Diener, D., and Ishikawa, T. (2011). Cryoelectron tomography of radial spokes in cilia and flagella. *J. Cell Biol.* **195**, 673-687.

Pigino, G., Maheshwari, A., Bui, K.H., Shingyoji, C., Kamimura, S., and Ishikawa, T. (2012). Comparative structural analysis of eukaryotic flagella and cilia from *Chlamydomonas*,

Tetrahymena, and sea urchins. *J. Struct. Biol.* **178**, 199-206.

Piperno, G., Huang, B., and Luck, D.J. (1977). Two-dimensional analysis of flagellar proteins from wild-type and paralyzed mutants of *Chlamydomonas reinhardtii*. *Proc. Natl. Acad. Sci. U.S.A.* **74**, 1600-1604.

Riedel-Kruse, I.H., Hilfinger, A., Howard, J., and Jülicher, F. (2007). How molecular motors shape the flagellar beat. *HFSP J.* **1**, 192-208.

Roberts, A.J., Kon, T., Knight, P.J., Sutoh, K., and Burgess, S.A. (2013). Functions and mechanics of dynein motor proteins. *Nat. Rev. Mol. Cell Biol.* **14**, 713-726.

Rupp, G., and Porter, M.E. (2003). A subunit of the dynein regulatory complex in *Chlamydomonas* is a homologue of a growth arrest–specific gene product. *J. Cell Biol.* **162**, 47-57.

Sakakibara, H., Kojima, H., Sakai, Y., Katayama, E., and Oiwa, K. (1999). Inner-arm dynein c of *Chlamydomonas* flagella is a single-headed processive motor. *Nature* **400**, 586-590.

Sakakibara, H., and Kamiya, R. (1989). Functional recombination of outer dynein arms with outer arm-missing flagellar axonemes of a *Chlamydomonas* mutant. *J. Cell Sci.* **92**, 77-83.

Sakakibara, H., and Nakayama, H. (1998). Translocation of microtubules caused by the αβ, β and γ outer arm dynein subparticles of *Chlamydomonas*. *J. Cell Sci.* **111**, 1155-1164.

Sakakibara, H., and Oiwa, K. (2011). Molecular organization and force-generating mechanism of dynein. *FEBS J.* **278**, 2964-2979.

Sakato, M., Sakakibara, H., and King, S.M. (2007). *Chlamydomonas* outer arm dynein alters conformation in response to Ca^{2+}. *Mol. Biol. Cell* **18**, 3620-3634.

Sanders, M.A., and Salisbury, J.L. (1995). Immunofluorescence microscopy of cilia and flagella. *Methods Cell Biol.* **47**, 163-169.

Sartori, P., Geyer, V.F., Scholich, A., Jülicher, F., and Howard, J. (2016). Dynamic curvature regulation accounts for the symmetric and asymmetric beats of *Chlamydomonas* flagella. *eLife* **5**, e13258.

Schaedel, L., John, K., Gaillard, J., Nachury, M.V., Blanchoin, L., and Thery, M. (2015). Microtubules self-repair in response to mechanical stress. *Nat. Mater.* **14**, 1156-1163.

Schmidt, H., Zalyte, R., Urnavicius, L., and Carter, A.P. (2014). Structure of human cytoplasmic dynein-2 primed for its power stroke. *Nature* **518**, 435-438.

Schmidt, H., and Carter, A.P. (2016). Review: Structure and mechanism of the dynein motor ATPase. *Biopolymers* **105**, 557-567.

Segal, R.A., Huang, B., Ramanis, Z., and Luck, D.J.L. (1984). Mutant strains of *Chlamydomonas reinhardtii* that move backwards only. *J. Cell Biol.* **98**, 2026-2034.

Shingyoji, C., Murakami, A., and Takahashi, K. (1977). Local reactivation of triton-extracted flagella by iontophoretic application of ATP. *Nature* **265**, 269-270.

Silflow, C.D., and Lefebvre, P.A. (2001). Assembly and motility of eukaryotic cilia and flagella. Lessons from *Chlamydomonas reinhardtii*. *Plant Physiol.* **127**, 1500-1507.

Smith, E.F., and Sale, W.S. (1992a). Regulation of dynein-driven microtubule sliding by the radial spokes in flagella. *Science* **257**, 1557-1559.

Smith, E.F., and Sale, W.S. (1992b). Structural and functional reconstitution of inner dynein arms in *Chlamydomonas* flagellar axonemes. *J. Cell Biol.* **117**, 573-581.

Smith, E.F., and Lefebvre, P.A. (1997). The role of central apparatus components in flagellar motility and microtubule assembly. *Cell Motil. Cytoskeleton* **38**, 1-8.

Spudich, J.A. (1994). How molecular motors work. *Nature* **372**, 515-518.

Sugino, K., and Naitoh, Y. (1982). Simulated cross-bridge patterns corresponding to ciliary beating in *Paramecium*. *Nature* **295**, 609-611.

Sui, H., and Downing, K.H. (2006). Molecular architecture of axonemal microtubule doublets revealed by cryo-electron tomography. *Nature* **442**, 475-478.

Takai, A., Nakano, M., Saito, K., Haruno, R., Watanabe, T.M., Ohyanagi, T., Jin, T., Okada, Y., and Nagai, T. (2015). Expanded palette of nano-lanterns for real-time multicolor luminescence imaging. *Proc. Natl. Acad. Sci. U.S.A.* **112**, 4352-4356.

Toba, S., Iwamoto, H., Kamimura, S., and Oiwa, K. (2015). X-ray fiber diffraction recordings from oriented demembranated *Chlamydomonas* flagellar axonemes. *Biophys. J.* **108**, 2843-2853.

Ueno, H., Bui, K.H., Ishikawa, T., Imai, Y., Yamaguchi, T., and Ishikawa, T. (2014). Structure of dimeric axonemal dynein in cilia suggests an alternative mechanism of force generation. *Cytoskeleton* **71**, 412-422.

Ueno, H., Yasunaga, T., Shingyoji, C., and Hirose, K. (2008). Dynein pulls microtubules without rotating its stalk. *Proc. Natl. Acad. Sci. U.S.A.* **105**, 19702-19707.

Wakabayashi, K., Yagi, T., and Kamiya, R. (1997). Ca^{2+}-dependent waveform conversion in the flagellar axoneme of *Chlamydomonas* mutants lacking the central-pair/radial spoke system. *Cell Motil. Cytoskeleton* **38**, 22-28.

Witman, G.B., Carlson, K., Berliner, J., and Rosenbaum, J.L. (1972). *Chlamydomonas* flagella : I. Isolation and electrophoretic analysis of microtubules, matrix, membranes, and mastigonemes. *J. Cell Biol.* **54**, 507-539.

Witman, G.B., Plummer, J., and Sander, G. (1978). *Chlamydomonas* flagellar mutants lacking radial spokes and central tubules. Structure, composition, and function of specific axonemal components. *J. Cell Biol.* **76**, 729-747.

Yamada, A., Yamaga, T., Sakakibara, H., Nakayama, H., and Oiwa, K. (1998). Unidirectional movement of fluorescent microtubules on rows of dynein arms of disintegrated axonemes. *J. Cell Sci.* **111**, 93-98.

Yanagisawa, H.A., Mathis, G., Oda, T., Hirono, M., Richey, E.A., Ishikawa, H., Marshall, W.F., Kikkawa, M., and Qin, H. (2014). FAP20 is an inner junction protein of doublet microtubules essential for both the planar asymmetrical waveform and stability of flagella in *Chlamydomonas*. *Mol. Biol. Cell* **25**, 1472-1483.

Yang, P., Diener, D.R., Rosenbaum, J.L., and Sale, W.S. (2001). Localization of calmodulin and dynein light chain LC8 in flagellar radial spokes. *J. Cell Biol.* **153**, 1315-1326.

Yang, P., Yang, C., Wirschell, M., and Davis, S. (2009). Novel LC8 mutations have disparate effects on the assembly and stability of flagellar complexes. *J. Biol. Chem.* **284**, 31412-31421.

Yang, P., and Sale, W.S. (1998). The M_r 140,000 intermediate chain of *Chlamydomonas* flagellar inner arm dynein is a WD-repeat protein implicated in dynein arm anchoring. *Mol. Biol. Cell* **9**, 3335-3349.